AGARD-AG-171

AGARD

ADVISORY GROUP FOR AEROSPACE RESEARCH & DEVELOPMENT

7 RUE ANCELLE 92200 NEUILLY SUR SEINE FRANCE

AGARDograph No. 171

on

Magnus Characteristics of Arbitrary Rotating Bodies

by

I.D.Jacobson

NORTH ATLANTIC TREATY ORGANIZATION

DISTRIBUTION AND AVAILABILITY
ON BACK COVER

NORTH ATLANTIC TREATY ORGANIZATION

ADVISORY GROUP FOR AEROSPACE RESEARCH AND DEVELOPMENT

(ORGANISATION DU TRAITE DE L'ATLANTIQUE NORD)

AGARDograph No.171

MAGNUS CHARACTERISTICS OF ARBITRARY ROTATING BODIES

by

I.D.Jacobson

School of Engineering and Applied Science,
University of Virginia, USA

Edited by

P.F.Yaggy

US Army Air Mobility Research and Development Laboratory,
Moffett Field, California, USA

This AGARDograph was prepared at the request of the Fluid Dynamics Panel of AGARD.

THE MISSION OF AGARD

The mission of AGARD is to bring together the leading personalities of the NATO nations in the fields of science and technology relating to aerospace for the following purposes:

- Exchanging of scientific and technical information;
- Continuously stimulating advances in the aerospace sciences relevant to strengthening the common defence posture;
- Improving the co-operation among member nations in aerospace research and development;
- Providing scientific and technical advice and assistance to the North Atlantic Military Committee in the field of aerospace research and development;
- Rendering scientific and technical assistance, as requested, to other NATO bodies and to member nations in connection with research and development problems in the aerospace field;
- Providing assistance to member nations for the purpose of increasing their scientific and technical potential;
- Recommending effective ways for the member nations to use their research and development capabilities for the common benefit of the NATO community.

The highest authority within AGARD is the National Delegates Board consisting of officially appointed senior representatives from each member nation. The mission of AGARD is carried out through the Panels which are composed of experts appointed by the National Delegates, the Consultant and Exchange Program and the Aerospace Applications Studies Program. The results of AGARD work are reported to the member nations and the NATO Authorities through the AGARD series of publications of which this is one.

Participation in AGARD activities is by invitation only and is normally limited to citizens of the NATO nations.

Published November 1973

532.582.82 : 533.696.5 : 623.451

Printed by Technical Editing and Reproduction Ltd
Harford House, 7–9 Charlotte St. London. W1P 1HD

CONTENTS

MAGNUS CHARACTERISTICS OF ARBITRARY ROTATING BODIES

Ira D. Jacobson
Assistant Professor
Department of Engineering Science and Systems
School of Engineering and Applied Science
University of Virginia, Thornton Hall
Charlottesville, Virginia 22901, U.S.A.

SUMMARY

This survey paper reviews both theoretical and experimental investigations of the Magnus effect on arbitrary bodies of revolution. The main emphasis is on spinning projectiles at angle of attack, both with and without fins. Flow visualization measurements are used to assess the accuracy of the existing theories. Laminar, turbulent, and mixed boundary layers are considered.

LIST OF SYMBOLS

AR	Aspect ratio
b	Span
C	Rotor chord length
C_D	Drag coefficient
C_L	Lift coefficient
C_{m_α}	Pitching moment curve slope coefficient
$C_{m_{p\alpha}}$	Magnus moment derivative coefficient
$(C_{m_q} + C_{m_{\dot{\alpha}}})$	Damping moment coefficient
C_{N_α}	Normal force curve slope coefficient
$C_n = \frac{M_{mag}}{q_\infty SD}$	Yawing moment coefficient
$C_y = \frac{F_{mag}}{q_\infty S}$	Side force coefficient
D	Maximum body diameter
F_{mag}	Magnus force
h	Parameter in Eq (14)
I	Rotor moment of inertia
k_x	Radius of gyration about longitudinal axis
k_y	Radius of gyration about transverse axis
L	Length of body
L'	Lift force/unit length
l_n	Length of nose section
M_e	Mach number at edge of boundary layer
M_∞	Free stream Mach number
M_{mag}	Magnus moment
m	Mass
$p = \omega$	Model spin rate
q_∞	Free stream dynamic pressure
R	Maximum radius of body

Re_C	Crossflow Reynolds number
$Re_D = \frac{V_\infty D}{\nu}$	Reynolds number based on body diameter
$Re_L = \frac{V_\infty L}{\nu}$	Reynolds number based on length
r_b	Local body radius
S	Reference area
s_d	Dynamic stability factor
s_g	Gyroscopic stability factor
V	Rotor tip speed
V_∞	Free stream velocity
α	Angle of attack
$\alpha^* = \alpha \frac{L}{R}$	Reduced angle of attack
β	$= \sqrt{\lvert M_\infty^2 - 1 \rvert}$
Γ	Circulation
γ	Glide path angle
Δ	Boundary layer displacement thickness
δ	Fin cant angle
δ'	Boundary layer thickness
θ	Azimuthal angle
ν	Kinematic viscosity
ρ	Air density
ω	Spin rate
$\omega^* = \frac{V_\infty}{\omega L}$	Inverse reduced Rossby number

INTRODUCTION

The purpose of this paper is to survey the state-of-the-art in both theoretical prediction and experimental measurement of the Magnus effect on arbitrary bodies. Classically,[1,2,3] the Magnus effect refers to the lift on a spinning cylinder moving through a fluid in a direction perpendicular to its spin axis (figure 1). This gives rise to a lift force per unit length, L', written as

$$L' = \rho V_\infty \Gamma \ . \tag{1}$$

Here ρ is the fluid density, V_∞ the free stream velocity, and Γ the circulation.

Robins,[4] in 1842, correctly observed that the dispersion of cannon balls was due to spin, this being the first record of an awareness of the importance spin plays in ballistics. Although the namesake of this effect, G. Magnus, made the first demonstration of the resulting force caused by a pressure differential due to spin,[5] it was Lord Rayleigh,[6] in 1877, who first treated the problem analytically and arrived at the familiar result described above for the Magnus effect.

In the early 1900's, based on discussions with Prandtl, Flettner[7] proposed the construction of a ship with Magnus rotors as replacements for sails. The spinning cylinders had an expected thrust which was many times greater than equivalent sails, as predicted from early tests.[8-11] However, these proved to be much less effective than anticipated. The discrepancies were due to the differences between the actual three-dimensional flow over the ship rotors and the two-dimensional tests and theory. In addition, the introduction of screw propulsion, which was far more reliable, ended the interest in this method of propulsion. Some of the first measurements on a two-dimensional cylinder were made by Lafay[12-13] as early as 1910; however, it was the 1920's that saw a flurry of experiments, most notably those by Thom.[14-19] These experiments, as well as others done on circular cylinders through the 1950's, are well summarized in two survey papers by Van Aken and Kelly[20] and by Swanson.[21] It is interesting to note that even the earliest

studies by Lafay indicated the existence of a negative Magnus effect (i.e., one giving rise to a net lift force in the opposite direction to the classical Magnus lift). This has been more closely examined recently by Griffiths and Ma[22] and will be explained in detail below. Although the applications of the classical Magnus effect had been limited to rotor ships and tennis and golf balls, it has more recently been applied to dispersible shapes and aerodynamic decelerators. An interesting application is being tested on the VIC 62 research vessel. Here a rotating cylinder extending the length of the leading edge of the rudder is used, enabling sharp turns to reduce stopping distance. The rotating cylinder improves the flow over the rudder making it more effective as well as producing a Magnus force which helps the craft turn.

The Magnus forces and moments acting on spinning missiles, rockets, and projectiles fall into a more complicated class of flows. At small angles and spin rates the boundary layer flow remains attached to the body and the Magnus effect is due mainly to the potential flow interaction with the asymmetries of the boundary layer. The concept of circulation, prevalent in the circular cylinder analysis, has been mentioned only very recently in analytical approaches, having been first suggested by Nikitin[23] and attempted by Power and Iversen.[24] At larger angles, the projectile more closely approximates a cylinder in crossflow and the analogy to the circular cylinder is perhaps in order. This is verified somewhat by papers by Iversen[25] and Fletcher[26] who show a considerable collapse in the data when plotted versus similarity parameters derived from the impulsively-started cylinder in crossflow. The addition of fins creates an even more complicated picture of the Magnus effect and this will be treated separately.

It is the Magnus effect on projectile-type bodies that will be examined in depth in this paper, although some data will be presented on two-dimensional dispersing shapes which basically behave as predicted by the classical Magnus effect.

To date there have been three survey papers written on the Magnus effect for projectiles: Platou,[27] in 1963; Regan,[28] in 1966; and Renevier and Giraud,[29] in 1967. In the course of this review, some repetition will be necessary to be as complete as possible. It is recommended, however, that the reader refer to these previous reviews as well for a broader interpretation of the literature.

IMPORTANCE OF MAGNUS EFFECT IN BALLISTICS

The importance of the Magnus effect, by now, has been well established. Details of the role it plays in dynamic stability of projectiles can be found in Murphy[30] or Nicolaides,[31] the latter having some humorous anecdotal references to past failures and the efforts to which designers have gone to eliminate the unstable behavior as a result of Magnus effects. For the present paper, it is sufficient to refer to figure 2. In this figure, the following definitions are used. The dynamic stability factor, s_d, is defined as

$$s_d = \frac{2(C_{N_\alpha} - C_D) + 2k_x^{-2} C_{m_{p\alpha}}}{C_{N_\alpha} - 2C_D - k_y^{-2}(C_{m_q} + C_{m_{\dot{\alpha}}})} \tag{2}$$

where C_{N_α} is the aerodynamic normal force curve slope coefficient, C_D the drag coefficient, C_{m_q} and $C_{m_{\dot{\alpha}}}$ aerodynamic damping moment coefficients, k_x and k_y radii of gyration in roll and yaw, respectively, and $C_{m_{p\alpha}}$ the Magnus moment coefficient. The gyroscopic stability factor, s_g, is given by

$$s_g = \frac{\omega^2}{4 \frac{\rho S D}{2m} k_y^{-2} C_{m_\alpha}} \tag{3}$$

where ω is the spin rate, S the reference area, D the reference length, m the mass, and C_{m_α} the pitching moment slope coefficient. As can be seen from this figure, along with Eq (2), the dynamic instability can occur for sufficiently large positive or negative values of the Magnus moment coefficient, $C_{m_{p\alpha}}$. This has been examined by Platou[32] along with other influences on dynamic instability and he has shown that for the "normal range" of geometries and aerodynamics, the Magnus effect along with the pitch damping are the main sources of concern for the projectile designer.

FLOW FIELD DESCRIPTION OF MAGNUS EFFECT ON NONFINNED BODIES

For the case of a spinning projectile at angle of attack, the flow patterns depend on many factors, including the angle of attack, spin rate, and Reynolds number. These affect the state of the boundary layer (i.e., laminar or turbulent) and the separation of lee side vortices. Before proceeding with the theoretical and experimental reviews, it will be helpful to enumerate the various possibilities for the flow patterns which result in Magnus forces. The flow field will be presented both schematically and with photographs where available for the cases of low and high angles of attack, and low and high spin rates. Martin,[33] Lando,[34] and Ingram, Lusardi and Nicolaides[35] have utilized

smoke flow visualization and hot wire measurements to determine the flow field for low subsonic speeds, and Sturek[36,37] has used spark photography to visualize the flow field over a cone in supersonic flow. An early study by Sieron[38] using a Schlieren system also gives some insight into the flow field.

From the work of Martin[33] and Lando[34] we see in figures 3 through 5 the flow patterns for small and large angles of attack. At sufficiently small angles of attack, the flow remains attached with the lee side vortices remaining embedded within the boundary layer. For sufficient small Reynolds numbers and spin rates, the boundary layer remains laminar and skewed in the direction of spin resulting in an asymmetric body with respect to the plane of the angle of attack. At higher Reynolds numbers, the boundary layer becomes turbulent.

For larger angles of attack and sufficiently small Reynolds numbers and spin rates, the boundary layer remains laminar; however, the vortices now become separated. Here, large is a very relative term with separation occurring at angles of 5° on some bodies. Increasing spin causes the separated vortex sheets to be altered, the one with vorticity in the direction of spin being forced closer to the body and eventually reattaching; the anticyclonic one having its point of separation shifted around the cylinder in the direction of spin. At high angles of attack where the vortex contribution dominates, this can give rise to negative Magnus forces.

Perhaps the most important flow condition for projectiles is for the case where the boundary layer undergoes transition from laminar to turbulent flow. As seen in Sturek's work,[36] hot wire and spark photography show the asymmetric shape of the transition line at small angle on a cone in supersonic flow (figures 6 and 7). The case where the boundary layer is laminar on the wind side and turbulent on the lee side yields a much greater Magnus force. This asymmetric pattern can be seen in Sieron's[38] shadowgraphs, as well.

THEORY

For the sake of bookkeeping, the various approaches to predicting the Magnus force and its associated moment will be broken into two distinct categories—nonfinned and finned bodies. Most of the work done to date has been on nonfinned projectiles, both theoretically and experimentally.

Nonfinned Projectiles—Attached Flow

Although nonfinned projectiles in principle refers to an arbitrary cross section body, all the work done to date involves bodies of revolution—cylinders, cones, ogive cylinders, etc. After the early work on the Magnus effect described in the historical background above ending in the early 1900's, the first attempt to predict theoretically this phenomenon for a projectile was undertaken by Martin,[39] in 1955. This effort still forms the basis for much of the later work in the area up to this time, and therefore will be discussed here in some detail.

In considering a yawed, spinning, semi-infinite cylinder, Martin, using a small perturbation theory in angle of attack and spin, solved for the laminar boundary layer velocity profiles. Based on these, he computed a laminar boundary layer displacement thickness which was skewed in the direction of the spin. The resulting "new" body, consisting of the original cylinder plus the displacement thickness, is asymmetric relative to the plane of the angle of attack (figure 8). Slender body potential flow theory for the "new" asymmetric body was used to predict the side force (Magnus force) and associated moment (Magnus moment). The analysis applies strictly, only to bodies whose boundary layers are wholly laminar and for small values of angle of attack, α (really $\alpha^* = \alpha\, L/R$) and "small" values of spin, ω (really $1/\omega^* = \omega L/V_\infty$). The restriction of "small" α^* and $1/\omega^*$ is due to Martin's use of series solutions for the velocity profiles and the resulting displacement thicknesses. His results can be summarized as

$$F_{mag} = \frac{13.15}{Re_L^{1/2}}\, q_\infty\, \frac{\alpha^*}{\omega^*}\, S \tag{4}$$

$$M_{mag} = \frac{7.89}{Re_L^{1/2}}\, q_\infty\, \frac{\alpha^*}{\omega^*}\, S\, L \tag{5}$$

where the Reynolds number, $Re_L = \frac{V_\infty L}{\nu}$, the dynamic pressure, $q_\infty = \frac{1}{2}\rho V_\infty^2$, the reference area, $S = \pi R^2$, the body radius is R, and the body length is L. These equations yield a constant center of pressure location of .6L (60% from the leading edge of the cylinder). Although Martin's theory was developed for a cylinder, he suggests using an effective cylinder equal to ½ the length of the nose section plus the length of the afterbody in applying it to projectiles. As will be seen later, a more appropriate effective length may be that obtained from a Mangler transformation for the nose. In addition, without any assumptions of the manner in which the boundary layer grows for the turbulent case, Martin was able to show that for a fully turbulent boundary layer, the center of pressure of the Magnus force would be located at .667L (67% from the leading edge).

As can be seen from Eq (4) and Eq (5), both the Magnus force and moment are linear in both spin and angle of attack. Although Martin did not have the benefit of hot wire or flow visualization, his description, albeit for a very restrictive set of assumptions, has been shown to be accurate.[27] Unfortunately, the fully laminar flow case does not often occur in practice and this greatly limits the applicability of his work.

Kelly and Thacker[40] extended this work to include higher-order spin terms, as well as the effect of radial pressure gradient in the boundary layer on a yawed, spinning cylinder. Their approach was essentially the same as Martin's and resulted in a Magnus force given by

$$F_{mag} = \frac{15.67}{Re_L^{1/2}} q_\infty \frac{\alpha^*}{\omega^*} S \left[1 - \frac{.53}{\omega^{*2}}\right] \tag{6}$$

with a center of pressure, X_{cp}, measured from the leading edge given by

$$X_{cp} = .6L \left[1 - \frac{.156}{\omega^{*2}}\right] . \tag{7}$$

Although Platou[27] indicates that there does not seem to be agreement with experimental data for this work, it is not clear that sufficiently small $1/\omega^*$ data exists for the fully laminar case to make the comparison valid. This author has not been able to find any documented flow conditions where all of the assumptions in both Martin's and Kelly and Thacker's work hold.

Both Sedney[41] and Feibig,[42] for the compressible flow over a cone with a laminar boundary layer, and Jacobson, Vollmer and Morton,[43] for the incompressible flow over a cone with a laminar boundary layer, used the same type of perturbation analysis as Martin to solve for the Magnus force and moment. Their results for a 10^o cone are

Incompressible:

$$F_{mag} = \frac{30.86}{Re_L^{1/2}} q_\infty \alpha \frac{\omega R}{V_\infty} S , \tag{8}$$

$$M_{mag} = \frac{21.6}{Re_L^{1/2}} q_\infty \alpha \frac{\omega R}{V_\infty} S L . \tag{9}$$

Compressible: (Mach No. = 2)

$$F_{mag} = \frac{91}{Re_L^{1/2}} q_\infty \alpha \frac{\omega R}{V_\infty} S , \tag{10}$$

$$M_{mag} = \frac{63.7}{Re_L^{1/2}} q_\infty \alpha \frac{\omega R}{V_\infty} S L . \tag{11}$$

A comparison of Eqs (8) and (10), and (9) and (11) shows that the effect of a favorable pressure gradient and incompressibility is to reduce the Magnus effect, although the location of the center of pressure is the same for both at approximately .71L. The reduction in magnitude is most probably due to the thinning effect that the favorable pressure gradient has on the boundary layer.

For the general compressible case, Sedney's[41] solution is

$$F_{mag} = \frac{3.46}{Re_L^{1/2}} \left(\frac{J_2 U}{\bar{u}'}\right) \sqrt{C}\, q_\infty \alpha \frac{\omega R}{V_\infty} S , \tag{12}$$

$$M_{mag} = \frac{2.47}{Re_L^{1/2}} \left(\frac{J_2 U}{\bar{u}'}\right) \sqrt{C}\, q_\infty \alpha \frac{\omega R}{V_\infty} S L \tag{13}$$

where $(J_2 U/\bar{u}')$ is a factor given in figure 9 for a variety of Mach numbers and cone half angles, and C is the proportionality constant in the viscosity temperature relationship which Sedney used (approximately 1). It is unfortunate that no experimental data for fully laminar boundary layer flow on cones exists to compare these theories.

Vaughn and Reis[44] determine the Magnus force and moment for arbitrary shapes using a transformation found by Vaughn and George[45] to transform the compressible flow on a spinning body of revolution at angle of attack into a flat plate Blasius flow. They include radial pressure gradient effects in addition to the boundary layer displacement effect without a gradient. The force and moment are given by

$$F_{mag} = -\frac{h}{R^2} \left\{ \int_o^{l_n} \delta_n' r_b \, dx + \frac{3}{2} \left[1 - 1.52|\alpha|\right] \int_{l_n}^{L} \delta_a' r_b \, dx \right\} q_\infty \alpha \frac{\omega R}{V_\infty} S , \tag{14}$$

$$M_{mag} = \frac{.5h}{R^3} \left\{ \int_o^{l_n} \delta_n' \, r_b \, dx + \frac{3}{2} \left[1 - 1.52|\alpha| \right] \int_{l_n}^{L} \delta_a' \, r_b \, x dx \right\} q_\infty \, \alpha \, \frac{\omega R}{V_\infty} \, S \tag{15}$$

where

$$h = 1.3 \left[\frac{T_\infty}{T'} + .03 + \frac{.95}{\beta} - \frac{.055}{\beta} \left(\frac{1}{\omega^*} \right)^2 + \frac{.0016}{\beta} \left(\frac{1}{\omega^*} \right)^4 \right] , \tag{16}$$

and

$$\frac{T_\infty}{T'} = 1 + .22r \left(\frac{\gamma - 1}{2} \right) M_e^2 + .5 \left(\frac{T_w}{T_\infty} - 1 \right) . \tag{17}$$

Here $\beta = \sqrt{|M_\infty^2 - 1|}$, r_b is the local body radius, r the recovery factor, δ_n' and δ_a' the nose and afterbody boundary layer thicknesses, respectively; and T_∞, T_w and T' the free stream, wall, and average boundary layer temperatures, respectively. These can be computed from the flat plate zero pressure gradient thickness given by

$$\delta_i' = \frac{5.2X}{Re_L^{1/2}} \left(\frac{T'}{T_\infty} \right)^{\frac{1+\omega'}{2}} M_{m_i} \tag{18}$$

where M_{m_i} is a constant determined from the Mangler transformation

$$M_{m_i} = \left[\frac{\int_o^L \pi \, r_b^2 \, dx}{\pi \, R^2 \, L} \right]^{1/2} .$$

ω' is related to viscosity and is assumed 1 for the range of temperatures experienced in wind tunnel testing, and .603 for low supersonic free flight.

For supersonic flow (M = 2) on a 10° cone, these reduce to

$$F_{mag} = \frac{80}{Re_L^{1/2}} \, q_\infty \, \alpha \, \frac{\omega R}{V_\infty} \, S \left[1 - .0215 \left(\frac{1}{\omega^*} \right)^2 + .00037 \left(\frac{1}{\omega^*} \right)^4 \right] , \tag{19}$$

$$M_{mag} = \frac{56.8}{Re_L^{1/2}} \, q_\infty \, \alpha \, \frac{\omega R}{V_\infty} \, S \, L \left[1 - .0215 \left(\frac{1}{\omega^*} \right)^2 + .00037 \left(\frac{1}{\omega^*} \right)^4 \right] . \tag{20}$$

Equations (19) and (20) yield a center of pressure location of .7L which agrees with Sedney's[41] result. The power of the above approach is its applicability to any shape projectile, although there still is the assumption of fully laminar flow to limit its use.

For a mixed flow or fully turbulent case, Vaughn and Reis[46] suggest a boundary layer as shown in figure 10 and develop equations to determine the Magnus force and moment for the case of boundary layer transition occurring symmetrically at any axial station. These will not be reproduced here since flow visualization and other analytic studies have shown that if transition does occur on a spinning body at angle of attack, it occurs asymmetrically (see figures 6 and 7). It should be noted, however, that for long bodies, when transition occurs over a short distance on the body, this approach may be adequate.

All of the above methods are for the completely laminar or completely turbulent case (with the exception of Vaughn and Reis' mixed flow approach) and all predict a center of pressure location which is independent of angle of attack and insensitive to Reynolds number. Jacobson[47] and Jacobson and Morton,[48,49] by investigating the stability of the laminar boundary layer on a yawed, spinning cylinder and a yawed, spinning cone, show that it is reasonable to believe that the boundary layer undergoes transition to a turbulent one asymmetrically (figure 11). This asymmetric transition gives rise to a substantially larger force and moment than predicted for the fully laminar case. In addition, the center of pressure no longer is independent of angle of attack and Reynolds number (figure 12).

To obtain these curves, the effects of spin and angle of attack on the stability of the laminar boundary layer on a semi-infinite cylinder were investigated. Assuming that the predicted instability eventually breaks down into turbulence at a constant distance along a body ray, the growth rates for laminar and turbulent boundary layers (assumed to follow those predicted by Martin's[39] theory for the laminar case and a modified version by Jacobson[47] for the turbulent case) were used to predict the Magnus force and moment as

$$F_{mag} = -2R^2 \, q_\infty \, I(L) \quad , \tag{21}$$

$$M_{mag} = -2R^2 q_\infty \left[I(L)\, L - \int_0^{2\pi} \Delta(L) \sin\theta d\theta \right] \tag{22}$$

where

$$I(L) = \int_0^{2\pi} \frac{\partial \Delta}{\partial x} \sin\theta d\theta \quad .$$

Here θ is the azimuthal angle, and Δ is the boundary layer displacement thickness. For the fully laminar and fully turbulent boundary layer conditions, these reduce to the same results as Martin.[39] Here, as in Martin's work, it is clear that the Magnus force depends only on the shape of the boundary layer at the base of the model. This general asymmetric behavior has been verified experimentally by hot wire and sound pressure measurements indicating the correct shape for transition (Jacobson and Morton,[50] figure 13). The drawback in this approach is that there are no methods at present for evaluating the relationship between instability and transition nor for determining the rate of turbulent boundary layer growth on a spinning body which is highly nonlinear with spin (figure 14). This theory appears to be in keeping with other measured and flow visualization data.

Power and Iversen, in a recent paper,[24] have included circulation in an attempt to account for the nonlinear behavior of the Magnus force with angle of attack on a semi-infinite circular cylinder. They postulate a potential flow which has circulation due to boundary layer separation and proceed as in previous analyses with a perturbation solution. They also include the effect of radial pressure gradient and skin friction. Although some success is achieved with this method, it would appear that it is valid only at large angles of attack when separated flow dominates, and the agreement with experimental data at small angles of attack is perhaps only coincidental. A similar behavior can be obtained by assuming a mixed (both laminar and turbulent) asymmetric boundary layer which is more in keeping with flow measurements for the Reynolds numbers involved. Figure 15 indicates the agreement they obtained with their calculated Magnus force given by

$$F_{mag} = \frac{15.2}{Re_L^{1/2}} q_\infty \frac{\alpha^*}{\omega^*} S \left[1 - \frac{.93}{Re_L} \left(\frac{L}{R}\right) + \frac{2.1 C_1 Re_C^{3/4} - 2.93}{Re_L^{1/2}} \left(\frac{L}{R}\right) \right] \tag{23}$$

where C_1 is a constant related to the local circulation, and Re_C is the crossflow Reynolds number. For small angles of attack and hence small crossflow Reynolds numbers, this reduces to first-order to Kelly and Thacker's results.[40]

Tetervin[51] has treated the fully turbulent flow over an ellipsoid of revolution at small angles of attack. Although this approach is interesting, it does not seem applicable at the present time to any bodies of experimental or practical interest and will not be discussed further.

Closing Comment on Theories for Nonfinned Bodies—Attached Flow

It would appear from the above discussions that the various theories which exist for predicting the Magnus effect are rather limited for practical applications. Although some insight is gained as to the manner in which the Magnus force manifests itself, the various approaches have restrictions that make them tenuous at best for prediction purposes. Here we will summarize the various theories and their drawbacks.

Martin's Theory[39] for a cylinder

Only applicable to bodies with totally laminar boundary layers and for flow conditions of small α^* and $1/\omega^*$. Strictly valid for a cylinder shape only with no means of estimating the effect of differing nose shape.

Kelly and Thacker's Theory[40] for a cylinder

Same as above.

Sedney's,[41] Feibig's,[42] and Jacobson et al.'s Theory[43] for a cone

Same as above except that it only applies to flow over a cone.

Jacobson's Theory[47] for a cylinder

Applies to all boundary layer conditions (laminar, turbulent, and mixed), however, requires knowledge of way in which boundary layer grows and how transition is affected by spin and angle of attack. Is restricted to attached flow (no separation). Strictly applies only for small values of α^* and $1/\omega^*$.

Vaughn and Reis' Theory[44]

Applies to attached laminar boundary layer on arbitrary bodies in supersonic flow. Does account for effects of nose shape and compressibility.

As can be seen, the one theory that does allow for mixed boundary layer requires as yet unavailable information on the effects of spin and angle of attack on transition and boundary layer growth. The others require a laminar boundary layer on the entire body—a condition which is very seldom found in experimental or full-scale tests. These problems make it virtually impossible to compare fairly these theories with available data in anything other than a qualitative manner. This will be done in the following chapter.

Before moving on, a comment on two contributors to the Magnus force and moment which appear to have been ignored by most investigators—wall shear stress and base effects. Although the transverse component of shear is most likely negligible, the longitudinal component for mixed boundary layers (especially on nose cones) may not be. The effects of the flow on the base have not been examined at all.

Nonfinned Bodies—Separated Flow

All of the work above except Powers[24] assumes the flow is attached everywhere. Some work has been done for the case where there is vortex shedding on the lee side of the body. In some instances this can lead to a negative Magnus force which has been described in detail by Fletcher,[26] who applies the two-dimensional explanations of Krahn[52] and extensive work by Swanson.[21]

To understand the negative Magnus force, it is convenient to examine the case of a two-dimensional cylinder. Although experimentally observed as early as 1910 by Lafay,[12,13] it was first explained by Krahn[52] in 1956. In the flow over a nonspinning cylinder, until a critical Reynolds number is reached, the laminar boundary layer separates at approximately 82° from the forward stagnation point. As the Reynolds number increases, the boundary layer becomes turbulent and separation moves downstream to approximately 130° from the forward stagnation point. As the cylinder begins to spin, for the case where the Reynolds number based on the free stream velocity is near the critical value (that which causes the boundary layer separation to switch from laminar to turbulent), the separation points are greatly affected. As is seen in figure 16, the side of the body on which the spin opposses the free stream "sees" a higher relative velocity and this induces a turbulent boundary layer separation; on the side for which the spin is in the same direction as the free stream, the relative velocity is lower and a laminar separation takes place. In actuality, the separation takes the form of a laminar bubble and turbulent reattachment for the turbulent case. On the side where separation is delayed, the pressure remains lower longer and the lift force is in the direction shown which is contrary to that expected using classical arguments (figure 1). The variation of the lift with Reynolds number is seen in figure 17 taken from Swanson,[21] where large negative lift coefficients are observed. Although the flow is not two-dimensional on a projectile at angle of attack, it follows that a similar effect should certainly be present and it is indeed observed.

Fletcher[26] shows that treating the body at angle of attack as an impulsively-started cylinder and taking into account body vortices yields a similar explanation for the three-dimensional projectile case.

Iversen,[25] in correlating the Magnus force for slender cylinders, again used the impulsive cylinder analogy to calculate a correlation parameter

$$C_y = -k \frac{\omega R}{V_\infty} \frac{x}{D} \frac{\tan \alpha \sin^{-5/4}|\alpha|}{Re_D^{1/4}} , \tag{24}$$

which when integrated over the body gives a Magnus force

$$F_{mag} = - \frac{\frac{2k}{\pi} \left(\frac{L}{D}\right)^2 \tan \alpha \sin^{3/4}|\alpha|}{Re_D^{1/4}} \tag{25}$$

and a center of pressure location of 2/3 the distance from the nose. For supersonic speeds with a crossflow Mach number of less than .4, figures 18 and 19 show the degree of correlation is excellent and insensitive to Mach number and spin rate. For subsonic speeds, the correlation appears to hold for small values of the parameter only and is limited by a spin ratio ($\omega R/V_\infty$) of .5 or less. This method does restrict the center of pressure location to a constant position and this is a serious drawback. Platou, in his review article,[27] shows that for values of the crossflow Mach number of .8 or greater, there exists a correlation of the Magnus force versus crossflow Mach number as the correlating parameter. Iversen[25] has investigated the case of both contributions due to the boundary layer and the separated vortices.

Effects of Fins

For the case of the finned projectile, three spin-related phenomena have been identified which influence the Magnus effect. These have been explained by Platou,[27] however they will be briefly described here for completeness.

The first method for generating a Magnus effect on fins is due to unequal normal forces, and was first described by Platou. A fin which is rotating at some angular rate, ω, induces an angle of attack (as shown in figure 20) due to the superposition of the

rotational velocity with the free stream velocity. This angle of attack varies with the position along the fin as shown, and is given by $\alpha = \omega y/V_\infty$. For the supersonic case, linear theory[1] yields the lift coefficient on each of the fins as

$$C_L = \frac{4\alpha}{\sqrt{M^2-1}} \quad . \tag{26}$$

When the projectile is at zero angle of attack, keeping in mind that the lift acts perpendicular to the fin, there is no net force, just a damping moment. At angle of attack, the lift force on the fin in the wake of the body has a reduced lift, resulting in a force on the tail section which acts through the center of pressure of the fins, as shown in figure 21.

For the body at this angle of attack and spin, ω, the Magnus force will be in the opposite direction but through a different center of pressure, figure 22. These two forces create a moment couple which is equal to the lesser of the two forces multiplied by the distance between them and the Magnus moment will be about the center of gravity, equal to this moment couple plus the moment due to the unbalanced force multiplied by the distance to the center of gravity. This resultant can be either positive or negative.

The second phenomenon is that due to canted fins. Benton[53] has shown that, provided the fins are canted differentially (which they generally are to induce rolling), a moment due to spin can be created. Consider a missile which is rolled due to fin cant, figure 23. The normal force on each of the fins can be broken down into components—one in the direction of the longitudinal axis and the other perpendicular to it. Due to the fact that the fins are differentially canted, they have angular deflections in opposite directions. This brings about a difference in direction between the longitudinal components.

Now if, in addition, the body has an angle of attack, keeping in mind the "induced" angle of attack due to spin, the total moment due to fin 1 is given by

$$N_1 y_1 = \int_{D/2}^{b/2} q_\infty C_{N_\alpha} \left(\alpha_B - \delta + \frac{\omega y}{V_\infty}\right) y \, dy \quad , \tag{27}$$

and due to fin 3

$$N_3 y_3 = \int_{D/2}^{b/2} q_\infty C_{N_\alpha} \left(\alpha_B + \delta - \frac{\omega y}{V_\infty}\right) y \, dy \quad . \tag{28}$$

The total torque is then

$$T = -C_{N_\alpha} q_\infty \alpha_B \delta D \left[\left(\frac{b}{2}\right)^2 - \left(\frac{D}{2}\right)^2\right] . \tag{29}$$

Figure 24 compares calculations based on Eq (29) with experimental results. The large discrepancies below Mach 2 are due to the uncertainty of the lift coefficient as one gets into the transonic regime.

The third mechanism considered is that of Magnus effects due to fin base pressures. Chapman, Wimbrow and Kester[55] showed experimentally that for thin wings or fins, the base pressure can change suddenly with angle of attack and seems to be associated with a high frequency vortex trail (8×10^4 Hz). The conditions for which this occurs are: laminar boundary layer, thickness ratio, $t/c < 0.075$; low supersonic Mach number; and thin trailing edge. When the critical angle is reached, there is a sudden change in base pressure which has been observed to as much as double in tests.

Many of the restrictions put on this case may seem to make it of purely academic interest, but this is to be seen. As before, consider a rotating missile and differentially canted fins. Then the angle of attack can be shown as before to be

$$\alpha_1 = \alpha_B - \delta + \frac{\omega y}{V_\infty} \quad ,$$

$$\alpha_3 = \alpha_B + \delta - \frac{\omega y}{V_\infty} \tag{30}$$

when at zero roll angle orientation.

It is obvious from this that the angle of attack of each fin is not necessarily the same. For a specific set of the variables, one fin can be at the lower base pressure and the other at a higher base pressure.

With multifin configurations, at least one set of fins may have unequal base pressures. This will produce a moment given by

$$C_{m_{p\alpha}} = \frac{\left[\left(\frac{P_b}{P_\infty}\right)_1 - \left(\frac{P_b}{P_\infty}\right)_3\right] S_b \, b\beta_\infty}{q_\infty \, S \, \alpha \, \frac{\omega R}{V_\infty} \, D} \tag{31}$$

where $(P_b/P_\infty)_i$ is the base pressure ratio for fin i, S_b the base area, b the span, and P_∞ the free stream pressure. Using reasonable values for these quantities, $C_{m_{p\alpha}}$ is of order of magnitude one. This is considerably less than the $C_{m_{p\alpha}}$ due to differential fin cant but more than that due to body fin interference. An interesting thing to note is that fins with a .075 t/c ratio or greater are not subject to a sudden change in base pressure.

When a body has two sets of fins, Benton[56] has shown that the downwash field on the tail set of fins (figure 25) contributes significantly to the Magnus effect. A semi-empirical theory based on the wake swirl of the forward set on fins which have an aileron deflection predicts the side force and moment as shown in figures 26a and 26b. The equations are not reproduced here since they are dependent on several empirical constants which will vary from case to case. Figures 26c and 26d show the results of Benton's experiments and theory and indicate the magnitude of the wing-tail interference term in the Magnus effect, which is seen to be considerable.

One other effect mentioned by Uselton and Carman,[57] and treated analytically by Thompson and Morrison[58] and Oberkampt and Nicolaides,[59] is the effect of body vortices on the fins. These vortices at angle of attack and spin are asymmetric and their impingement on the fins can give rise to side forces and moments. For the basic finner missile configuration, Oberkampt and Nicolaides[59] compute the side force and side moment coefficients both for variations in angle of attack and fin deflection angle (figure 27). It can be seen that the interaction can be significant. This body vortex/fin interaction due to vortex asymmetries can also be produced by a model undergoing "coning motion." The induced vortex asymmetries as in the spin case can give rise to side forces and moments. This phenomenon has been investigated by Kuhn, Spangler and Nielson.[60]

EXPERIMENTAL DATA—PROJECTILES

Before proceeding to summarize the experimental data obtained to date, a short description of the types of facilities used and test apparatus for measuring the Magnus effect is in order. The primary source of Magnus data is from conventional wind tunnels. The ability to measure the forces involved is hampered by the fact that the Magnus force is generally an order of magnitude or more smaller than the normal force, providing a challenging situation for the experimentor. Most of the wind tunnel systems currently being used are of the type shown in figure 28 which is described by Platou et al.,[61] and Regan,[62] and consists of an air-turbine-driven model mounted on bearings with an internal strain gauge balance. Due to the high spin rates involved, model design and dynamic balancing become an integral and important part of the experiment.

Some of the sources of error[63] are due to model-induced oscillations due to free stream turbulence, flow angularity and curvature, and test section Mach number variation. In addition, when testing canted fin or self-rotating configurations, Platou[64] has shown that a normal force interaction term exists which is due to a side force existing at zero spin. Since self-rotating configurations generally are not tested at zero spin, this can result in a serious error. An example which shows the magnitude of this error is reproduced in figure 29.

A second source of Magnus data is through the free-flight or constrained free-flight test technique. Here the projectile is allowed to move in varying degrees of freedom ranging from total free-flight (as in a ballistic tunnel, range, magnetic suspension or actual flight) to constrained free-flight (as in the case of a tunnel balance which allows only angular motions). In general, the measured motion is curve fit analytically in a least squares sense to a quasi-linear model of motion. These models are usually of the tricyclic or quadricyclic theory form, and damping and frequencies obtained from the fit are used to predict the aerodynamics, including the Magnus terms.

Other methods include resonance tests, full 6-D equation fits, and forced oscillation testing techniques. Errors in these free-flight-type approaches are due in general to the lack of sufficient data for an accurate fit, inaccuracies in measuring angles and displacements of a moving projectile, and the usually implicit assumptions of linear aerodynamics over a cycle of motion which can involve large changes in angle of attack over which the aerodynamics may be highly nonlinear. A description of the above techniques can be found in a variety of references, among them Eikenberry,[65] Murphy,[30] Knadler,[66] Chapman and Kirk,[67] Ragunath,[68] and Jacobson, Junkins and Jancaitis.[69]

Experimental Data—Nonfinned Bodies

Nonfinned bodies for which substantial data is available includes the shapes shown in figure 30, with several configurations being tested with different nose shapes. The simplest shape is that of a cone (10° half angle) which has been investigated by several experimentors—Nicolaides and Brady,[70] in 1959, for a Mach number of 2, Curry, Reed and

Ragsdale,[71] in 1971, for a range of supersonic Mach numbers and a range of Reynolds numbers, and Sturek,[36] in 1972, again for supersonic Mach numbers. Figures 31 and 32 and Table I compare their results and indicate that at M = 2 there is quite a discrepancy between results. The values in Table I indicate the probable cause for the discrepancy.

TABLE I

		Transition Location			
		Curry, et al.[71] (Re = 1.8 x 10^6)		Sturek[36] (Re = 1.9 x 10^6)	
M	α	Lee Side	Wind Side	Lee Side	Wind Side
2	0°	>1	>1	N/A	N/A
	2°	.98	>1	.25	.71
	4°	.46	.92	.19	.68
3	0°	>1	>1	N/A	N/A
	4°	.41	>1	.45	>1

N/A—Not available.

Here it is seen that transition on the cone for M = 2 occurs at different locations for the two experiments and thus differing portions of the body are bathed in laminar and turbulent boundary layers for the two sets of measurements. An interesting behavior pattern for the center of pressure location is seen in figure 33. It is interesting to note that this "type" of behavior for the center of pressure is predicted for mixed boundary layer conditions by Jacobson[47] as was seen in figure 10. Although not applicable for these flow conditions, Sedney's[41] theory is superimposed to show the effect a mixed boundary layer has on the magnitude of the forces and moments, and even more drastically on the center of pressure. Sturek[36] indicates that there is better agreement at M = 3 for the two sets of wind tunnel data (Curry, et al.,[71] and Sturek[36]). As is seen in Table I, the transition data, although sparse, indicates essentially the same boundary layer configuration for this case, which implies the same flow conditions on the body. Although it is unfortunate that no data exists to check Sedney's[41] theory, it is important to realize that in real-flight conditions, the totally laminar boundary layer seldom exists. For this reason, the importance of the effect of mixed asymmetric boundary layers on the Magnus force and moment should be recognized and more work in this area stimulated.

The next simplest series of shapes are the Army-Navy spinner and tangent-ogive-type configurations. Reports containing information on these shapes are summarized in Table II.

TABLE II

Shape	Mach No.	Reynolds Number Based on Body Length	Angle of Attack (Degrees)	$\omega R/V_\infty$	Author/s	Ref. No.
Spinner (3 cal)	.9 → 1.7	.65 x 10^6	0 → 5	0 → .4	Platou	72
Spinner (5,7 cal)	Subsonic	2.2 → 5.1 x 10^6	0 → 28	0 → 1.8	Greene	73
Spinner (5,7 cal)	.2 → 2.5	1.75 → 6.1 x 10^6	0 → 25	0 → .4	Greene	74
Spinner (7 cal)	.3 → 2.5	2 → 4.6 x 10^6	0 → 20	0 → 2	Luchuk & Sparks	75
Spinner (7,8,9,10 cal)	2 → 2.7	3 → 6.3 x 10^6	0 → 20	0 → .1	Holmes, Regan & Falusi	76
Ogive Cylinder (4.4-8.25 cal)	.2	.4 x 10^6	0 → 30	0 → 1	Fletcher	77
Ogive Cylinder (approx. 10 cal)	Subsonic	.6 → 1.8 x 10^6	0 → 20	0 → 1	Nikitin	23
Ogive Cylinder (25 cal)	2 → 6	10 → 24 x 10^6	0 → 16	0 → .03	Uselton & Carman	57
Ogive Cylinder (24 cal)	3,5	9 → 29 x 10^6	0 → 16	0 → .02	Uselton	78

Some of the results are shown in figures 34 and 35. Once again, there is a discrepancy between facilities (figure 34) due in part to the asymmetries in the boundary layer development on the bodies and in part to measurement inaccuracies. Figure 35 illustrates the trend in increasing fineness ratio for the smaller angles of attack. Although a considerable scatter exists, there is a general trend toward longer bodies having higher Magnus forces. At higher angles of attack, there is a trend for the Magnus center of pressure to become constant in location at about .3L from the base, which is in relatively good agreement with Iversen's[25] crossflow analogy result of .33L. Figure 36 illustrates this trend with representative data curves; many more could have been included, all resulting in approximately the same asymptote at about an angle of attack of 20 degrees.

The effects of nose shape have been investigated by Greene[74] and Luchuk.[79] Both observed significant variations in the Magnus effect due to nose shape and typical results are shown in figures 37 and 38. Once again, notice the relatively constant asymptote at high angles and the general shape versus angle of attack. These curve types are predictable with a theory based on an asymmetric transition on the body (again see figure 13). The nose shapes having different pressure gradients affect the boundary layer growth and will thus have an effect on transition. It is known that boundary layer instability and transition on a flat plate is greatly affected by pressure gradients and this pressure gradient effect is undoubtedly reflected in the projectile shapes tested. In the low angle of attack range ($0-4^\circ$), a large nonlinear variation is seen which can cause difficulties in estimating the Magnus effect.

Since the boundary layer state and distribution are of prime importance in determining the Magnus force and moment, the application of grit to artificially "trip" the boundary layer can be expected to have a large effect. This can be seen in the data by Platou,[72] Sieron,[38] and Uselton.[78] All three show significant changes in the Magnus forces and moments due to grit addition—Platou for Mach 2, Sieron at transonic speeds (M = .9 → 1.1), and Uselton for high Mach numbers (M = 5). These effects occur at all angles and spin rates, including changes in sign for large angles (figure 39).

Another factor which has been investigated is the effect of base shape by Platou,[72] and by Platou and Nielson.[80] In both cases, there were significant changes in the Magnus effect as a result of rounding the base or boattailing it. This, as in the case of nose shapes, is to be expected since a change in base shape will, through pressure gradient effects, modify the boundary layer and hence the Magnus force. To better understand the questions concerning the effect of the boundary layer at the base, Regan and Schermerhorn[81] attempted to use base bleed to thin the base boundary layer. Due to an increase in base pressure from suction pumping, the results were inconclusive, but indicated only minimal reductions in the Magnus force.

Still another variable affecting the Magnus force are body variations. Most artillery and bullets have various serrations and protuberances which will affect the boundary layer. The effect of body serrations is extensively investigated by Sylvester and Braun[82] for both a 5-caliber cone cylinder and a 5-caliber A-N spinner model (figure 40). Figure 41, for the cone-cylinder model, indicates that except for an initial side force offset due to the aerodynamic asymmetries of the serrations, the Magnus coefficient (i.e., C_{y_p}) is unaffected by the serrations. The results are somewhat obscured in that a boundary layer trip was used to simulate more closely the turbulent boundary layer existing on the serrated model. This implies that the effects on the growth and distribution of the boundary layer are mainly a function of the state of the boundary layer (i.e., laminar or turbulent) and the angle of attack and spin rate, and are not additionally affected by the serrations. Similar results are obtained on the A-N spinner model. When a boundary layer trip is not used, the serrations may influence the state of the boundary layer and hence the Magnus force. An interesting phenomenon exists at very low angles of attack for the serrated models (figure 42). When the Reynolds number based on diameter is 2×10^5, the model exhibits both a large side force in the notch-spin condition (i.e., a spin rate equal to the free-flight steady state value obtained from the serrations), as well as gross changes for the cases of underspin and overspin relative to notch-spin rate. The significance of these changes at the lower Reynolds number is not obvious, however one explanation may be that the state of the boundary layer is less sensitive to effects of spin and angle of attack for cases where natural transition to turbulence is moved toward the nose tip (higher Re/ft free stream values). This is exhibited somewhat in figure 12 where the effects of angle of attack are negligible for high unit Reynolds numbers, yet important for lower unit Reynolds numbers.

Another body variation which commonly occurs on projectiles is a sub-caliber extension from the base (e.g., the 107-mm mortar shell). The effect on the Magnus moment slope coefficient from the work of MacAllister, et al.[83] is shown in figure 43 where the extension length is seen to greatly change the Magnus effect, especially at low Mach numbers for small yaw angles. At large yaw angles, the effects are even greater as can be seen in figure 44. These booms (especially the long boom of one caliber length and 1/3-caliber diameter) can create sufficiently large positive Magnus moments to drive the projectile unstable.

In addition to the basic shapes and studies discussed above, considerable testing has been done on special shapes—these include bullets, artillery, and mortar rounds. Table III summarizes some of these experiments (see page 13).

In summary, it is evident that the Magnus force, moment, and center of pressure location are highly sensitive to anything which can have an effect on the boundary layer state or growth. These include: boundary layer trips; nose shape and base shape; pressure gradients; body roughness due to serrations; rings, grooves, etc.; and afterbody booms. The impact of all of this is the realization that to apply experimental data to free-flight conditions for many bodies will require a better understanding of the boundary layer which exists in free-flight as well as on the test body. This will be especially true if small variations in boundary layer configuration alter the Magnus effect drastically. It is perhaps essential that all Magnus testing in the future be accompanied by a determination of the test body's sensitivity to boundary layer changes by using different trip configurations.

Experimental Data—Finned Bodies

Some early reports, among them those by Murphy,[90] Piddington,[91] and Platou[92] indicate that the effects of fins on the Magnus forces and moments of bodies of revolution not only can change the sign of the forces and moments, but can be an order of magnitude greater. As an example, figure 45 shows the effect of fins on two 6.6-caliber bodies. This concept of a reversal in sign is in keeping with the theory of body interference (proposed by Platou[92]) of the flow on the lee side fin.

Several specific finned shapes have received attention through the years. They are illustrated in figure 46. Tests on the Tomahawk model by Uselton,[78] and by Curry and Reed[93] on the same model in the same facility for the identical test conditions (M = 5, Re_L = 27.3×10^6), illustrate the nonrepeatability of the data (figure 47). Both authors

TABLE III

Shape	Mach No.	Reynolds Number Based on Body Length	Angle of Attack (Degrees)	$\omega R/V_\infty$	Author/s	Ref. No.
30-mm bullet	1.5 → 2.5	.5 → 1.3 x 10^6	0 → 40°	0 → .3	Platou & Sternberg	84
20-mm & 30-mm bullet	.8 → 1.18	.13 → .44 x 10^6	0 → 40°	0 → .5	Sieron	85
20-mm & 30-mm bullet	.2 → 1.18	.2 → .8 x 10^6	0 → 40°	0 → .5	Sieron	38
5" projectile	.7 → 2.3	N/A	0 → 11°	N/A	Chadwick	86
5" projectile	.7 → 2.5	N/A	0 → 5°	N/A	Donovan & MacAllister	87
4.2 M329A1E1 projectile	.3 → .95	1.25 → 3.5 x 10^6	0 → 40°	0 → .7	Kline & Gazdayka	88
XM549 artillery shell	.5 → 2.2	.2 → 2 x 10^6	0 → 20°	0 → >1	Platou & Nielson	80
5" projectile	.05	.28 x 10^6	0 → 4°	.22 → .45	Kline	89

N/A—Not available.

indicate that at zero spin and angle of attack, an asymmetric vortex pattern exists on the model which is unpredictable and not repeatable from one tunnel installation to the next, but is stable for a given run. The behavior for the nonspinning model has been observed by other authors,[94,95] however still others[77,34] have not observed them.

This effect, of course, cannot be a "real" one in that there is no mechanism for net vorticity to be generated—a condition which the asymmetric pattern implies. It must then be due to flow and body irregularities as Thompson and Morrison[58] have indicated in a paper where they show that these vortex asymmetries can give rise to rolling moments and side forces and moments through interactions with the fins. These irregularities can be expected to change from one tunnel installation to another, since it is highly unlikely for the "exact" same tunnel/model/balance setup to be repeated. Some possibilities for the cause of this flow asymmetry might be changes in flow inclination or generation of flow shears in the test section due to blockage changes and complex shock-boundary layer interactions. From calculations made by Curry and Reed,[93] they state that it is not certain whether the asymmetries are due to flow and model asymmetries or to a "real" effect in the perfectly aligned flow case. Typical patterns which may exist under actual experimental conditions are shown in figure 48. Effects of these asymmetric patterns have been shown to be more pronounced at lower Mach numbers for supersonic flow.[57]

Uselton[78] points out that although the asymmetric vortex pattern at zero spin causes the behavior of the Magnus force at spin to be nonsymmetric about zero for positive and negative fin cants, δ, the difference between the two seems to be independent of the zero spin condition (i.e., $\Delta C_y = C_{y_{\delta+}} - C_{y_{\delta-}}$ is independent of $C_{y_{\delta=0}}$). This is illustrated in figure 49. This tends to substantiate the explanation given above. Consider that for the zero deflection angle case, the asymmetric vorticity causes the apparent deflection angle to be some angle different than zero, ε, and yields a side force. Then both the positive and negative deflection angles really represent angles of $\delta - \varepsilon$ and $-\delta - \varepsilon$ which are certainly not equal and opposite. If, however, the change in side force due to a change in deflection angle varies linearly, which can be expected for small deflection angles, then the total change in side force for both positive and negative deflections will be equivalent to the symmetric case. For example, in the asymmetric case:

$$\left.\begin{aligned} C_{y_{\delta+}} &\sim \delta - \varepsilon \\ C_{y_{\delta-}} &\sim -\delta - \varepsilon \end{aligned}\right\} \Rightarrow \Delta C_y \sim 2\delta \qquad (32)$$

and in the symmetric case:

$$\left.\begin{aligned} C_{y_{\delta+}} &\sim \delta \\ C_{y_{\delta-}} &\sim -\delta \end{aligned}\right\} \Rightarrow \Delta C_y \sim 2\delta \quad . \qquad (33)$$

Thus, the correct side force for a given deflection angle, δ, can be found by dealing with differences only.

It is also interesting to note that for the Tomahawk vehicle, Stone[96] has computed the Magnus moment coefficient derivative for several actual flights using a free-flight reduction technique. Although this data is for a Mach number of 7.7, it is compared by Curry and Reed[93] with their data for similar cases of $\omega R/V_\infty$ (figure 50). There are some differences, especially at small angles of attack, however reasonable agreement exists considering the Reynolds and Mach number differences. It should be noted that here the tunnel data has been corrected to account for apparent zero side loads. Uselton and

Carman[57] have shown that for the Tomahawk vehicle, as Mach number increases or Reynolds number decreases, the Magnus force decreases.

Figure 51 shows a comparison of the data for the Apache vehicle versus the Tomahawk. Although the vehicles are slightly different, the differences appear to be insignificant when comparing the side force coefficients in difference form, ΔC_y, as suggested by Uselton.[78] Once again, the actual C_y shows considerable variation, both at 0-spin and at spin due to vortex asymmetries; however, as expected from the above argument, ΔC_y is nearly the same for both vehicles.

Several recent papers have investigated the M823 research store: Regan, Shannon and Tanner[97]; Regan[98]; and Regan and Falusi[99] with fixed and freely spinning stabilizers. Typical results are shown in figure 52 for a 5-degree fin cant. Here it can be seen that the moment does not go to zero when the force does for the freely spinning stabilizer. There are three possible causes for a pure moment as was described in the theory section. Differential base pressure (positive moment for low $\omega R/V_\infty$), differential fin cant moment (negative moment), and body vortex interaction with fins (positive or negative depending on asymmetry of zero spin vortices). Thus, in general, it is not a simple matter to predict the net moment. In the case of the fixed stabilizer (body spinning as well), an additional moment is present due to the couple formed by the body Magnus and fin Magnus. Since both the location of and the sign of the body Magnus can vary, this couple can be either positive or negative.

Several attempts[34,89,100] have been made to eliminate or reduce the Magnus effect, generally through the use of vanes or fins of various types. An example of the effect of nose vanes is shown in figure 53 (from Lando[34]) and of boattail fins in figure 54 (from Kline[89]), both for low subsonic speeds. It is evident that the Magnus effect can be greatly affected by both types of modifications.

MAGNUS ROTORS

The Magnus rotor is basically any cylindrical shape of arbitrary cross section (for the purpose of this paper, this includes the flat plate and Flettner shapes). A typical example is shown in figure 55, along with a force balance diagram. Most rotors autorotate due to asymmetric cross sections or asymmetric vortex shedding. These phenomenon have been described by Nicolaides[101] and Iversen,[102] the latter having an excellent history of the development and applications of the Magnus rotor, including its use as an aerodynamic decelerator.

There are three basic areas which need to be understood in predicting and evaluating the behavior of these rotors. These are the prediction of autorotation rates, glide angles ($\gamma = \tan^{-1}(C_D/C_L)$), and directional stability. It should be noted that terminal steady-state velocities for these rotors are all subsonic.

As is indicated in figure 56 from Iversen,[102] autorotation rates increase with increasing aspect ratio. Iversen shows that much of this data can be collapsed onto a single curve by correlating with the moment of inertia-aspect ratio parameter ($I\text{Æ}R/\rho C^5$, where I is the mass moment of inertia in roll, ÆR the aspect ratio, ρ the air density, and C the rotor chord) and can be approximated by

$$\frac{\bar{V}}{V_\infty} = \frac{7}{3}\left(\frac{I\text{Æ}R}{\rho C^5}\right)^{1/4} \tag{33}$$

where $\bar{V}$ is the tip speed of the rotor.

It is evident that increasing aspect ratio increases the tip speed ratio, $\bar{V}/V_\infty$. Flatau's[103] data shows that the addition of end plates increases the effective aspect ratio, with larger end plates yielding larger effective aspect ratios. Increasing aspect ratio also produces an increasing ratio of lift-to-drag yielding longer glide paths. Iversen[102] suggests the expression

$$\frac{C_L}{C_D} = 0.5\sqrt{\text{Æ}R_{\text{effective}}}\ , \tag{34}$$

although the reader is cautioned that this approximation appears to be valid only for small effective aspect ratios (i.e., $\text{Æ}R_{\text{eff}} < 4$). For larger aspect ratios, actual cross-sectional profile appears to become important.

Little data is available on stability characteristics in yaw for most rotor shapes. The interested reader is referred to the literature[96,104,105] for further information.

Several other types of rotor shapes have been investigated which make use of the Magnus force to produce lift. These include spherical shapes[105,106] and disc shapes of various types,[107] such as a circular disk looking much like a frisbee.[108]

CONCLUSION—NEED FOR FUTURE RESEARCH

In examining the state-of-the-art in determining the Magnus effect on projectiles, one is forced to conclude that there is still much to be learned. It appears that the key to developing a viable means of predicting the Magnus forces and moments on full-scale flight projectiles hinges on a better understanding of and a better means of predicting the flow fields on these bodies. This requires a means of predicting boundary layer transition, growth rates, and separation phenomena. While this is a difficult problem, it is an essential step which should be taken.

Two areas which have received little attention in the literature are the effects of wall shear stress and base effects. These need further examination, along with the effects of interaction of body vortices with fins and pure fin effects.

REFERENCES

1. Kuethe, A. M. and Schetzer, J. D., Foundations of Aerodynamics, 2nd Edition, John Wiley and Sons, Inc., New York, New York, 1961.
2. Shames, I. H., Mechanics of Fluids, McGraw-Hill Book Company, Inc., New York, New York, 1962.
3. Batchelor, G. K., An Introduction to Fluid Mechanics, Cambridge University Press, Great Britain, 1967.
4. Robins, B., New Principles of Gunnery, London, 1842.
5. Magnus, G., "On the Deflection of a Projectile," Poggendorffs Annalen der Physik und Chemie, Vol. 88, No. 1, 1853.
6. Rayleigh, Lord, "On the Irregular Flight of a Tennis Ball," Messenger of Math., Vol. 7, 1877, p. 14.
7. Flettner, A., "The Flettner Rotor Ship," Engineering, Vol. 19, January 23, 1925, pp. 117-120.
8. Betz, A., "Der Magnuseffekt, die Grundlage der Flettner-Walze," VDI, 1925, p. 9; English translation, NACA TM 310, 1925.
9. Prandtl, L., "Magnuseeffekt und Windkraftschiff," Die Neturwissenschaften, 1925, p. 93; English translation, NACA TM 367, 1926.
10. Buseman, A., "Messungen an Rotierenden Zylindern," Ergibnisse der Aerodynamik Versuchsanstalt zu Göttingen, IV Lieferung, 1932, p. 101.
11. Rizzo, R., "The Flettner Rotor Ship in the Light of the Kutta-Joubowski Theory and of Experimental Results," NACA TN 228, 1925.
12. Lafay, "Sur l'Inversion du Phénomène de Magnus," Comptes Rendus, Vol. 151, 1910.
13. Lafay, "Contribution Experimentale a l'Aerodynamique du Cylindre," Revues Mechanique, Vol. 30, 1912.
14. Thom, A., "The Aerodynamics of a Rotating Cylinder," Thesis, University of Glasgow, 1926.
15. Thom, A., "Experiments on the Air Forces on Rotating Cylinders," ARC R and M 1018, 1925.
16. Thom, A., "The Pressures Round a Cylinder Rotating in an Air Current," ARC R and M 1082, 1926.
17. Thom, A., "Experiments on the Flow Past a Rotating Cylinder," ARC R and M 1410, 1931.
18. Thom, A. and Sengupta, S. R., "Air Torque on a Cylinder Rotating in an Air Stream," ARC R and M 1520, 1932.
19. Thom, A., "Effects of Discs on the Air Forces on a Rotating Cylinder," ARC R and M 1623, 1934.
20. Van Aken, R. W. and Kelly, H. R., "The Magnus Force on Spinning Cylinders," NAVORD Report 5583, NOTS 1784, China Lake, California, June 1957.
21. Swanson, W. H., "The Magnus Effect: A Summary of Investigations to Date," J. Basic Engineering, September 1961, pp. 461-470.
22. Griffiths, R. T. and Ma, C. Y., "Differential Boundary-Layer Separation Effects in the Flow over a Rotating Cylinder," Aero. J. of RAS, Vol. 73, June 1969, pp. 524-526.
23. Nikitin, S. A., "Aerodynamic Characteristics of a Spinning Body of Revolution Situated at an Angle of Incidence in a Flow," (In Russian), Izvestiia, Seriia, Fizicheskikh: Tekhnicheskikh Nauk, No. 6, 1967, pp. 63-70.
24. Power, H. L. and Iversen, J. D., "Magnus Effect on Spinning Bodies of Revolution," AIAA Journal, Vol. 11, No. 4, April 1973, pp. 417-418.
25. Iversen, J. D., "Correlation of Magnus Force Data for Slender Spinning Cylinders," AIAA Paper No. 72-966, September 1972.
26. Fletcher, C. A. J., "Negative Magnus Forces in the Critical Reynolds Number Regime," Journal of Aircraft, Vol. 9, No. 12, December 1972, pp. 826-834.
27. Platou, A. S., "Magnus Characteristics of Finned and Nonfinned Projectiles," AIAA Journal, Vol. 3, No. 1, January 1965, pp. 83-90.
28. Regan, F. J., "Magnus Effects," in AGARD CP No. 10, The Fluid Dynamic Aspects of Ballistics, September 1966.
29. Renevier, J. P. and Giraud, M., "Contribution a l'etude experimentale de l'effect Magnus lere partie: Note de documentation," Institut Franco-Allemand de Recherches de Saint-Louis, Note De Documentation Bibliographische Notiz D2/67, 1967, N69-19541.
30. Murphy, C. H., "Free Flight Motion of Symmetric Missiles," BRL Report No. 1216, Aberdeen Proving Ground, Maryland, July 1963.
31. Nicolaides, J. D., "Missile Flight and Astrodynamics," TN 100, Bureau of Naval Weapons, Washington, D.C., 1961.
32. Platou, A. S., "The Influence of the Magnus Moment on the Dynamic Stability of a

Projectile," BRL Memorandum Report No. 2155, Aberdeen Proving Ground, Maryland, January 1972.
33. Martin, J. M., "An Experimental Correlation Between the Flow and Magnus Characteristics of a Spinning Ogive-Nose Cylinder," Ph.D. Dissertation, University of Notre Dame, Notre Dame, Indiana, August 1971.
34. Lando, D. W., "An Investigation to Control the Magnus Characteristics of Symmetrical Fin and Nonfin Bodies," Ph.D. Dissertation, University of Notre Dame, Notre Dame, Indiana, May 1972.
35. Ingram, C. W., Lusardi, R. J. and Nicolaides, J. D., "Effects of Rifling and N-Vanes on the Magnus Characteristics of Bodies of Revolution," AIAA Paper No. 72-970, September 1972.
36. Sturek, W. B., "Boundary Layer Studies on a Spinning Cone," BRL Report No. 1649, Aberdeen Proving Ground, Maryland, May 1973.
37. Sturek, W. B., "Boundary Layer Studies on a Spinning Cone," AIAA Paper No. 72-567, September 1972.
38. Sieron, T. R., "On the 'Magnus Effects' of an Inclined Spinning Shell at Subsonic and Transonic Speeds," WADD TR 50-212, Wright-Patterson Air Force Base, Ohio, April 1961.
39. Martin, J. C., "On Magnus Effects Caused by the Boundary Layer Displacement Thickness on Bodies of Revolution at Small Angles of Attack," BRL Report No. 870 (Revised), Aberdeen Proving Ground, Maryland, June 1955; also J. Aeronaut. Sci., June 1957.
40. Kelly, H. R. and Thacker, G. R., "The Effect of High Spin on the Magnus Force on a Cylinder at Small Angles of Attack," NAVORD Report 5036, NOTS 1381, China Lake, California, February 1956.
41. Sedney, R., "Laminar Boundary Layer on a Spinning Cone at Small Angles of Attack in a Supersonic Flow," J. Aeronaut. Sci., June 1957, pp. 430-436.
42. Feibig, M., "Laminar Boundary Layer on a Spinning Circular Cone in Supersonic Flow at Small Angles of Attack," OSR TN 56-532, Cornell University, Ithaca, New York, June 1956.
43. Jacobson, I. D., Vollmer, A., and Morton, J. B., "Calculation of the Velocity Profiles of the Incompressible Laminar Boundary Layer on a Yawed Spinning Cone and the Magnus Effect," RLES Report No. ESS-3318-104-73U, University of Virginia, Charlottesville, January 1973.
44. Vaughn, H. R. and Reis, G. E., "A Magnus Theory," AIAA Paper No. 73-124, January 1973.
45. Vaughn, H. R. and George, O. L., Jr., "The Characteristics of a Laminar Boundary Layer on a Spinning Tangent Ogive Cylinder at Angle of Attack," Sandia Laboratories Report SC-RR-71-0851, Albuquerque, New Mexico, March 1972.
46. Vaughn, H. R. and Reis, G. E., "A Magnus Theory for Bodies of Revolution," Sandia Laboratories Report SC-RR-72-0537, Albuquerque, New Mexico, January 1973.
47. Jacobson, I. D., "Influence of Boundary Layer Transition on the Magnus Effect," Ph.D. Dissertation, University of Virginia, Charlottesville, June 1970.
48. Jacobson, I. D. and Morton, J. B., "Boundary Layer Stability on a Yawed Spinning Body of Revolution and its Effect on the Magnus Force and Moment," NASA CR-2060, June 1972.
49. Jacobson, I. D. and Morton, J. B., "Final Report on BRL Contract DAAD05-72-C-0131," RLES Report No. ESS-3318-106-73U, University of Virginia, Charlottesville, January 1973.
50. Jacobson, I. D. and Morton, J. B., "Transition on a Spinning Cylinder," Unpublished report, University of Virginia, Charlottesville, 1973.
51. Tetervin, N., "Calculation of Magnus Forces on Axisymmetric Bodies at Small Angles of Attack with Incompressible Turbulent Boundary Layers," NOLTR 72-80, White Oak, Maryland, March 1972.
52. Krahn, E., "Negative Magnus Force," J. Aeronaut. Sci., April 1956, pp. 377-378.
53. Benton, E. R., "Supersonic Magnus Effect on a Finned Missile," AIAA Journal, Vol. 2, No. 1, January 1965, pp. 153-155.
54. Nicolaides, J. D. and MacAllister, L. C., "A Review of Aeroballistic Range Research on Winged and/or Finned Missiles," Ballistic TN No. 5, Bureau of Ordnance, Dept. of the Navy, Washington, D.C., 1955.
55. Chapman, D. R., Wimbrow, W. R., and Kester, R. H., "Experimental Investigation of Base Pressure on Blunt-Trailing-Edge Wings at Supersonic Velocities," NACA TN 2611, January 1952.
56. Benton, E. R., "Wing-Tail Interference as a Cause of 'Magnus' Effects on a Finned Missile," J. Aeronaut. Sci., November 1962, pp. 1358-1367.
57. Uselton, J. C. and Carman, J. B., "A Study of the Magnus Effects on a Sounding Rocket at Supersonic Speeds," AIAA Paper No. 70-207, January 1970.
58. Thompson, K. D. and Morrison, D. F., "On the Asymmetric Shedding of Vortices from Slender Cylindrical Bodies at Large Angles of Yaw," TN HSA 106, Weapons Research Establishment, Salisbury, South Australia, May 1965.
59. Oberkampt, W. L. and Nicolaides, J. D., "Aerodynamics of Finned Missiles at High Angle of Attack," AIAA Paper No. 71-50, January 1971.
60. Kuhn, G. D., Spangler, S. B., and Nielson, J. N., "Theoretical Study of Vortex Shedding from Bodies of Revolution Undergoing Coning Motion," AIAA Paper No. 70-72, January 1960; also NASA CR-1448, October 1969.
61. Platou, A. S., Colburn, R., and Pedgoray, J. S., "The Design and Dynamic Balancing of Spinning Models and a Testing Technique for Obtaining Magnus Data in Wind Tunnels," BRL Memorandum Report No. 2019, Aberdeen Proving Ground, Maryland, October 1969.
62. Regan, F. J. and Horanoff, E. V., "Wind-Tunnel Magnus Measurements at the Naval Ordnance Laboratory," AIAA Journal, Vol. 5, No. 6, June 1967, pp. 1193-1194.

63. Platou, A. S., "The Influence of Wind Tunnel Flow Distribution and Turbulence on the Measurement of Magnus Forces," BRL Memorandum Report No. 1969, April 1969.
64. Platou, A. S., "Wind Tunnel Magnus Testing of a Canted Fin or Self-Rotating Configuration," AIAA Journal, Vol. 10, No. 7, June 1972, pp. 965-967.
65. Eikenberry, R. S., "Analysis of the Angular Motion of Missiles," Sandia Laboratories Report SC-CR-70-6051, Albuquerque, New Mexico, February 1970.
66. Knadler, C. E., Jr., "A Wind Tunnel Free-Flight Data-Reduction Program for Either Spinning or Nonspinning Models Utilizing Data from a Single Plane," NOLTR 68-87, White Oak, Maryland, June 1968.
67. Chapman, G. T. and Kirk, D. B., "A New Method for Extracting Aerodynamic Coefficients from Free Flight Data," AIAA Journal, Vol. 8, No. 4, April 1970, pp. 753-758.
68. Ragunath, B. S., "Error Analysis in the Evaluation of Aerodynamic Derivatives from the University of Virginia Wind-Tunnel Cold Magnetic Balance System," Ph.D. Dissertation, University of Virginia, Charlottesville, 1971.
69. Jacobson, I. D., Junkins, J. L., and Jancaitis, J. J., "Data Acquisition and Reduction for the UVA Superconducting Magnetic Suspension and Balance Facility," Second International Symposium on Electro-Magnetic Suspension, University of Southampton, Southampton, England, July 1971, pp. K1-K14.
70. Nicolaides, J. D. and Brady, J. D., "Magnus Moment of Pure Cones in Supersonic Flight," NAVORD Report 6183, White Oak, Maryland, 1959.
71. Curry, W. H., Reed, J. F., and Ragsdale, W. C., "Magnus Data on the Standard 10° Cone Calibration Model," Sandia Laboratories Report SC-DC-71-3821, Albuquerque, New Mexico, March 1971.
72. Platou, A. S., "The Magnus Force on a Short Body of Supersonic Speeds," BRL Report No. 1062, Aberdeen Proving Ground, Maryland, January 1959.
73. Greene, J. E., "Static Stability and Magnus Characteristics of the 5-Caliber and 7-Caliber Army-Navy Spinner Rocket at Low Subsonic Speeds," NAVORD Report 3884, White Oak, Maryland, December 1954.
74. Greene, J. E., "A Summary of Experimental Magnus Characteristics of a 7- and 5-Caliber Body of Revolution at Subsonic Through Supersonic Speeds," NAVORD Report 6110, White Oak, Maryland, August 1958.
75. Luchuk, W. and Sparks, W., "Wind Tunnel Magnus Characteristics of the 7-Caliber Army-Navy Spinner Rocket," NAVORD Report 3813, White Oak, Maryland, September 1954.
76. Holmes, J. E., Regan, F. J., and Falusi, M. E., "Supersonic Wind Tunnel Magnus Measurements of the 7-, 8-, 9-, and 10-Caliber Army-Navy Spinner Projectile," NOLTR 68-172, White Oak, Maryland, October 1968.
77. Fletcher, C. A. J., "Investigation of the Magnus Characteristics of a Spinning Inclined Ogive-Cylinder Body at M = 0.2," TN HSA 159, Weapons Research Establishment, Salisbury, South Australia, October 1969.
78. Uselton, J. C., "Aerodynamic Characteristics of a High Fineness Ratio Model with Various Spin Rates at M_∞ = 3 and 5," AEDC-TR-66-171, Arnold Air Force Station, Tennessee, September 1966.
79. Luchuk, W., "The Dependence of the Magnus Force and Moment on the Nose Shape of Cylindrical Bodies of Fineness Ratio 5 at a Mach No. of 1.75," NAVORD Report 4425, White Oak, Maryland, April 1957.
80. Platou, A. S. and Nielson, G. I. T., "Some Aerodynamic Characteristics of the Artillery Projectile XM549," BRL Report No. 2284, Aberdeen Proving Ground, Maryland, April 1973.
81. Regan, F. J. and Schermerhorn, V. L., "The Effect of Base Bleed on the Drag and Magnus Characteristics of a Rotating Body of Revolution," NOLTR 72-204, White Oak, Maryland, August 1972.
82. Sylvester, M. A. and Braun, W. F., "The Influence of Helecal Serrations and Bullet Engraving on the Aerodynamic and Stability Properties of a Body of Revolution with Spin," AIAA Paper No. 70-557, May 1970.
83. MacAllister, L. C., Oskay, V., Reiter, B. J., Klein, R., and Gazdayka, W., "The Effect of a Subcaliber Cylindrical Afterbody on the Behavior of Spin-Stabilized Projectiles," AIAA Paper No. 70-558, May 1970.
84. Platou, A. S. and Sternberg, J., "The Magnus Characteristics of a 30-mm Aircraft Bullet," BRL Report No. 994, Aberdeen Proving Ground, Maryland, September 1959.
85. Sieron, T. R., "The Magnus Characteristics of the 20-mm and 30-mm Projectiles in the Transonic Range," WADC TN 59-320, October 1959.
86. Chadwick, W. R., "Dynamic Stability of a 5-in. Projectile with Nonlinear Magnus Moment," J. of Spacecraft, Vol. 4, No. 9, September 1967, pp. 1263-1265.
87. Donovan, W. F. and MacAllister, L. C., "Transonic Range Tests of 5-inch/54 Rocket-Assisted Projectile (Inert)," BRL Memorandum Report No. 2107, Aberdeen Proving Ground, Maryland, July 1971.
88. Kline, R. W. and Gazdayka, W., "Aerodynamic Characteristics and Sucsonic Flight Performance of the Spin-Stabilized 4.2 Inch M329A1E1 Mortar Projectile," Picatinny Arsenal Report PA-TR-4300, Dover, New Jersey, June 1972.
89. Kline, R. W., "Subsonic Aerodynamic Stabilization of Long, Low Drag Bodies of Revolution Using Boattail Fins," Picatinny Arsenal Report TA-TR-4307, Dover, New Jersey, June 1972.
90. Murphy, C. H., "Effect of Roll on Dynamic Stability of Symmetric Missiles," J. Aeronaut. Sci., Vol. 21, No. 9, September 1954.
91. Piddington, M., "The Effects of Magnus Moment at Subsonic Velocities in the 105-mm Mortar Projectile T-53," BRL Memorandum Report No. 1354, Aberdeen Proving Ground, Maryland, June 1961.
92. Platou, A. S., "The Magnus Force on a Finned Body," BRL Report No. 1193, Aberdeen Proving Ground, Maryland, March 1963.
93. Curry, W. H. and Reed, J. F., "Measurements of Magnus Effects on a Sounding Rocket Model in a Supersonic Wind Tunnel," AIAA Paper No. 66-754, September 1966.

94. Gowen, F. E., "Buffeting of a Vertical Tail on an Inclined Body at Supersonic Mach Numbers," NACA RM A53A09, March 1953.
95. Cooper, M., Gapcimski, J. P., and Hasel, L. E., "A Pressure-Distribution Investigation of a Fineness-Ratio-12.2 Parabolic Body of Revolution (NACA RM-10) at M = 1.59 and Angles of Attack up to 36°," NACA TM L52G14a, October 1952.
96. Stone, G. W., "The Magnus Instability of a Sounding Rocket," AIAA Paper No. 66-62, January 1966.
97. Regan, E. J., Shannon, J. H., and Tanner, F. J., "Wind Tunnel and Computer Studies of a Low Drag Bomb with Various Tail Stabilizers," AGARD CP No. 10, September 1966, pp. 292-317.
98. Regan, F. J., "Magnus Measurements on a Freely Spinning Stabilizer," AIAA Paper No. 70-559, May 1970.
99. Regan, F. J. and Falusi, M. E., "The Static and Magnus Aerodynamic Characteristics of the M823 Research Store Equipped with Fixed and Freely Spinning Stabilizers," NOLTR 72-291, White Oak, Maryland, December 1972.
100. Sears, E. S., "A Method for Eliminating the Magnus Instability of a Finned Missile," AFATL TR 71-149, November 1971.
101. Nicolaides, J. D., "Theory of Flight for Magnus Rotors," Unpublished report, University of Notre Dame, Notre Dame, Indiana, 1966.
102. Iversen, J. D., "The Magnus Rotor as an Aerodynamic Decelerator," AIAA Paper No. 68-962, September 1968.
103. Flatau, A., "An Investigation of the Rotational and Aerodynamic Characteristics of High Aspect Ratio Rotors," CRDL TM 1-4, Edgewood Arsenal, Maryland, September 1964.
104. Zipfel, P. H., "On Flight Dynamics of Magnus Rotors," Tech Report 117, Dept. of the Army, Fredrick, Maryland, November 1970.
105. Anon., "Wind Tunnel Testing of Self Dispersing Shapes," Final Report, Phase III, Contract No. DA18-064-AMC-325(A), AVCO Corporation, Missile Systems Division, Wilmington, Massachusetts, April 1966.
106. Barkla, H. M. and Auchterlonie, L. J., "The Magnus Effect on Rotating Spheres," J. Fluid Mech., Vol. 47, 1971, pp. 437-447.
107. Bird, J. D. and Llewellyn, C. P., "An Analysis of the Stability of Spinning Disks During Atmospheric Reentry," NASA TM X-248, March 1960.
108. Stilley, G. D. and Carstens, D. L., "Adaptation of the Frisbee Flight Principle to Delivery of Special Ordnance," AIAA Paper No. 72-982, September 1972.

ACKNOWLEDGMENTS

The author wishes to thank Dr. J. B. Morton for his many useful discussions and Mrs. A. Symmers for her help in preparing the manuscript.

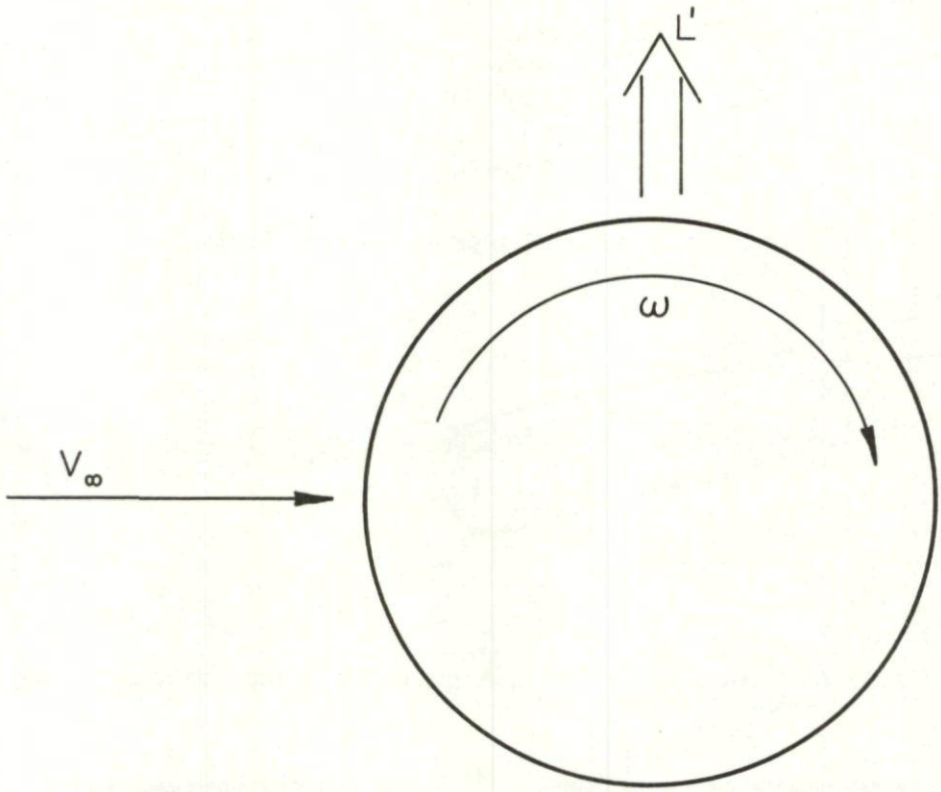

FIGURE 1. CLASSICAL MAGNUS EFFECT

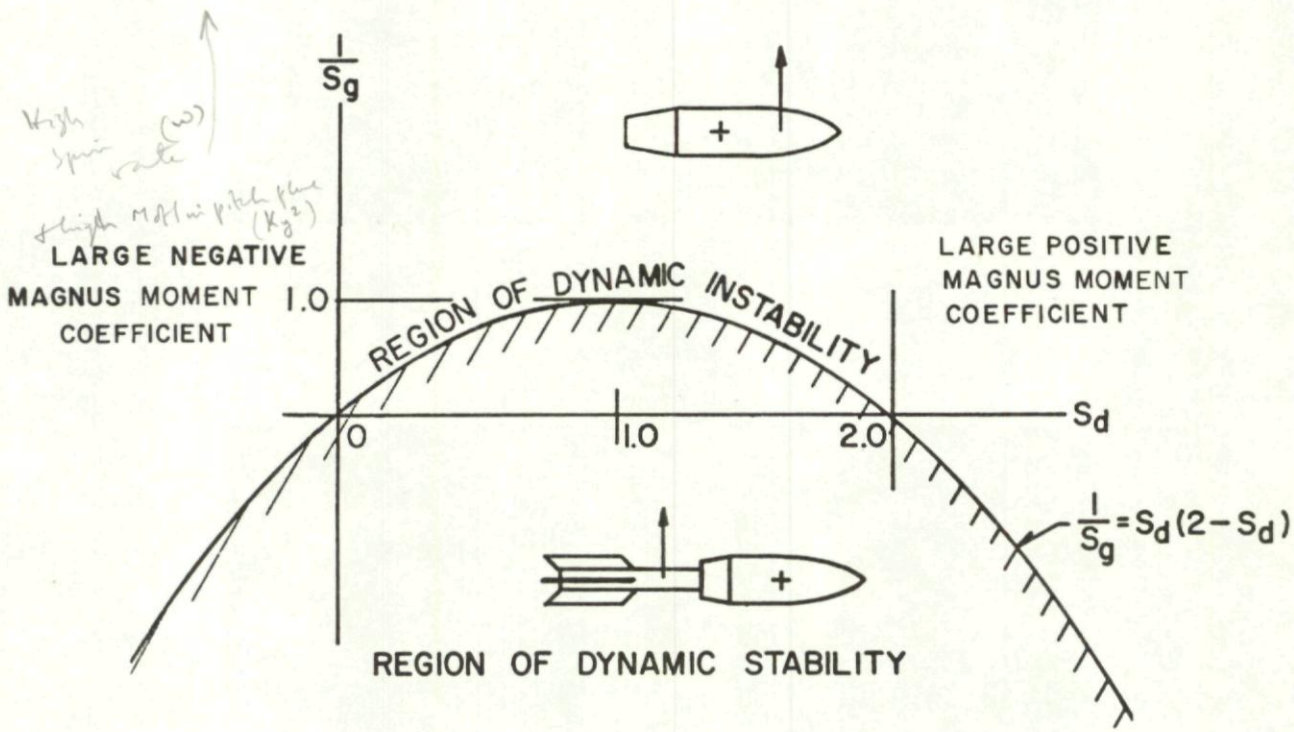

FIGURE 2. DYNAMIC STABILITY OF A PROJECTILE
(from reference 31)

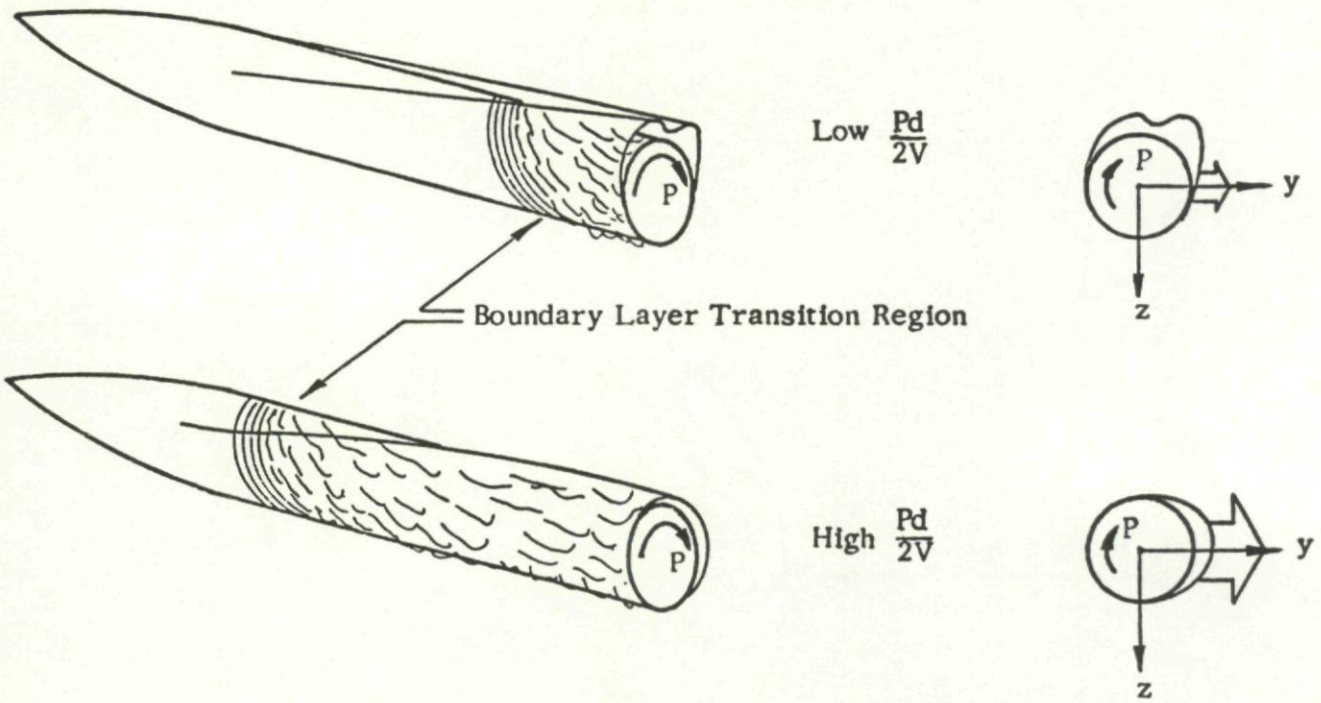

FIGURE 3. LOW ANGLE OF ATTACK FLOW CHARACTERISTICS FOR A CLEAN BODY (from reference 34)

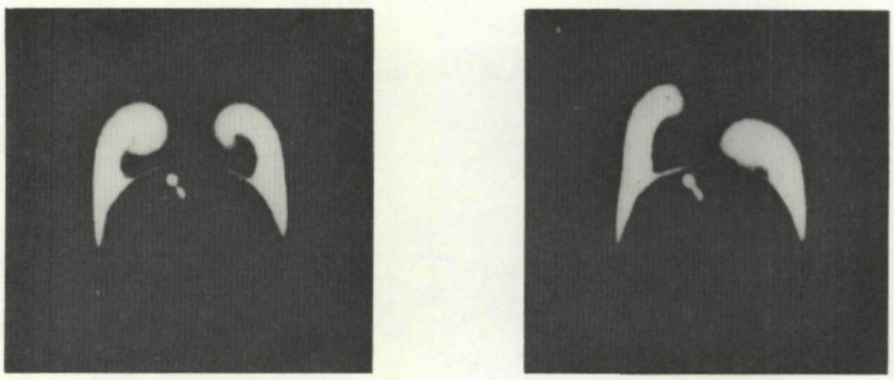

A) Zero Pd/2V

B) Low Pd/2V

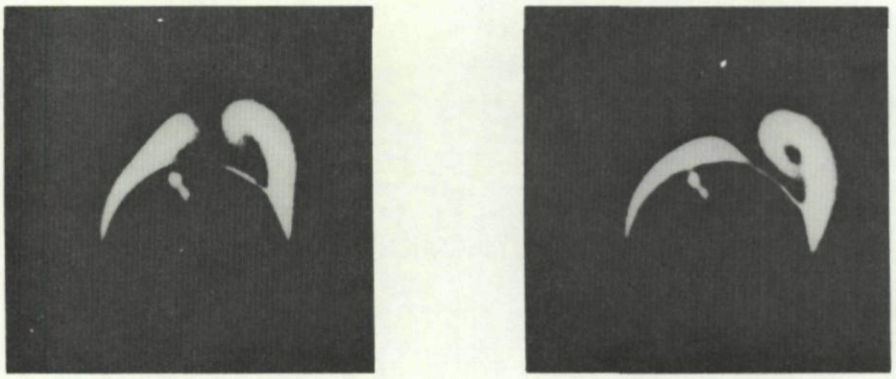

C) Moderate Pd/2V

D) High Pd/2V

FIGURE 4. QUALITATIVE SMOKE FLOW PHOTOGRAPHS ALONG MODEL AXIS $\alpha = 20^{o}$, $V_{\infty} = 60$ FT/SEC., P = CLOCKWISE, NO VANES (from reference 34)

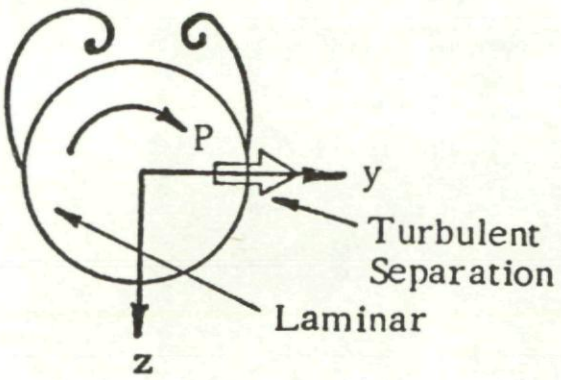

Low Pd/2V

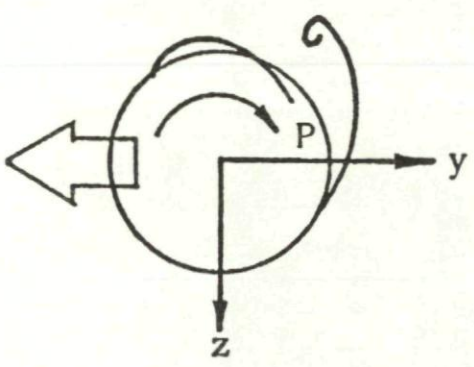

High Pd/2V

FIGURE 5. LARGE ANGLE OF ATTACK VORTEX PATTERNS (from reference 33)

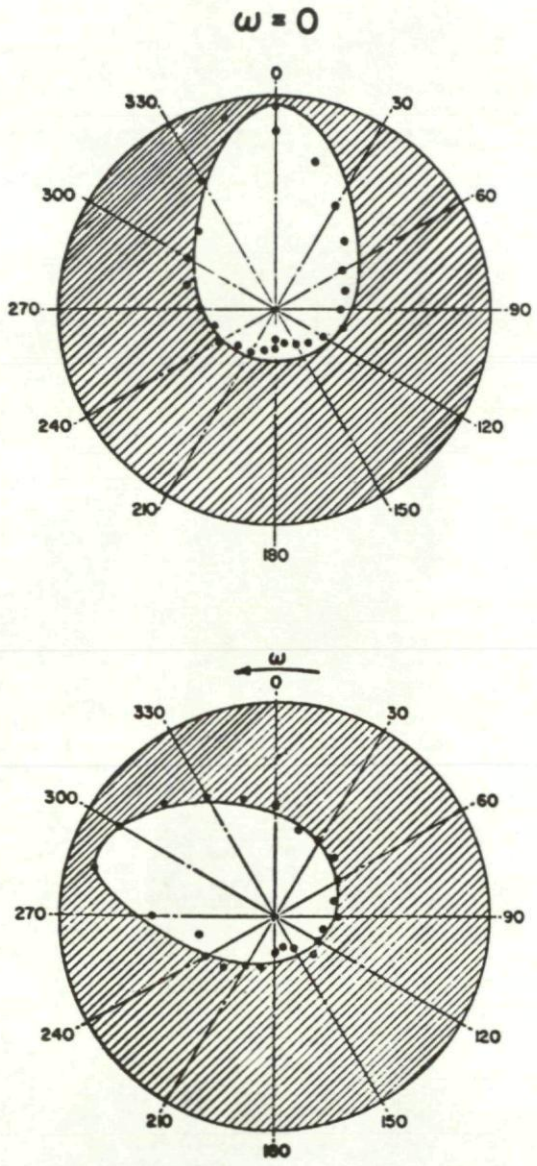

FIGURE 6. PROFILE OF BOUNDARY LAYER TRANSITION ABOUT CIRCUMFERENCE OF 10^{0} CONE, $M_{\infty} = 2$, $\alpha = 4^{0}$, $\omega = 30{,}000$ RPM, $Re_{L} = 5.97 \times 10^{6}$ (from reference 36)

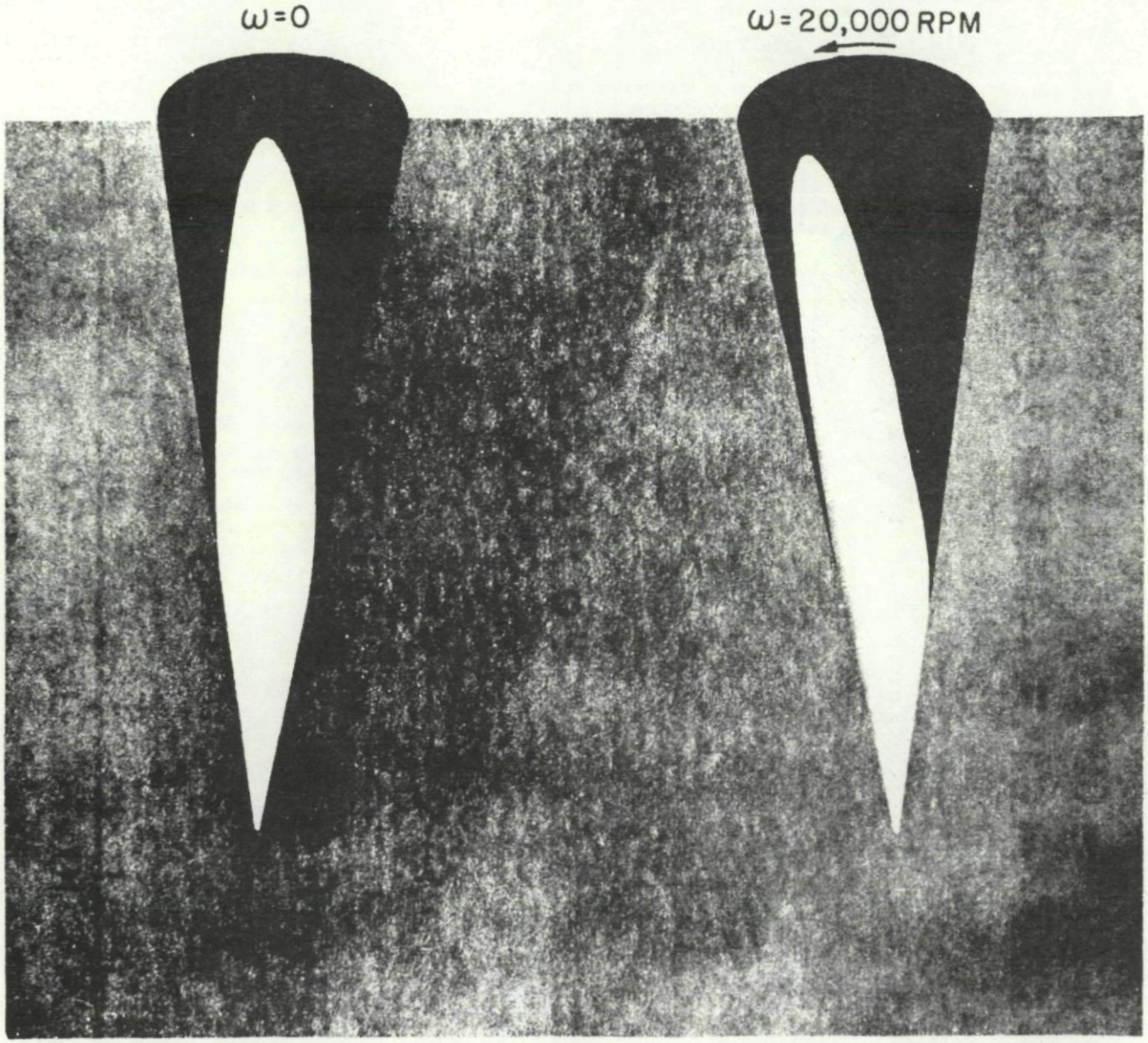

FIGURE 7. CONE MODELS PAINTED TO REVEAL REGIONS OF LAMINAR (WHITE) AND TURBULENT (BLACK) BOUNDARY LAYER, $M_\infty = 2$, $\alpha = 4^o$, $Re_L = 5.97 \times 10^6$
(from reference 36)

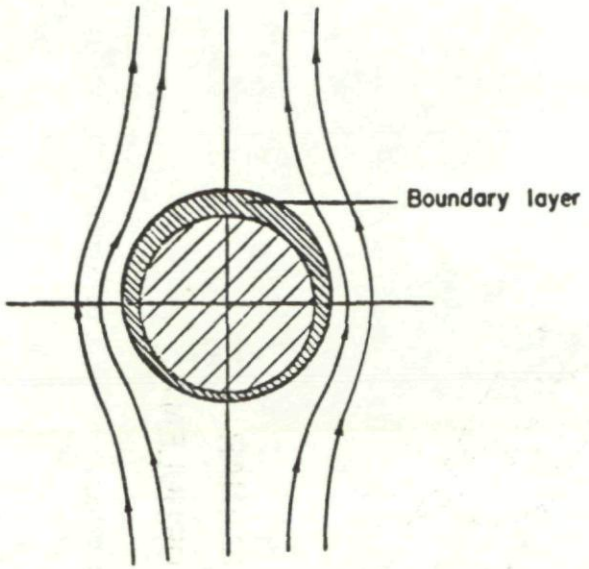

(a) Boundary layer on a cross section of a non-spinning body.

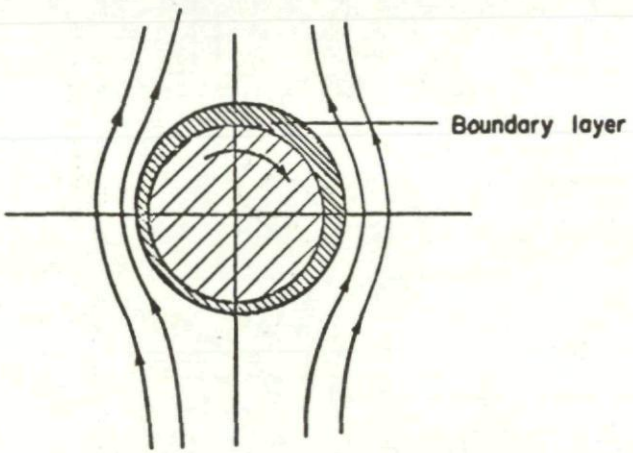

(b) Boundary layer on a cross section of a spinning body.

FIGURE 8. EFFECT OF SPIN ON BOUNDARY LAYER DISPLACEMENT THICKNESS (from reference 39)

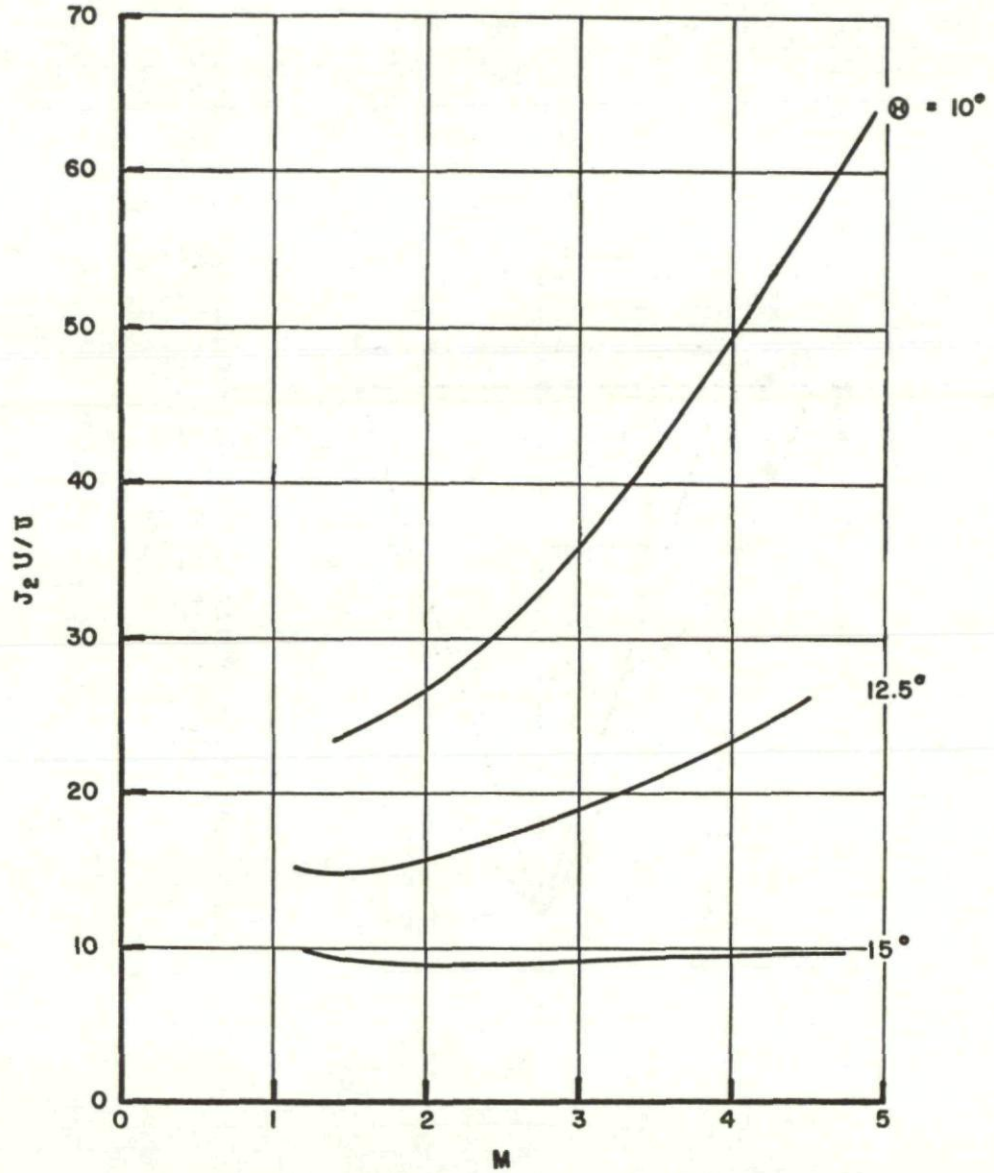

FIGURE 9. CONTRIBUTION OF INTERACTION TERM TO DISPLACEMENT THICKNESS (from reference 41)

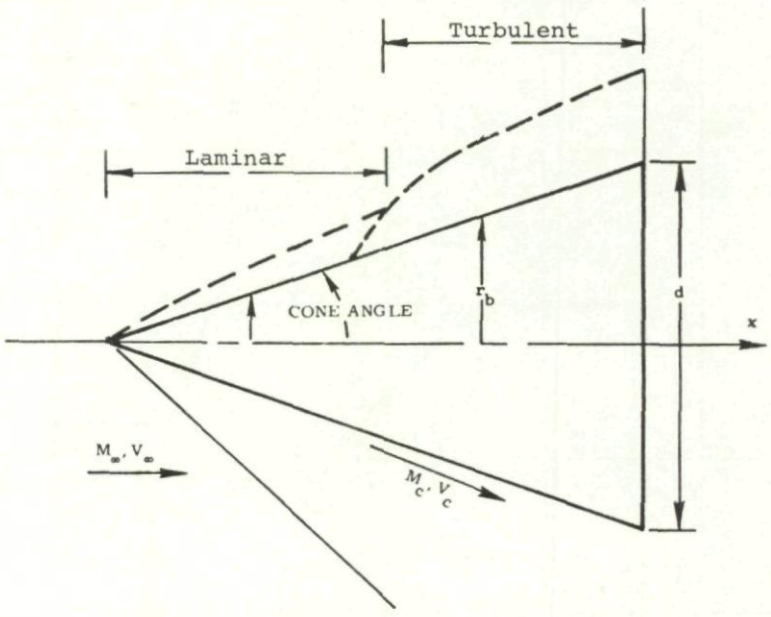

FIGURE 10. CONE BOUNDARY LAYER GEOMETRY
(from reference 46)

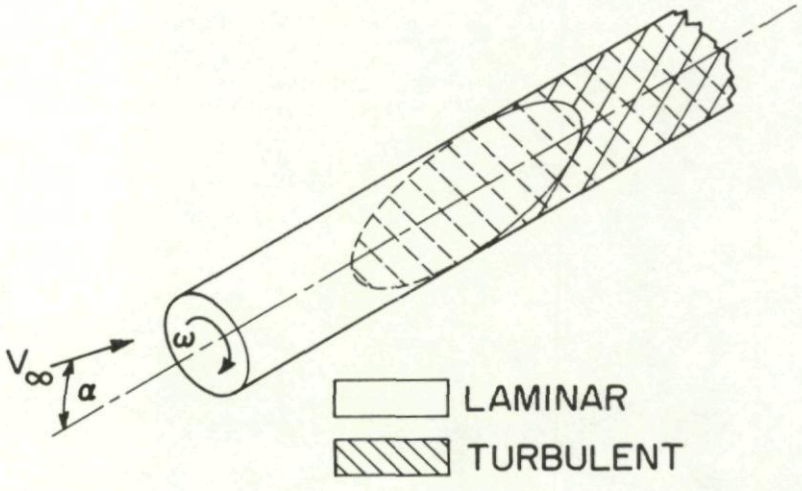

FIGURE 11. ASYMMETRIC BOUNDARY LAYER TRANSITION ON A CYLINDER
(from reference 48)

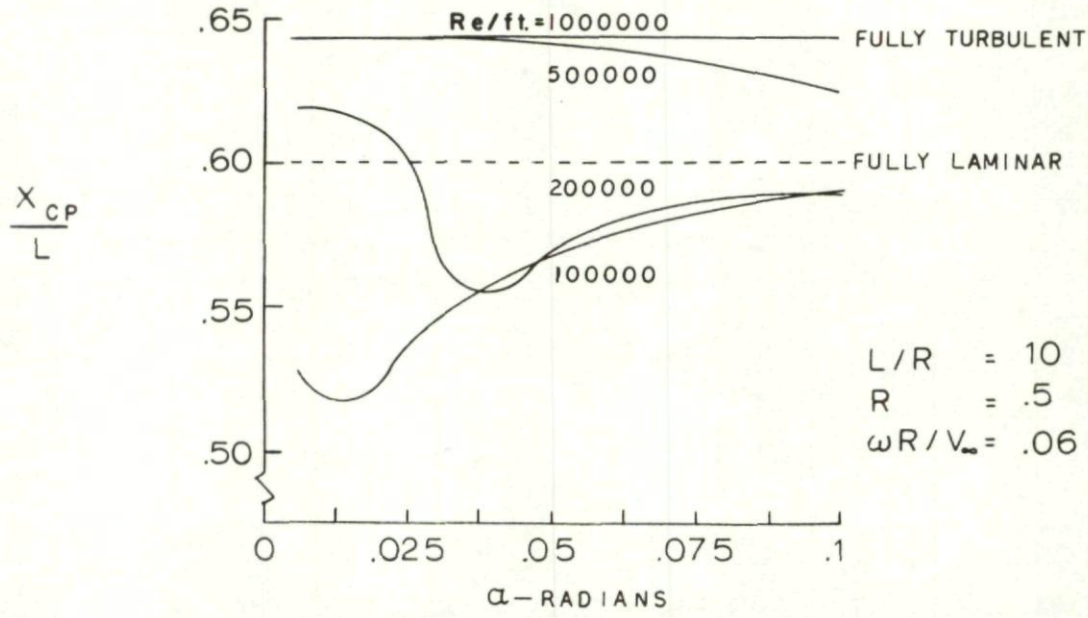

FIGURE 12. MAGNUS CENTER OF PRESSURE LOCATION (MEASURED FROM NOSE) VS. ANGLE OF ATTACK ($Re_{transition}$ = 200,000) (from reference 48)

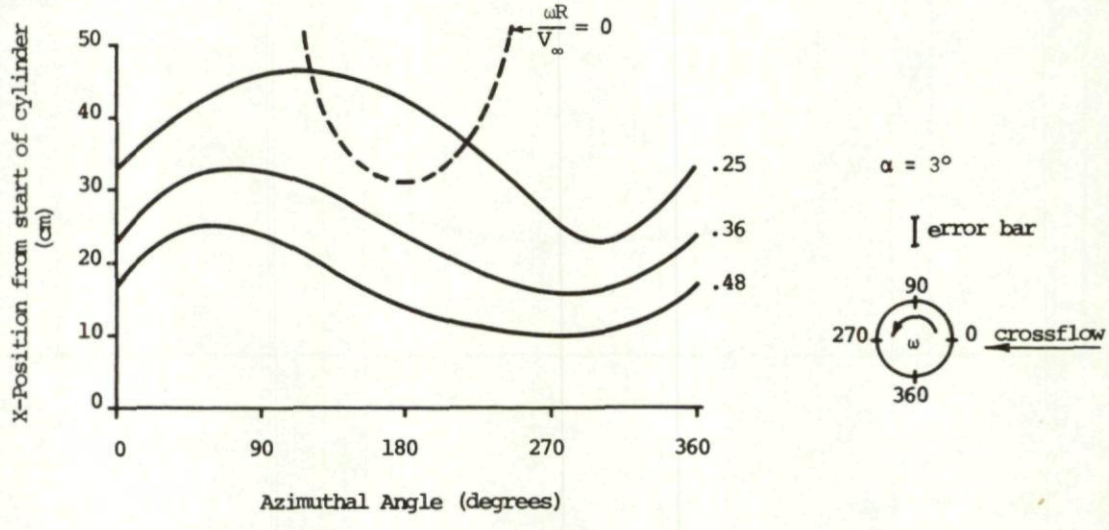

FIGURE 13. AZIMUTHAL VARIATION OF TRANSITION LINE ON A CIRCULAR CYLINDER (from reference 50)

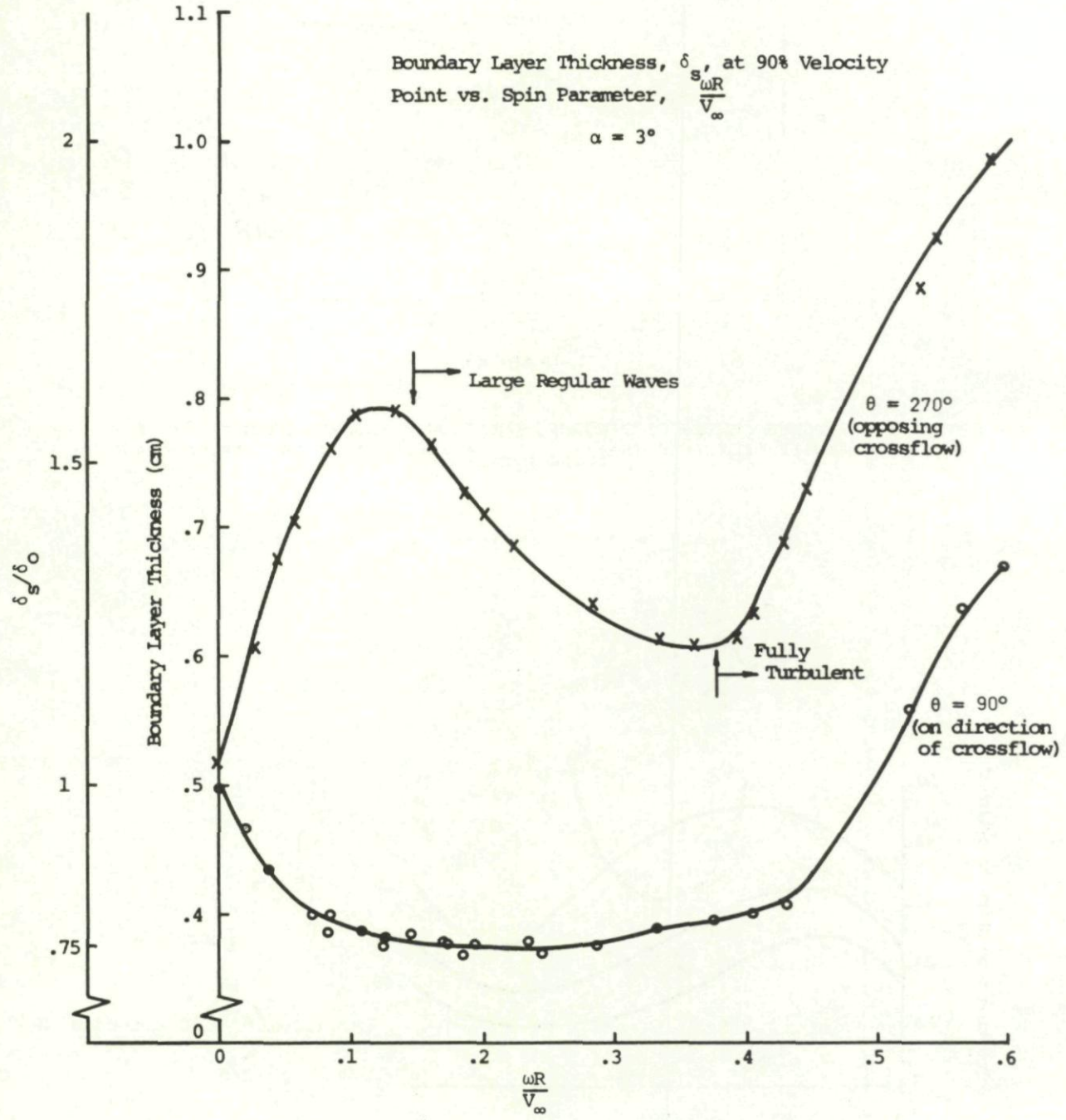

FIGURE 14. EFFECT OF SPIN RATE ON BOUNDARY LAYER THICKNESS (from reference 50)

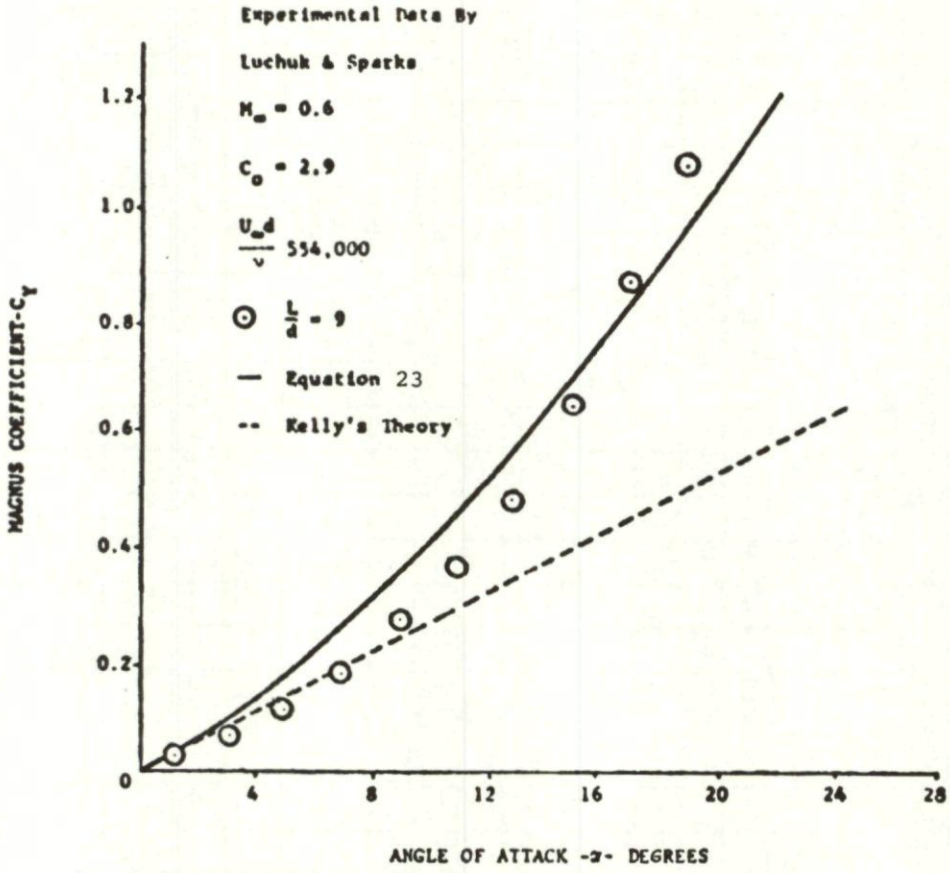

FIGURE 15. SIDE FORCE COEFFICIENT COMPARISON, M_∞ = 0.6 (from reference 24)

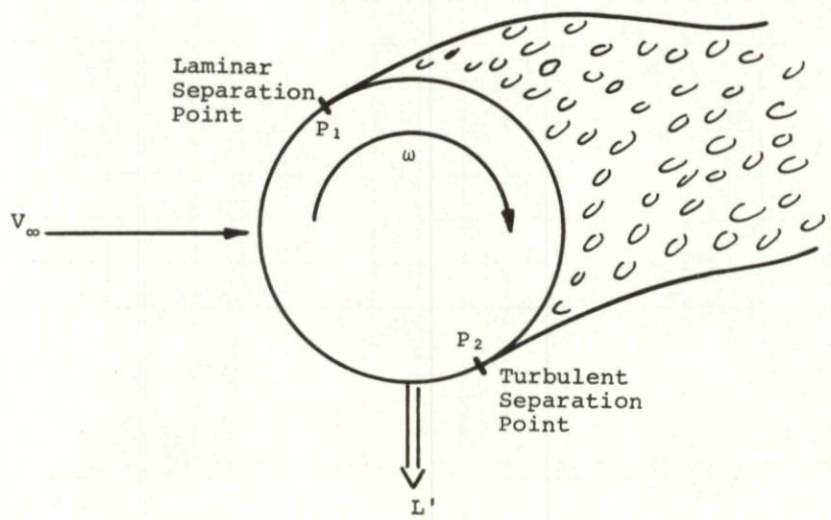

FIGURE 16. EFFECT OF ROTATION ON SEPARATION FOR TWO DIMENSIONAL CYLINDER IN CRITICAL REYNOLDS NUMBER RANGE

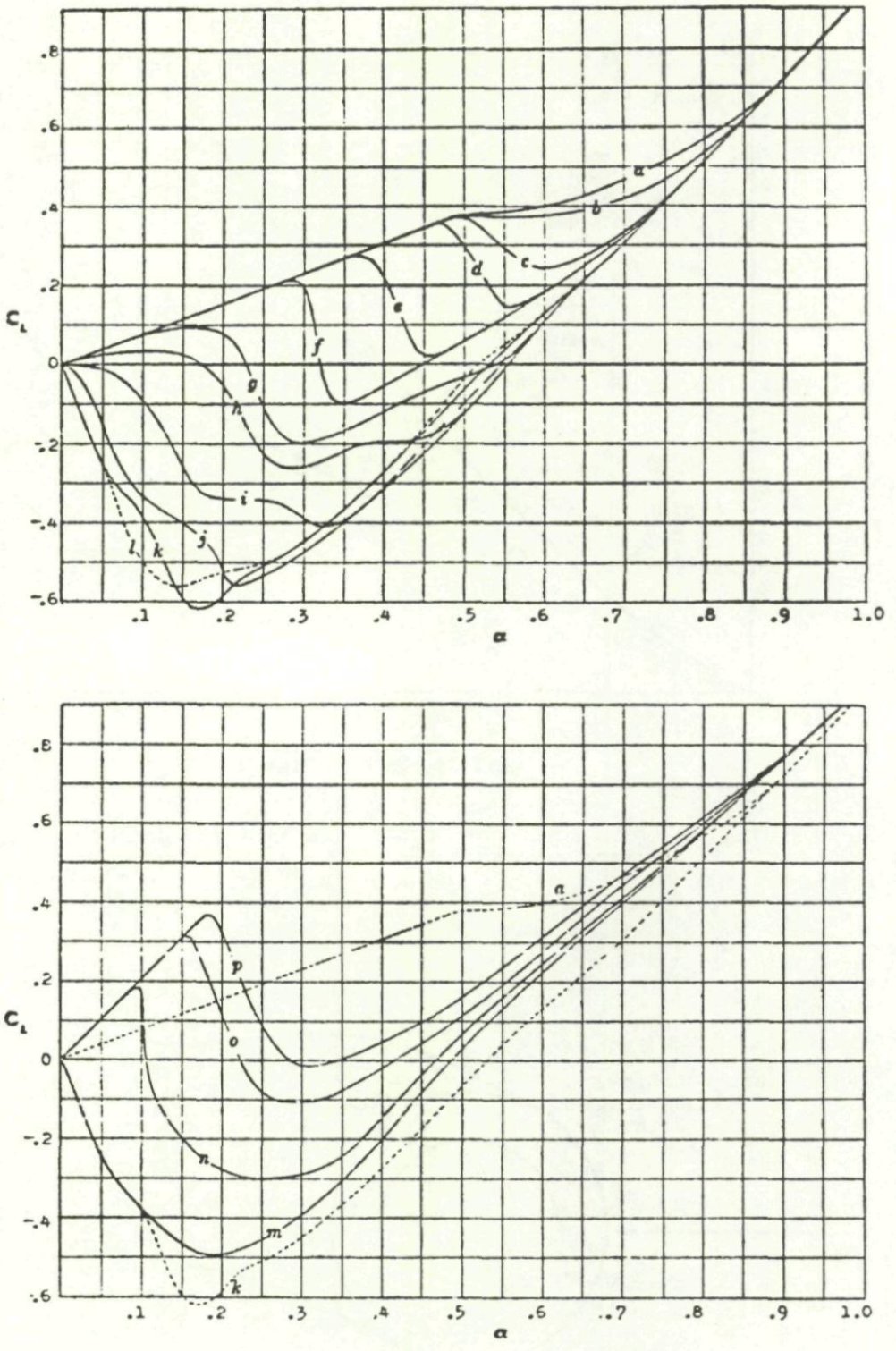

Curve Designation	Reynolds No.	Curve Designation	Reynolds No.
a	3.58×10^4	i	22.5×10^4
b	4.9	j	26
c	6.07	k	29.5
d	7.91	l	32.5
e	9.9	m	36.5
f	12.8	n	42
g	15.2	o	45
h	18.15	p	50.1

FIGURE 17. LIFT COEFFICIENT C_L VERSUS VELOCITY RATIO α (from ref. 21)

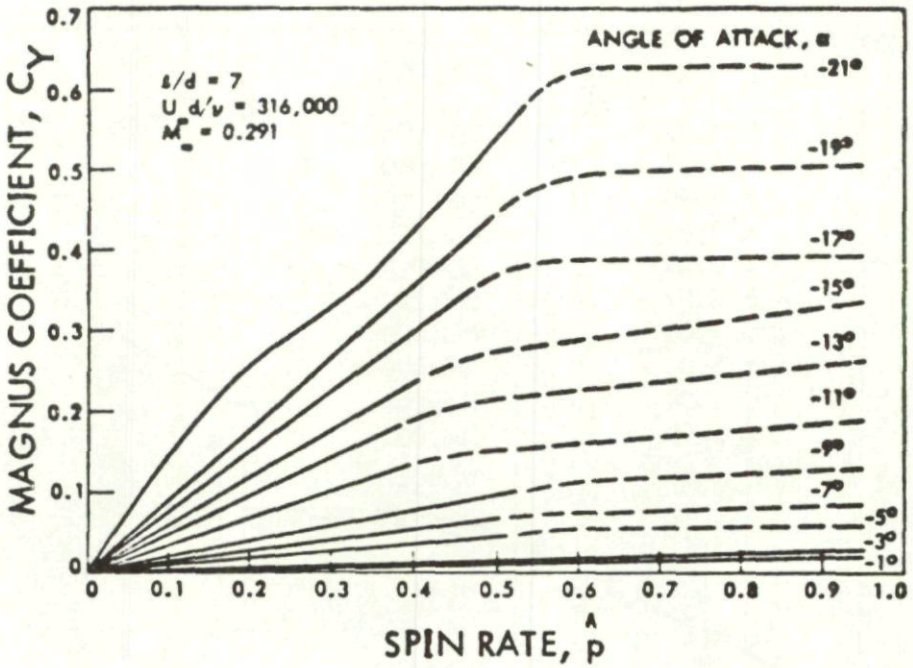

Side force coefficient vs spin rate

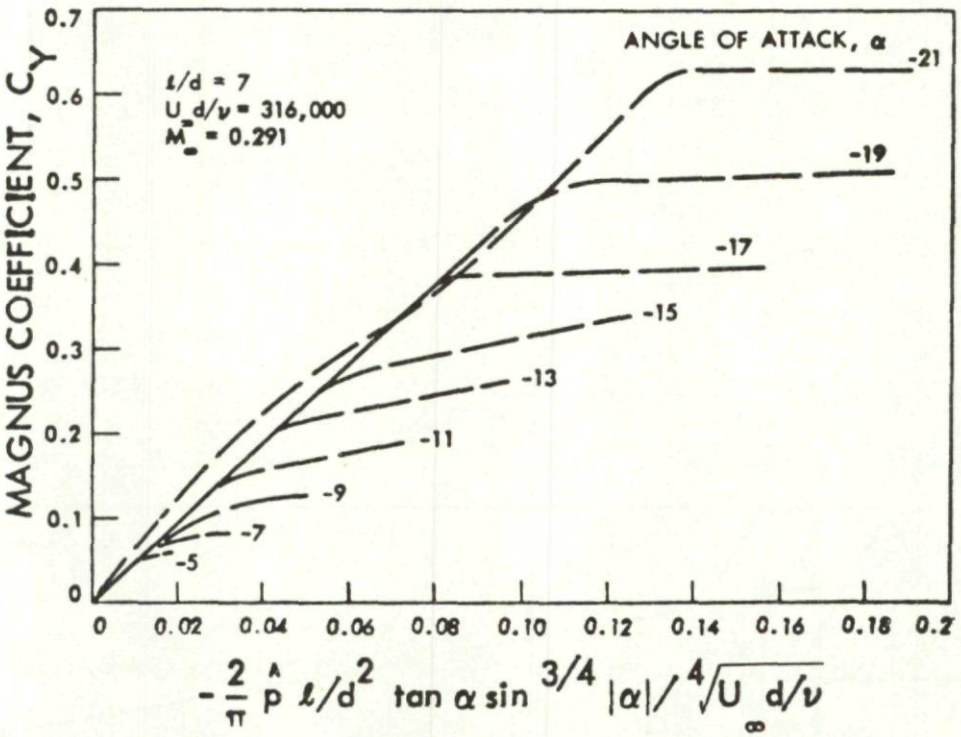

Side force coefficient vs product of spin rate and cross-flow analogy parameter

FIGURE 18. CORRELATION OF MAGNUS FORCE COEFFICIENT VS. CROSSFLOW ANALOGY PARAMETER
(from reference 25)

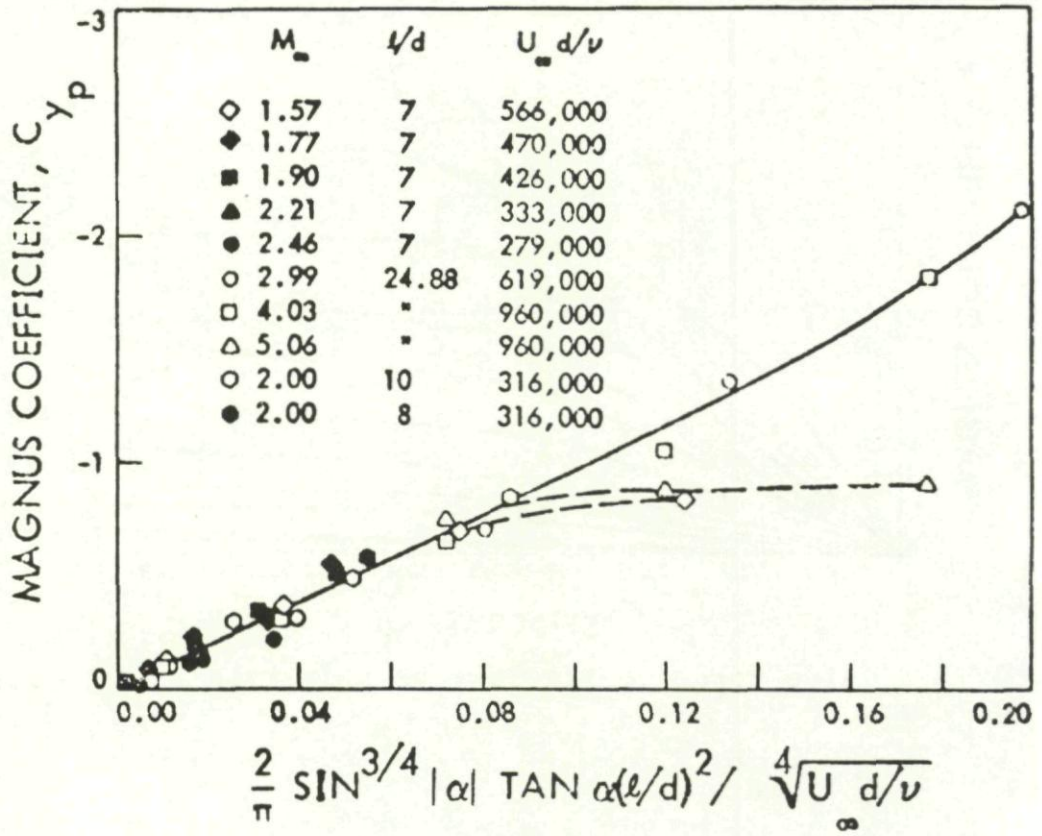

FIGURE 19. MAGNUS FORCE COEFFICIENT VS. CROSSFLOW ANALOGY PARAMETERS (from reference 25)

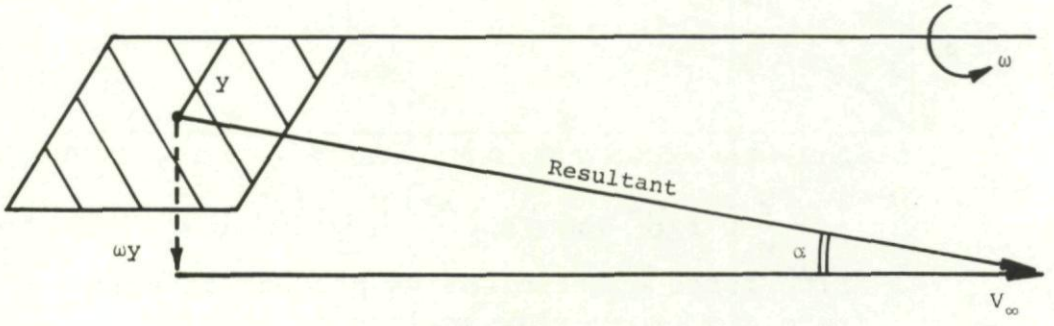

FIGURE 20. INDUCED ROLL ANGLE

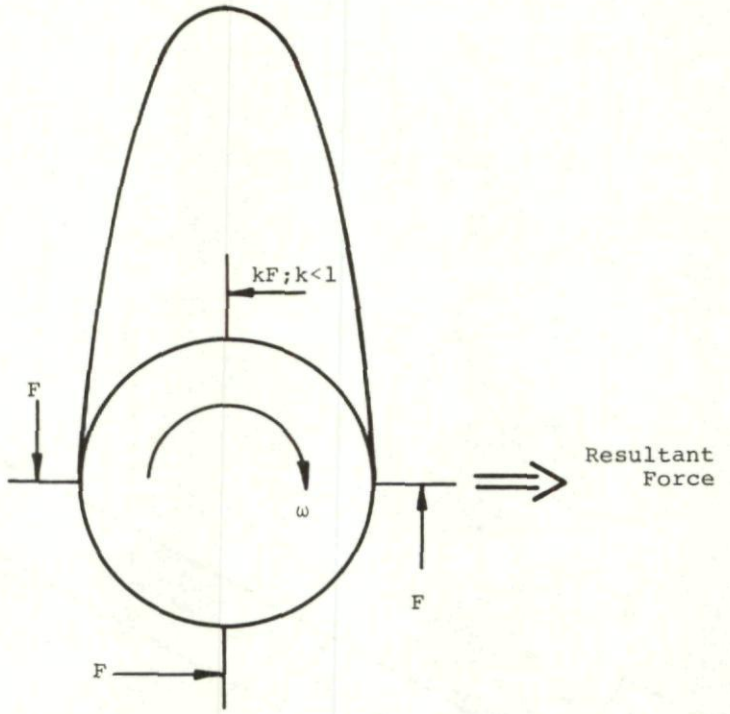

FIGURE 21. LEEWARD FIN BLOCKAGE

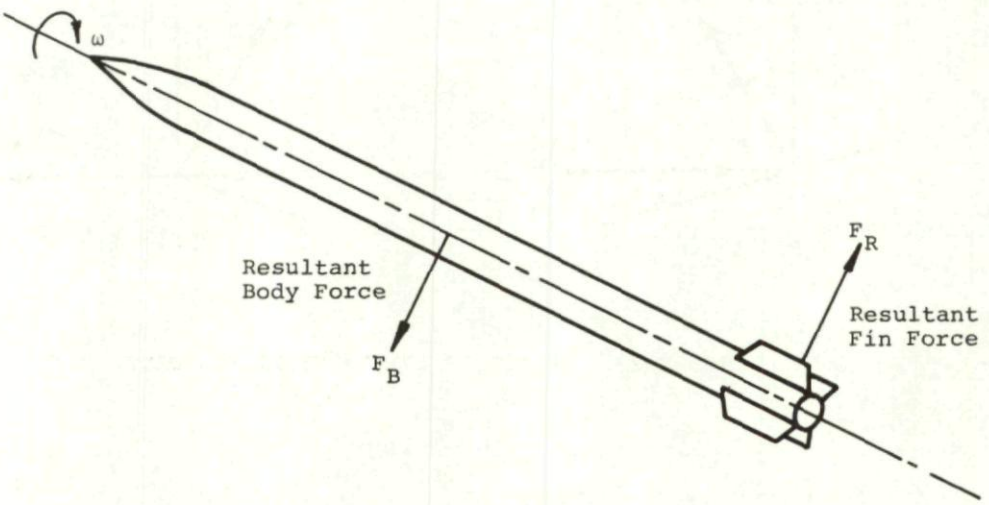

FIGURE 22. RESULTANT BODY AND FIN MAGNUS FORCES

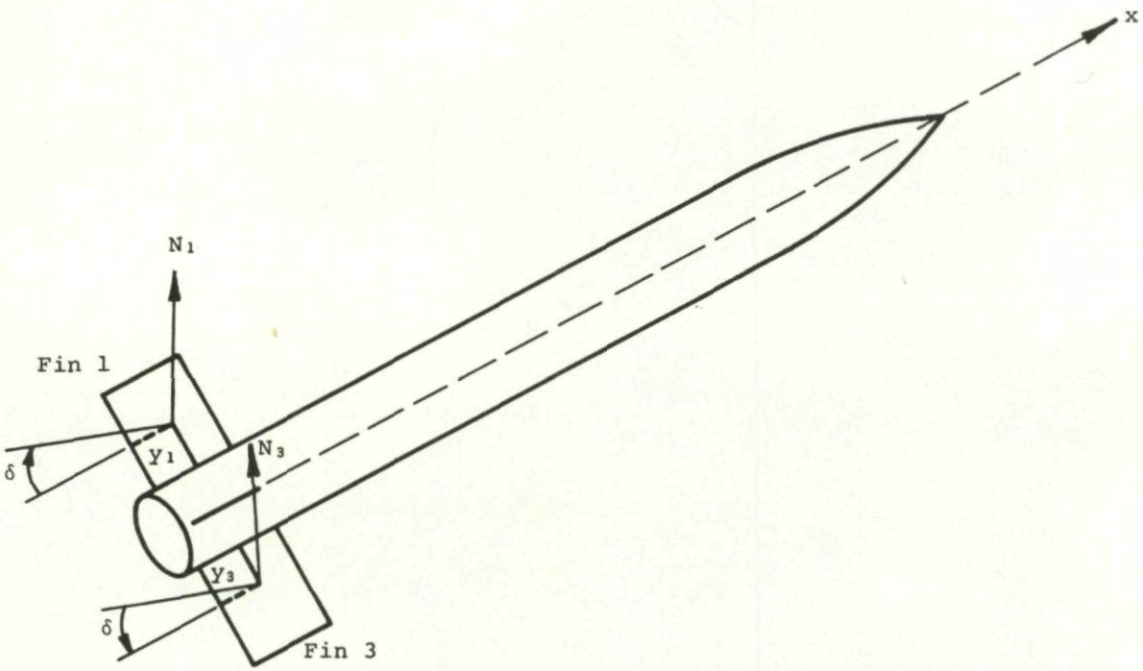

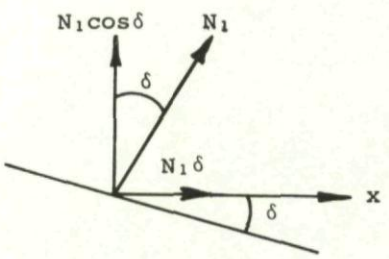

Fin 1

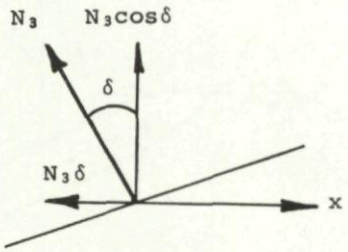

Fin 3

FIGURE 23. EFFECT OF DIFFERENTIAL FIN CANT

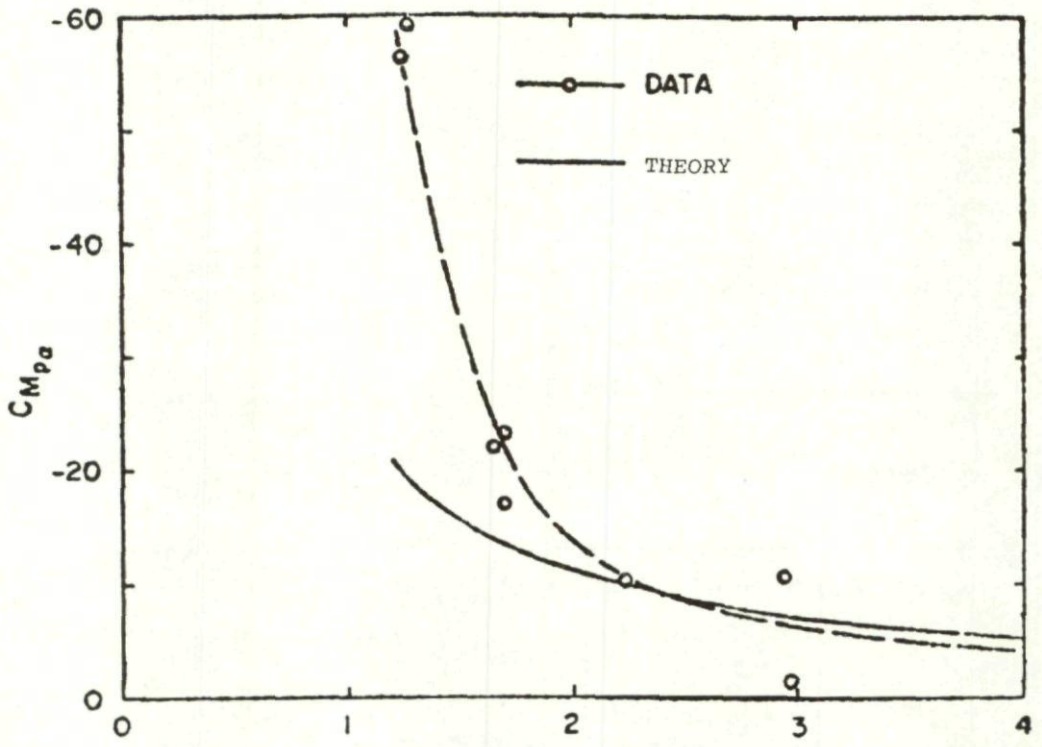

FIGURE 24. MAGNUS MOMENT COEFFICIENT DERIVATIVE AS A FUNCTION OF MACH NUMBER (from reference 53)

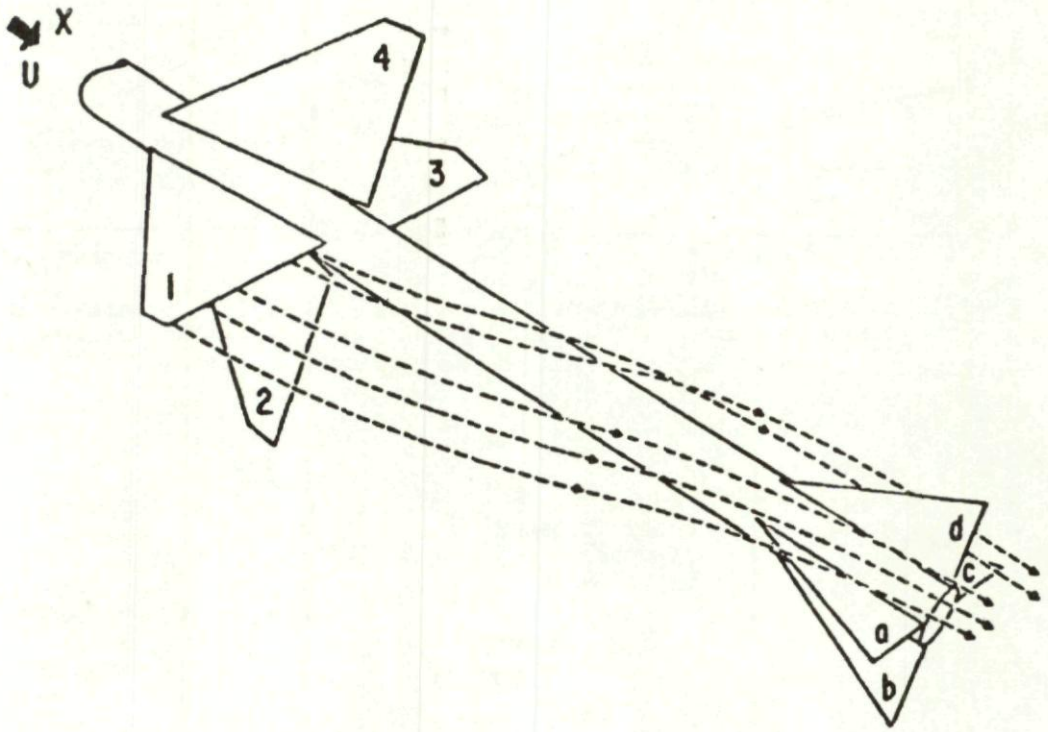

FIGURE 25. SCHEMATIC OF SWIRLING VORTEX LINES BEHIND WING PANEL 1 WHEN $\alpha = \omega = 0$ (from reference 56)

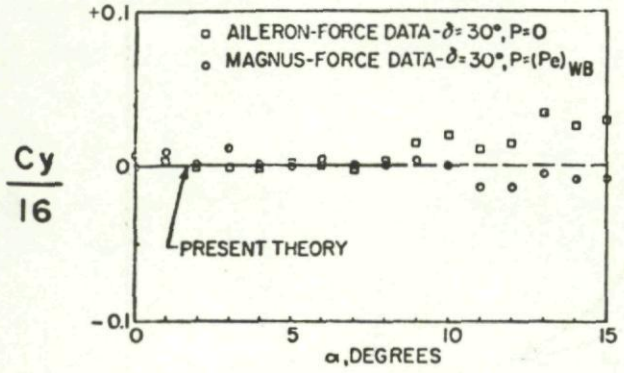

a. Side Forces Wing-Body Alone

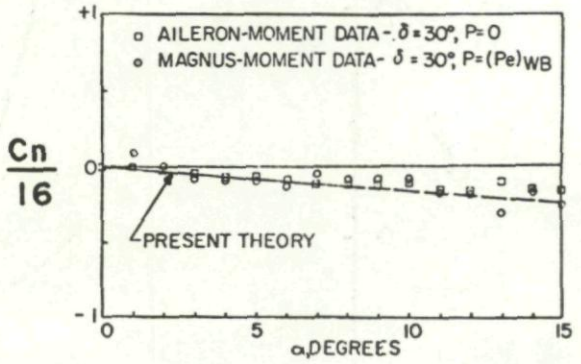

b. Side Moments Wing-Body Alone

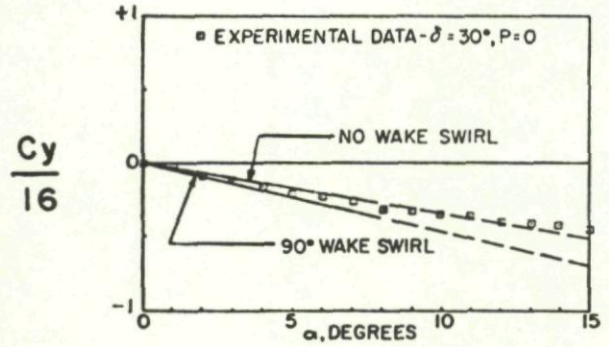

c. Side Forces Wing-Body-Tail Configuration

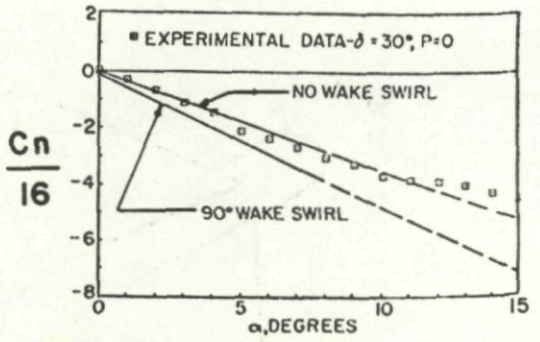

d. Side Moments Wing-Body-Tail Configuration

FIGURE 26. COMPARISON OF MAGNUS EFFECT ON WING-BODY-TAIL COMBINATION VS. WING-BODY ALONE (from reference 56)

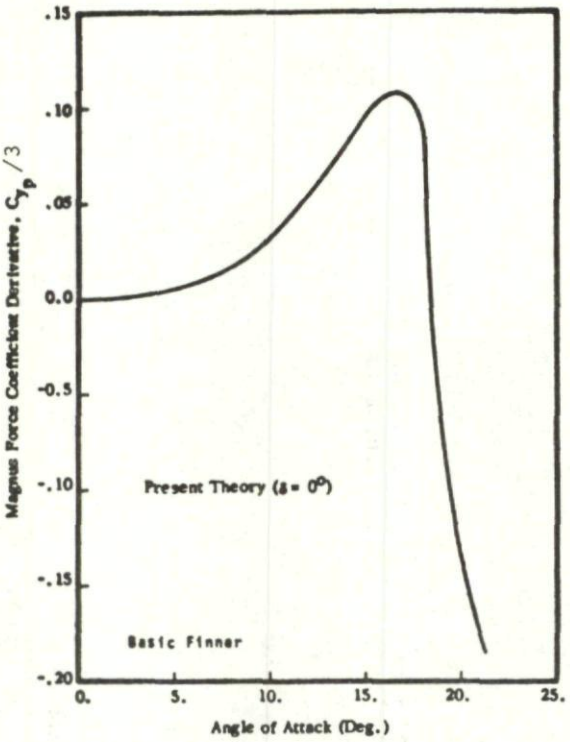

a. Magnus Force

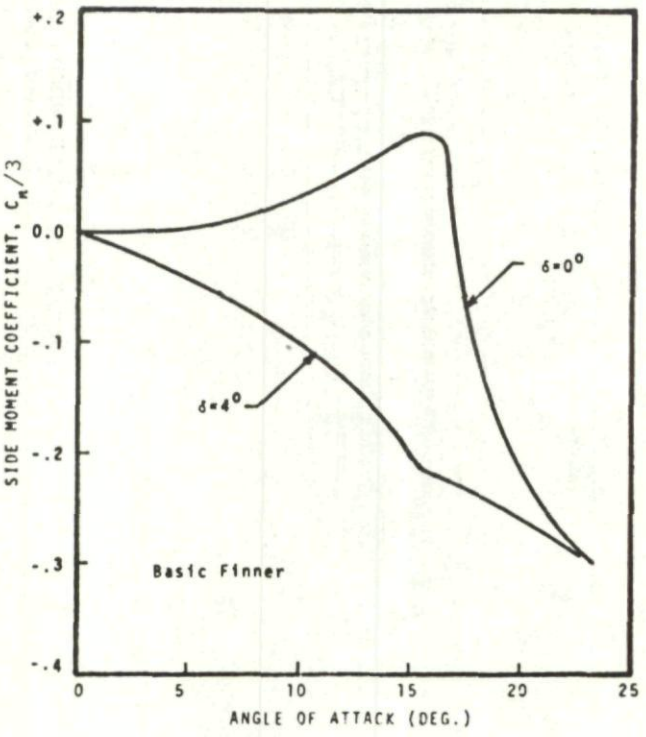

b. Magnus Moment

FIGURE 27. BODY VORTEX/FIN INTERFERENCE MAGNUS EFFECT (from reference 59)

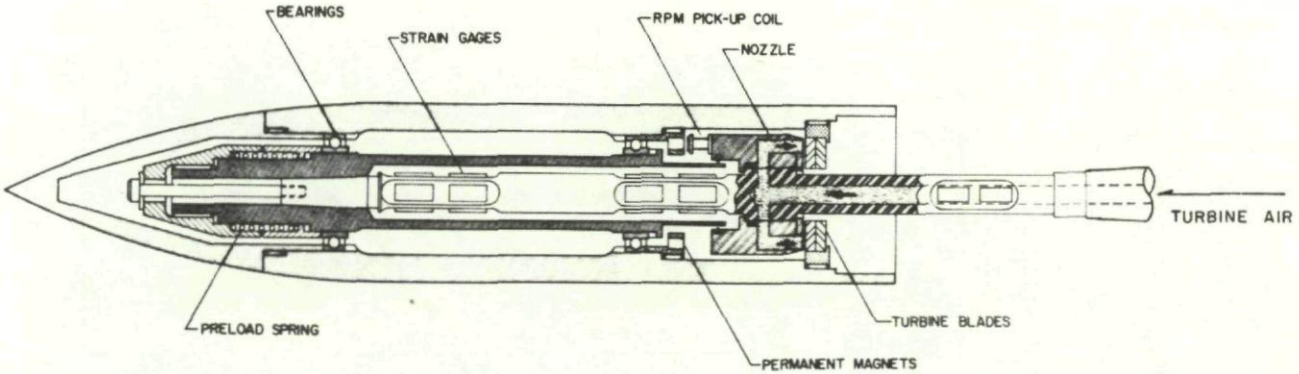

FIGURE 28. WIND TUNNEL BALANCE SYSTEM
(from reference 63)

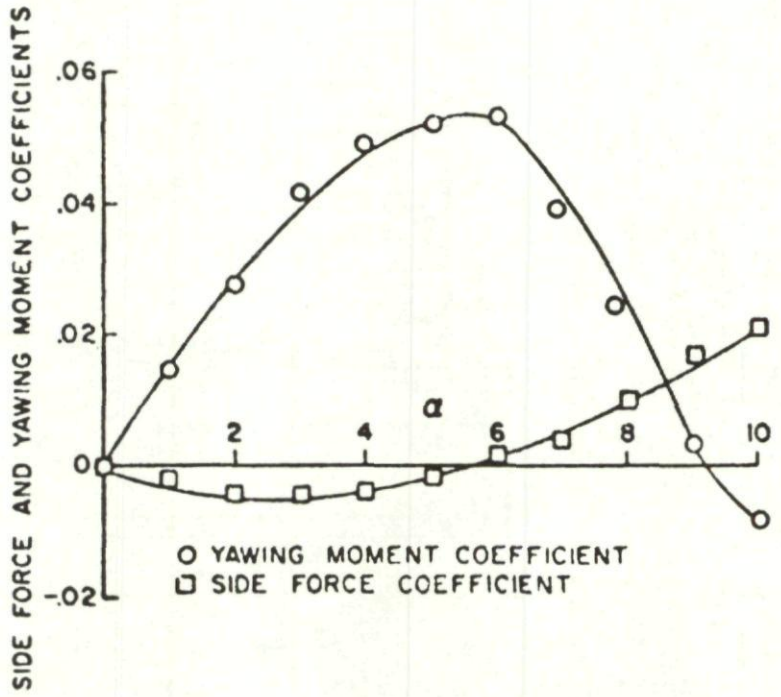

a. Side Force and Yawing Moment Coefficients vs. Angle of Attack for a 4° Fin Cant at Mach Number 0.90, Re_L = 1.5 x 10^6

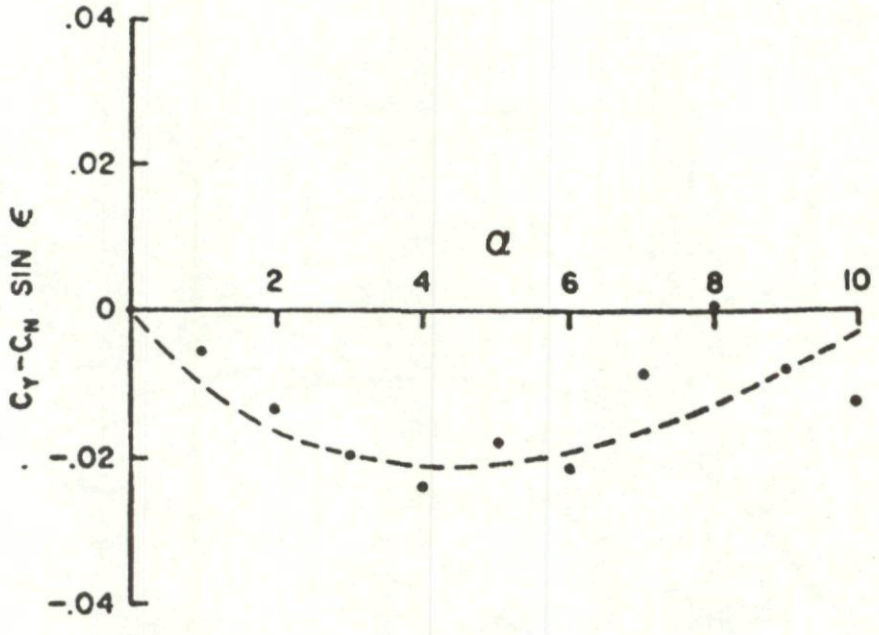

b. Side Force Coefficient Corrected for Normal Force Interaction

FIGURE 29. NORMAL FORCE INTERACTION EFFECT
(from reference 64)

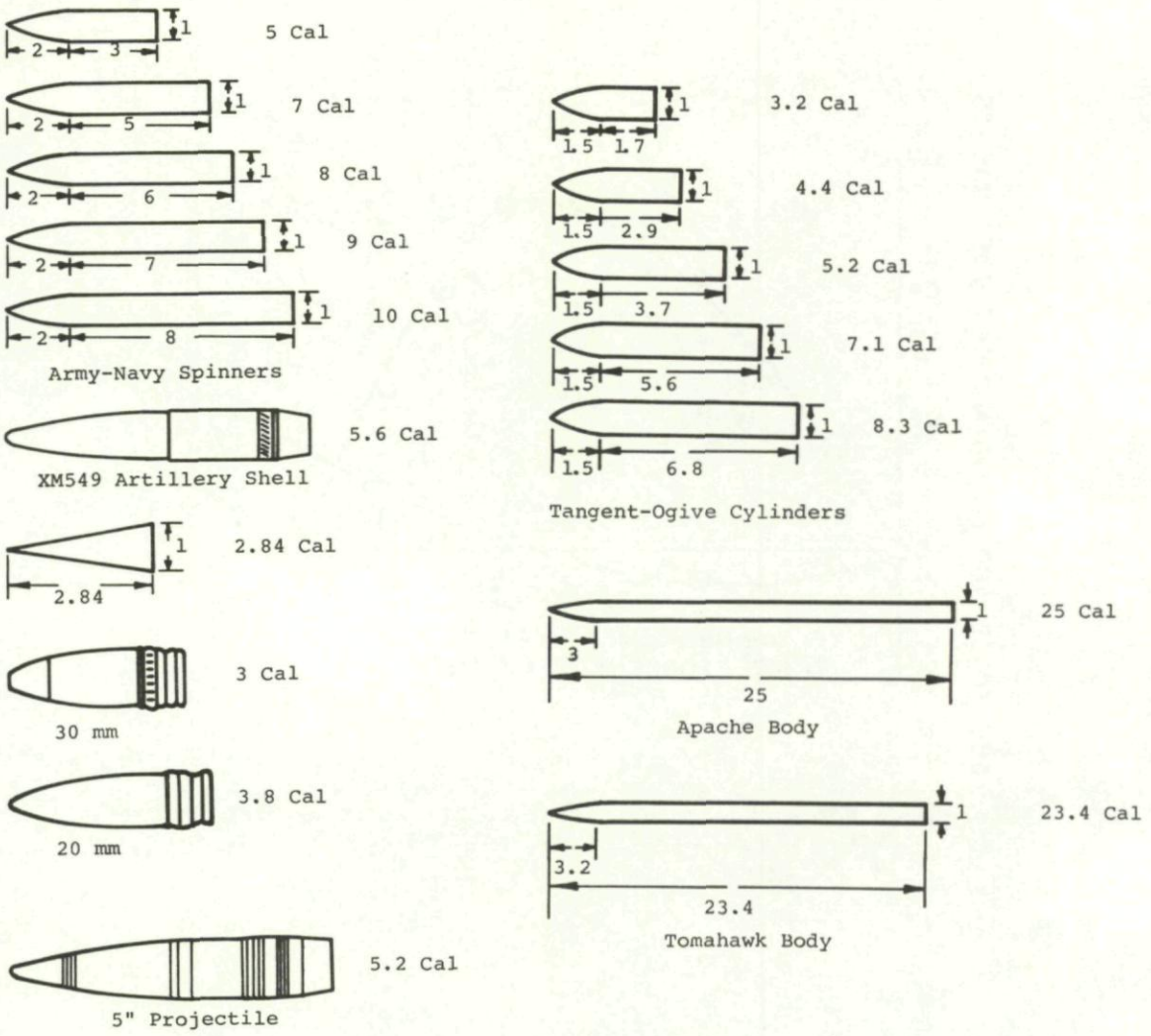

FIGURE 30. NONFINNED BODY MODELS

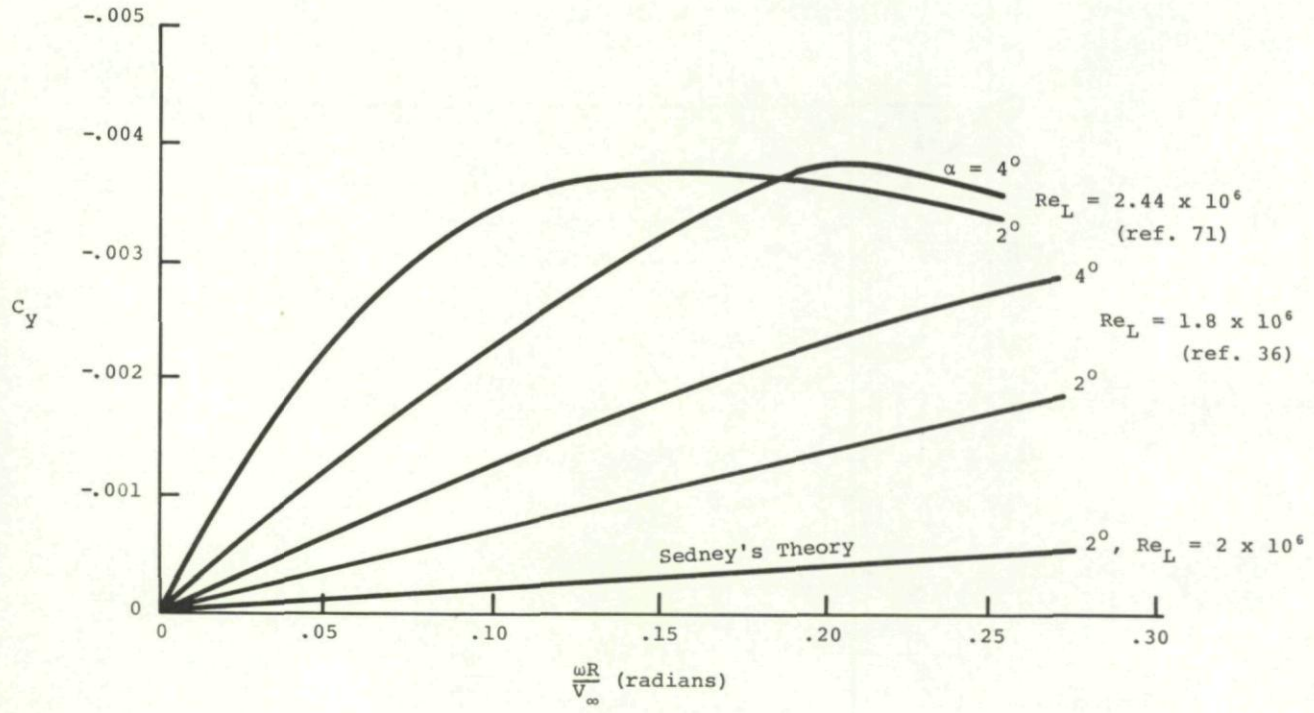

FIGURE 31. COMPARISON OF CONE MAGNUS FORCE DATA (M_∞= 2)

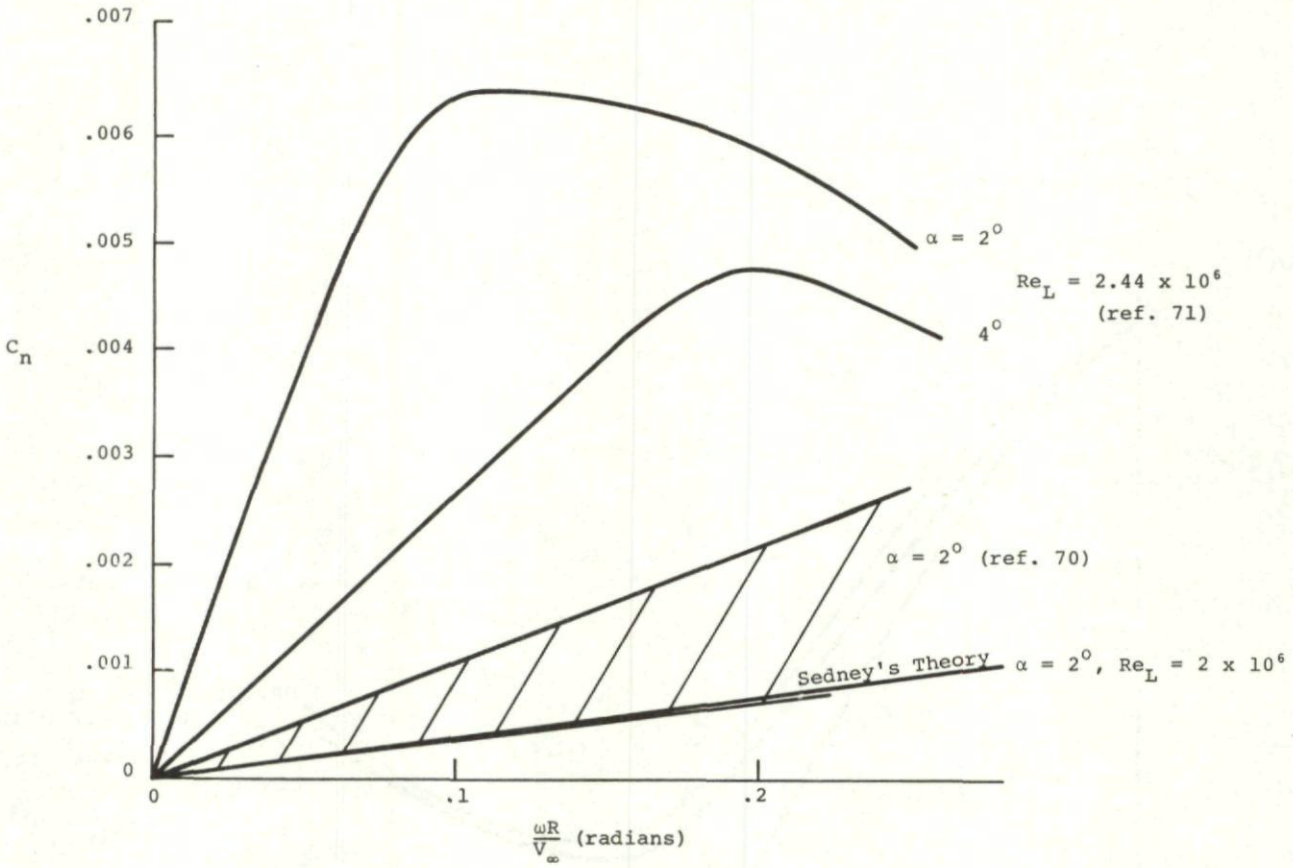

FIGURE 32. COMPARISON OF CONE MAGNUS MOMENT DATA ($M_\infty = 2$)

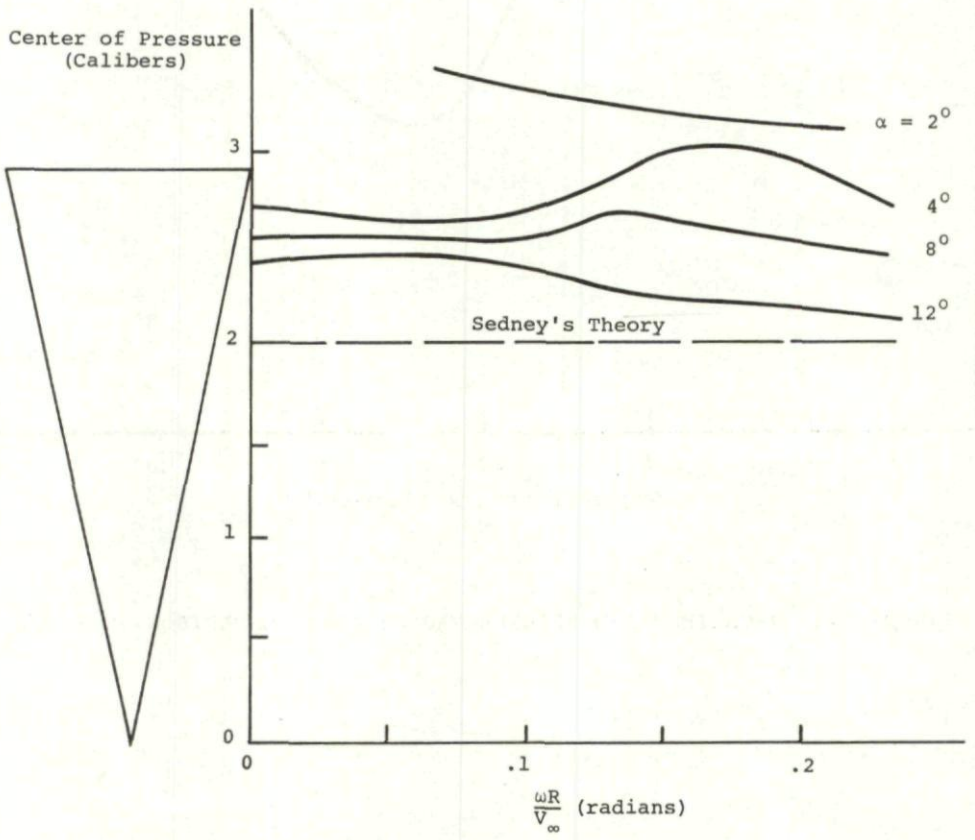

FIGURE 33. CONE CENTER OF PRESSURE (data taken from reference 71)

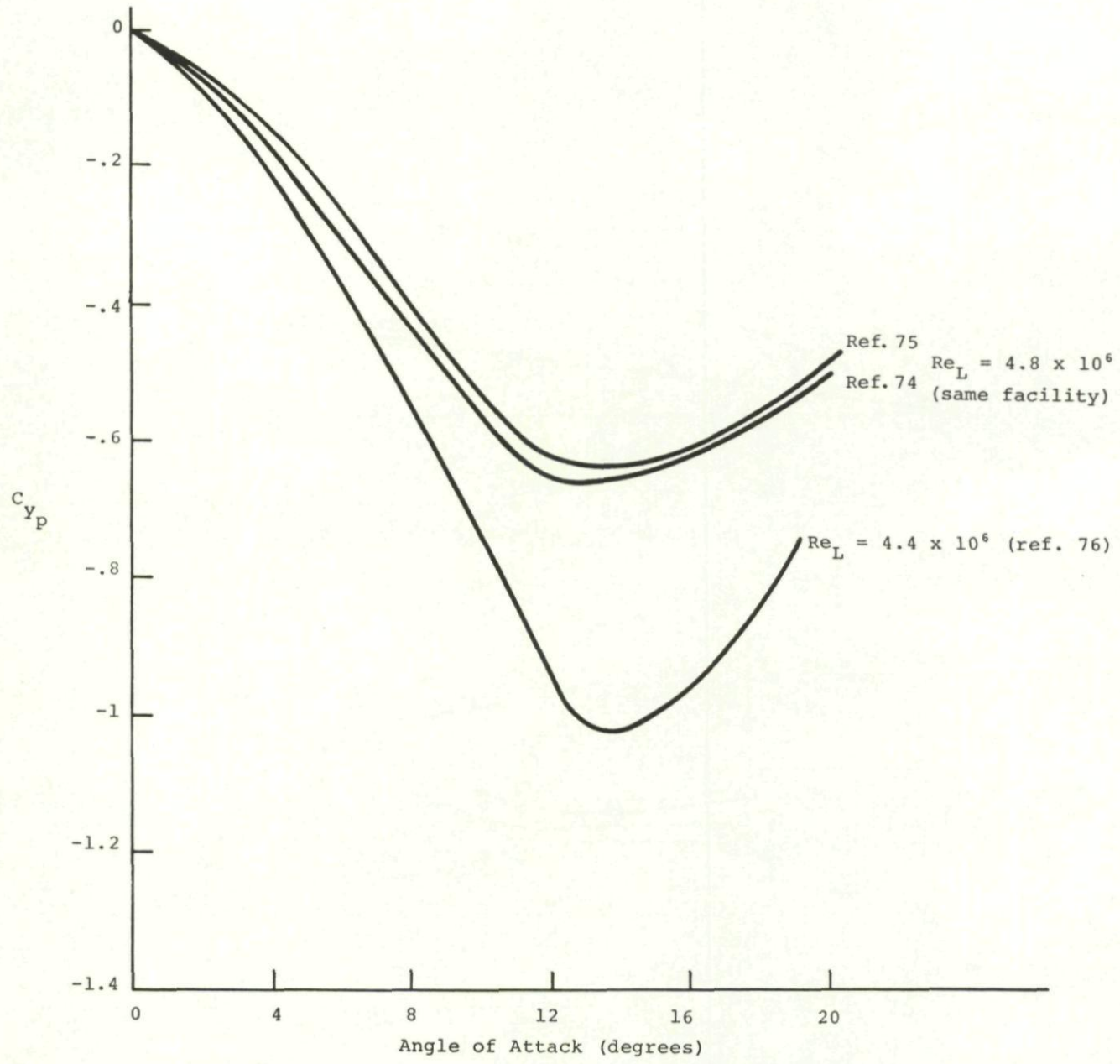

FIGURE 34. 7-CALIBER A-N SPINNER MAGNUS DATA COMPARISON (M_∞ = 2)

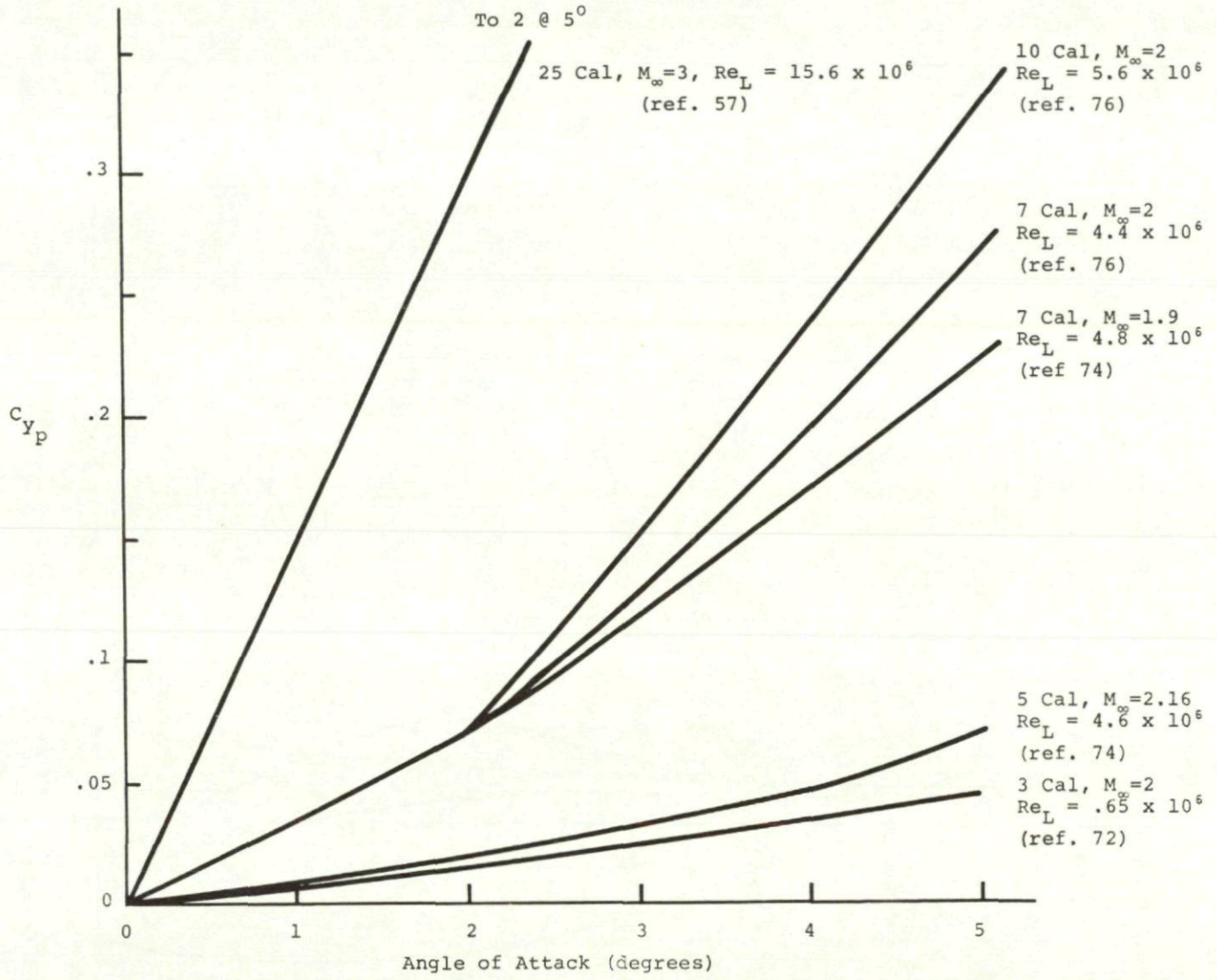

FIGURE 35. EFFECT OF FINENESS RATIO ON MAGNUS FORCE AT LOW ANGLES OF ATTACK

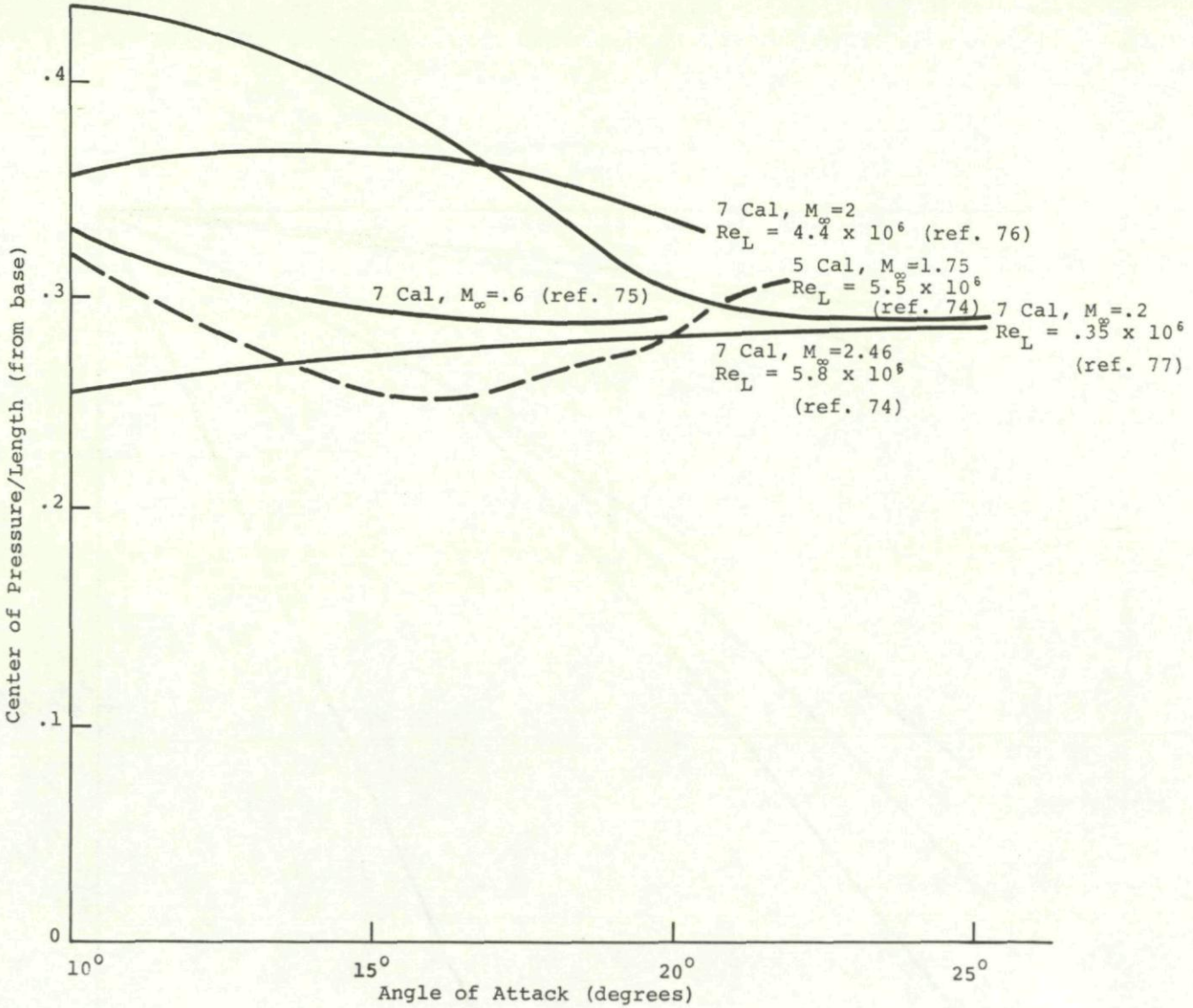

FIGURE 36. MAGNUS CENTER OF PRESSURE

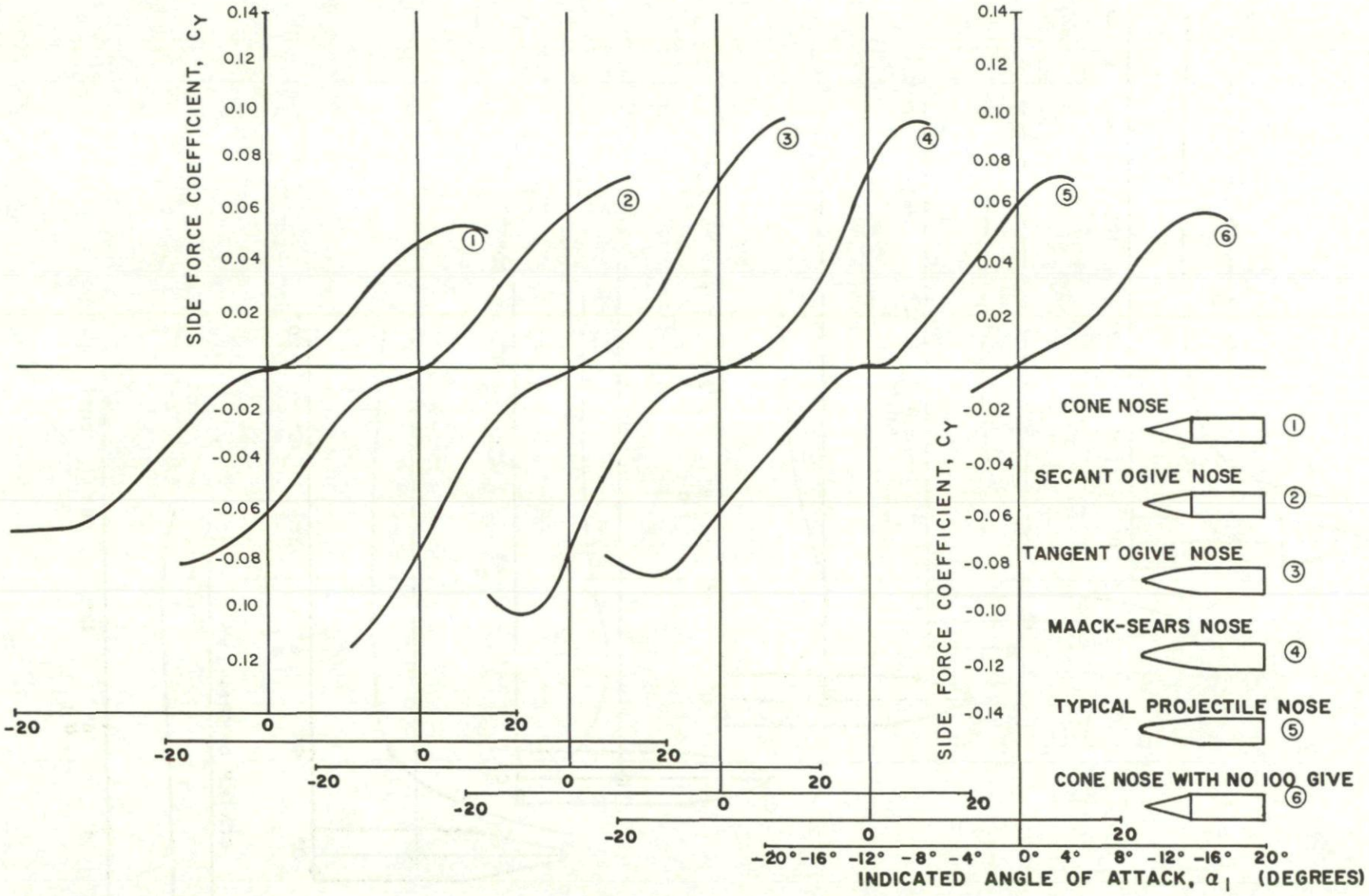

FIGURE 37. THE EFFECT OF NOSE SHAPE ON THE SIDE FORCE COEFFICIENT, C_y
(P = 458 RPS)
(from reference 79)

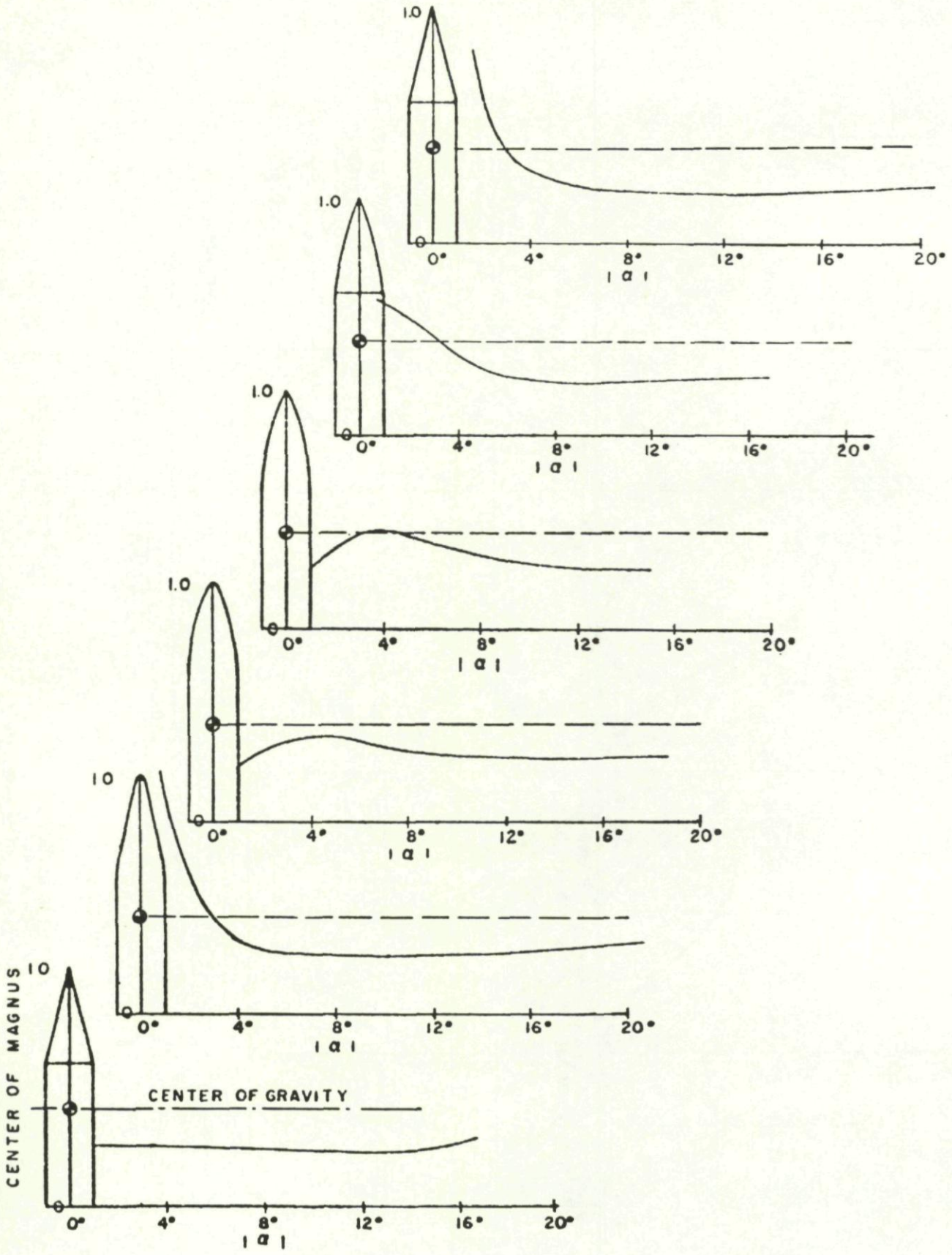

FIGURE 38. THE EFFECT OF NOSE SHAPE ON THE MAGNUS CENTER OF PRESSURE (P = 458 RPS) (from reference 79)

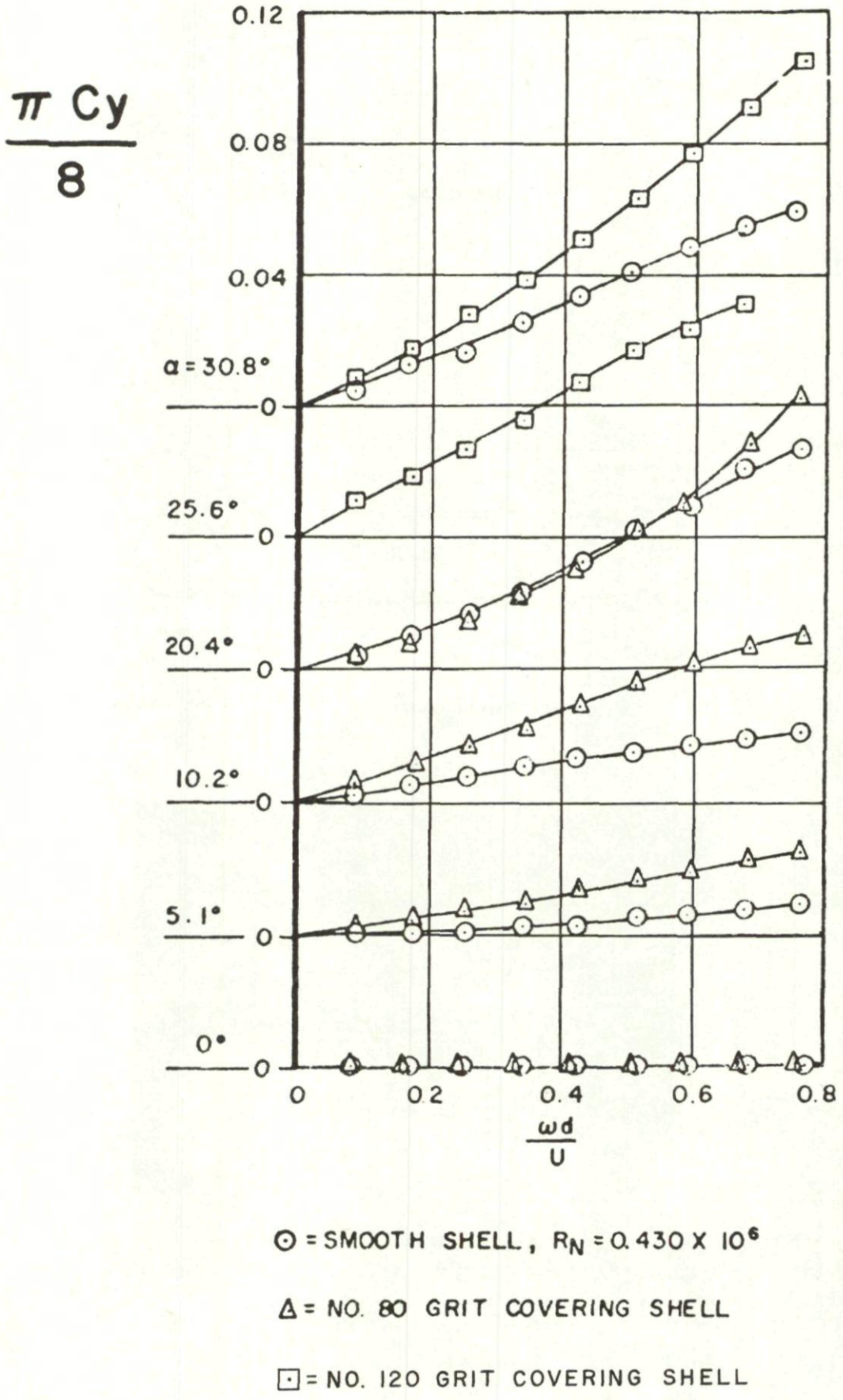

FIGURE 39. EFFECT OF GRIT ON MAGNUS FORCE COEFFICIENT (from reference 38)

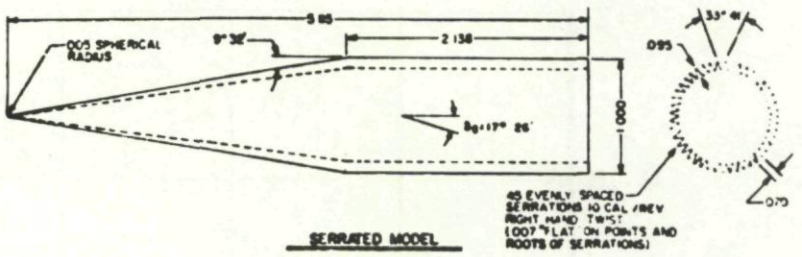

a. CONE-CYLINDER

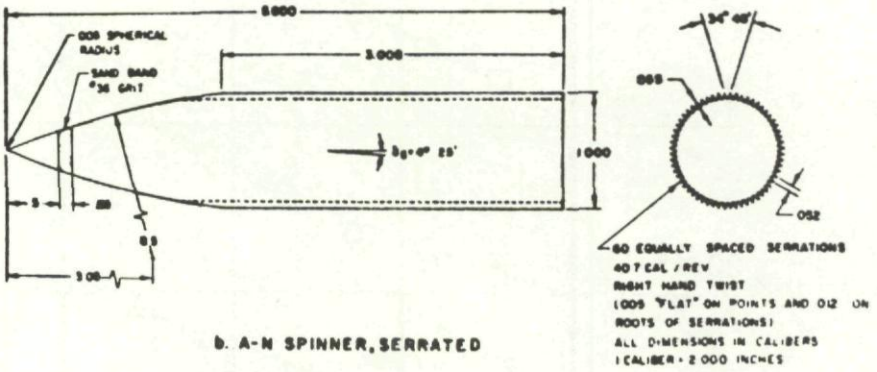

b. A-N SPINNER, SERRATED

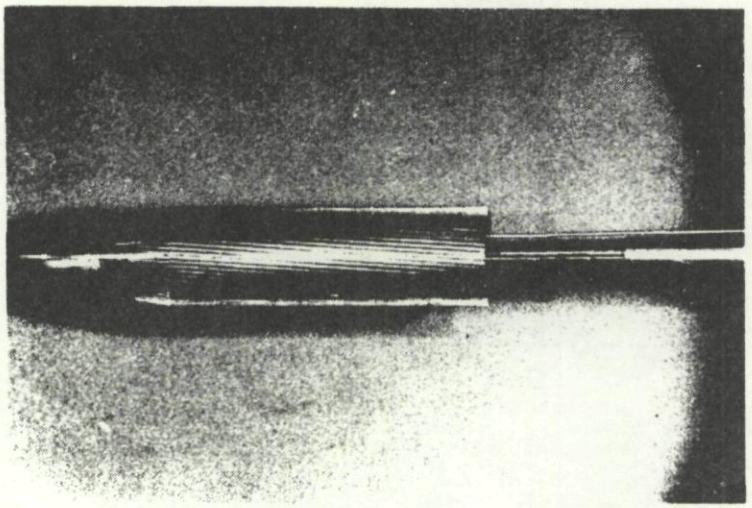

c. A-N SPINNER, SERRATED

FIGURE 40. SERRATED MODELS
(from reference 82)

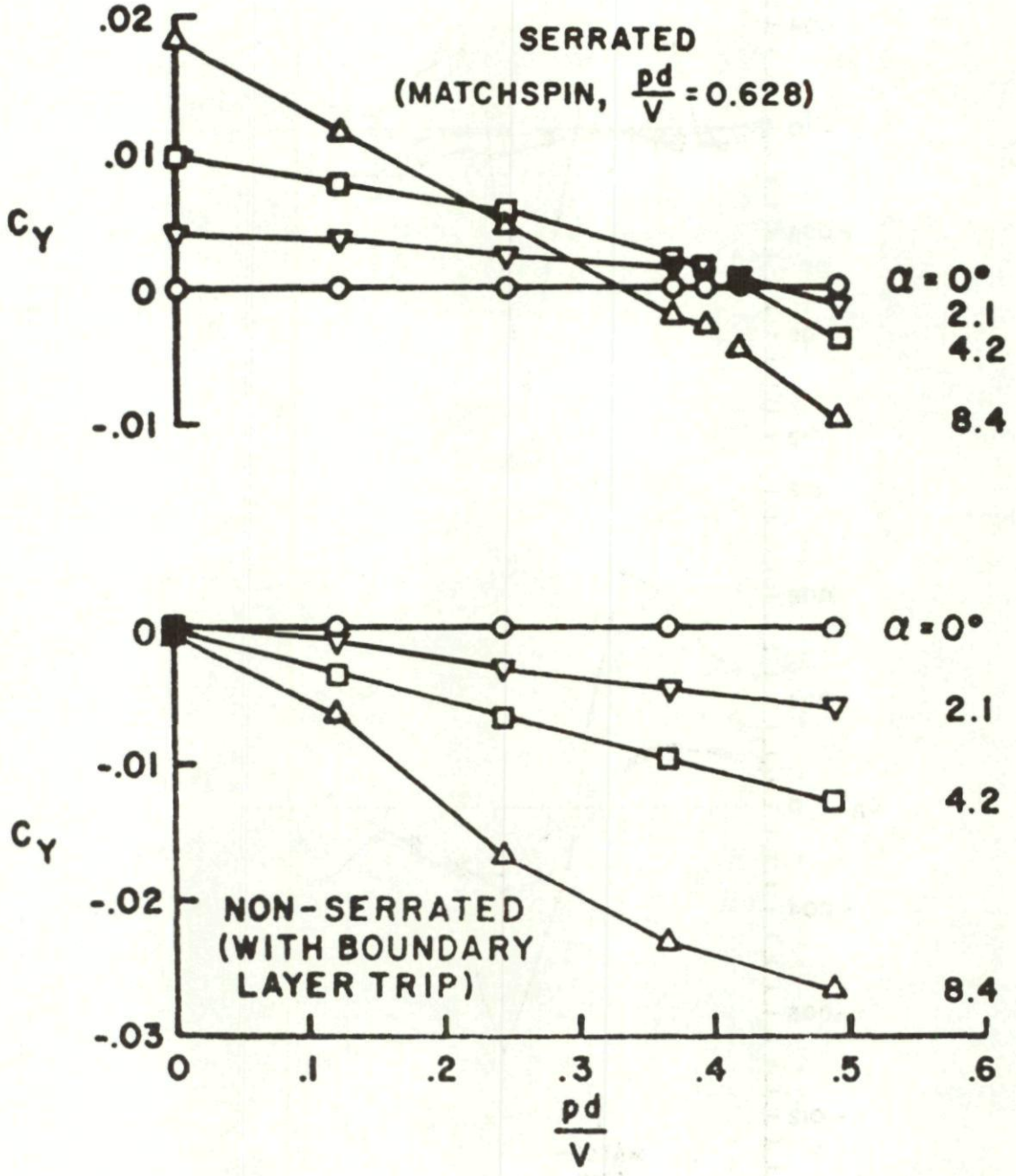

FIGURE 41. COMPARISON OF TYPICAL SERRATED AND NONSERRATED RESULTS FOR THE CONE-CYLINDER MODELS: $M_\infty = 1.5$, $Re_L = 5.1 \times 10^6$ (from reference 82)

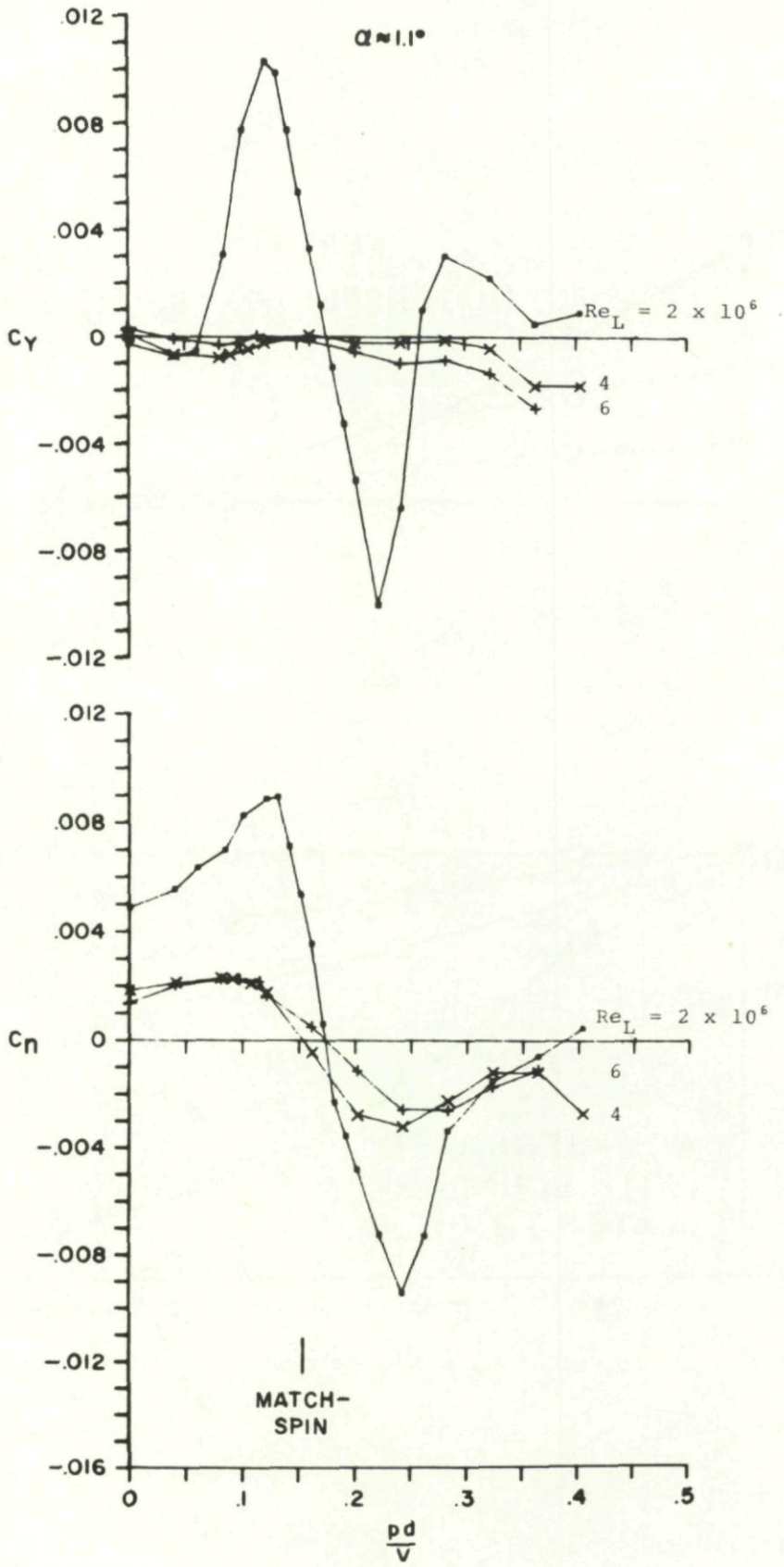

FIGURE 42. EFFECT OF REYNOLDS NUMBER ON THE YAW FORCE AND MOMENT CHARACTERISTICS OF THE SERRATED A-N SPINNER: $\alpha \approx 1.1$ DEGREE (MOMENTS REFERRED TO MODEL BASE)

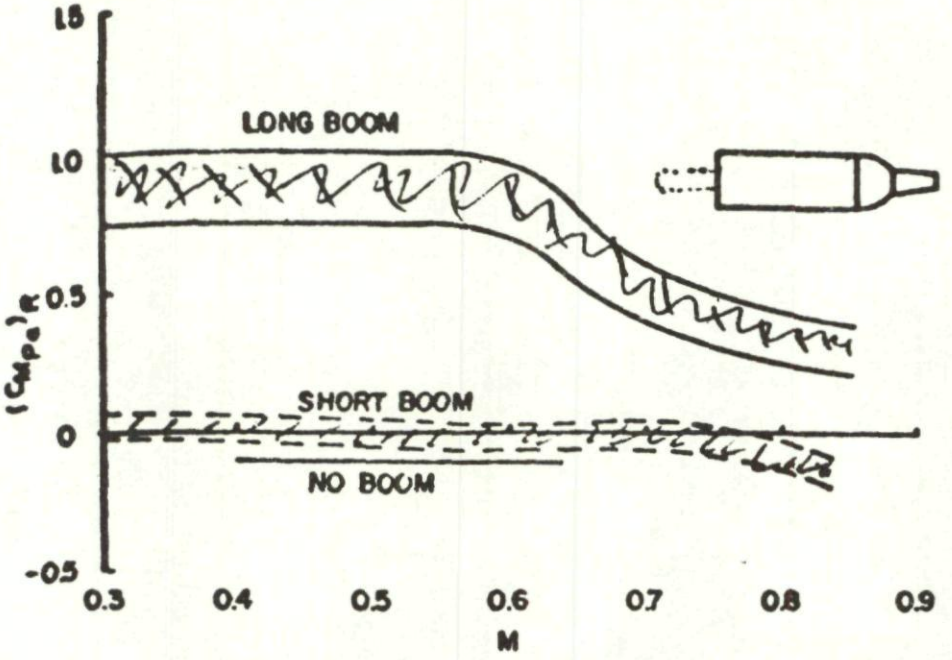

FIGURE 43. MAGNUS MOMENT COEFFICIENT DERIVATIVE VS. MACH NUMBER FOR DIFFERENT BOOM LENGTHS AT SMALL ANGLES OF ATTACK (from reference 83)

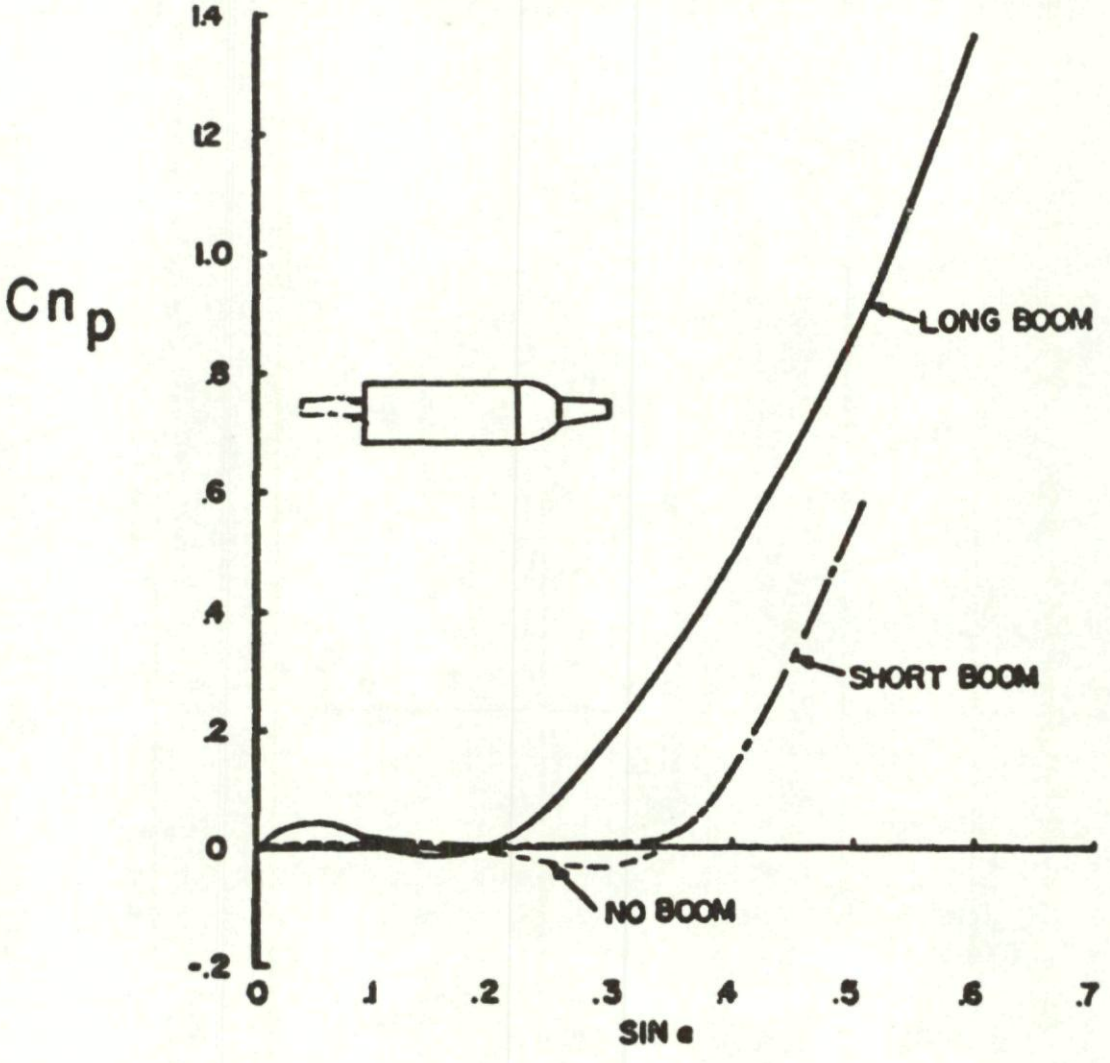

FIGURE 44. EFFECT OF BOOM ON MAGNUS MOMENT COEFFICIENT VS. ANGLE OF ATTACK FOR SQUARE BASED SHELL (from reference 83)

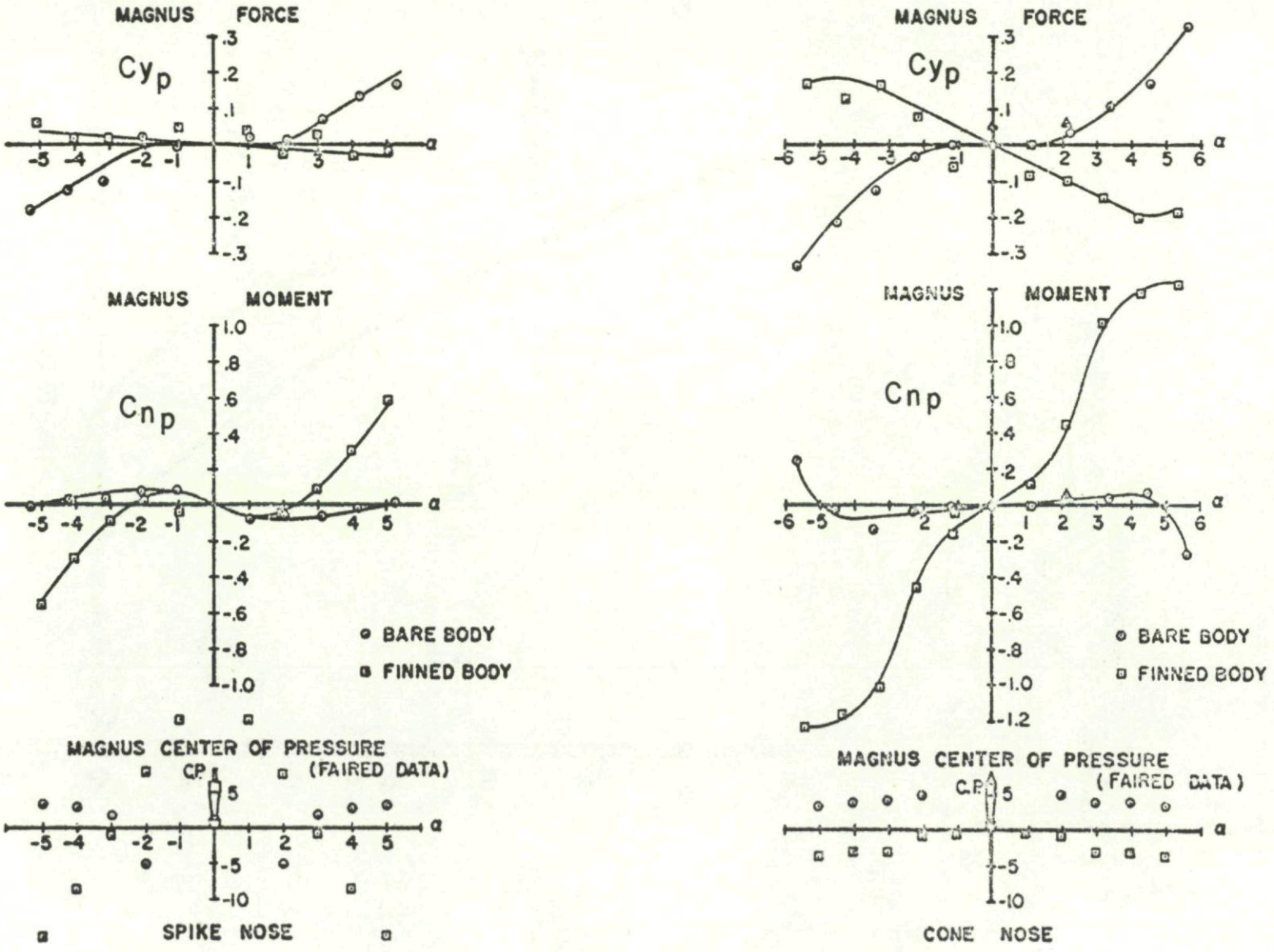

FIGURE 45. THE MAGNUS CHARACTERISTICS OF FINNED PROJECTILES AT $M_\infty = 1.75$, $Re_L = .71 \times 10^6$ (from ref. 92)

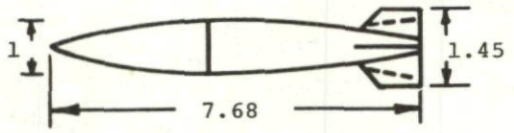

M823 Research Store

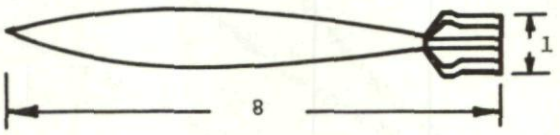

105 mm Mortar

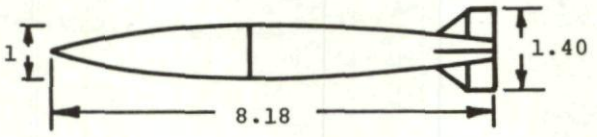

Navy Low Drag Bomb

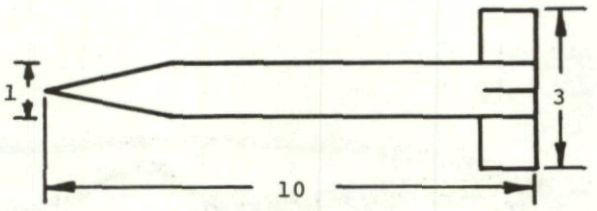

Basic Finner

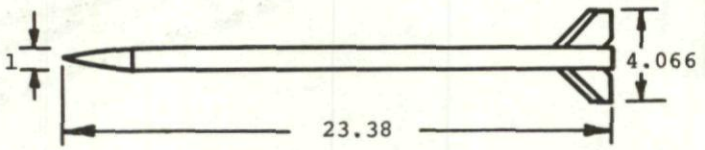

Tomahawk

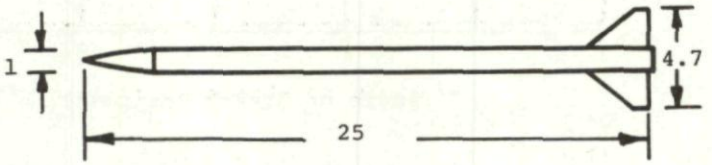

Apache

FIGURE 46. FINNED BODY MODELS
(Dimensions in Calibers)

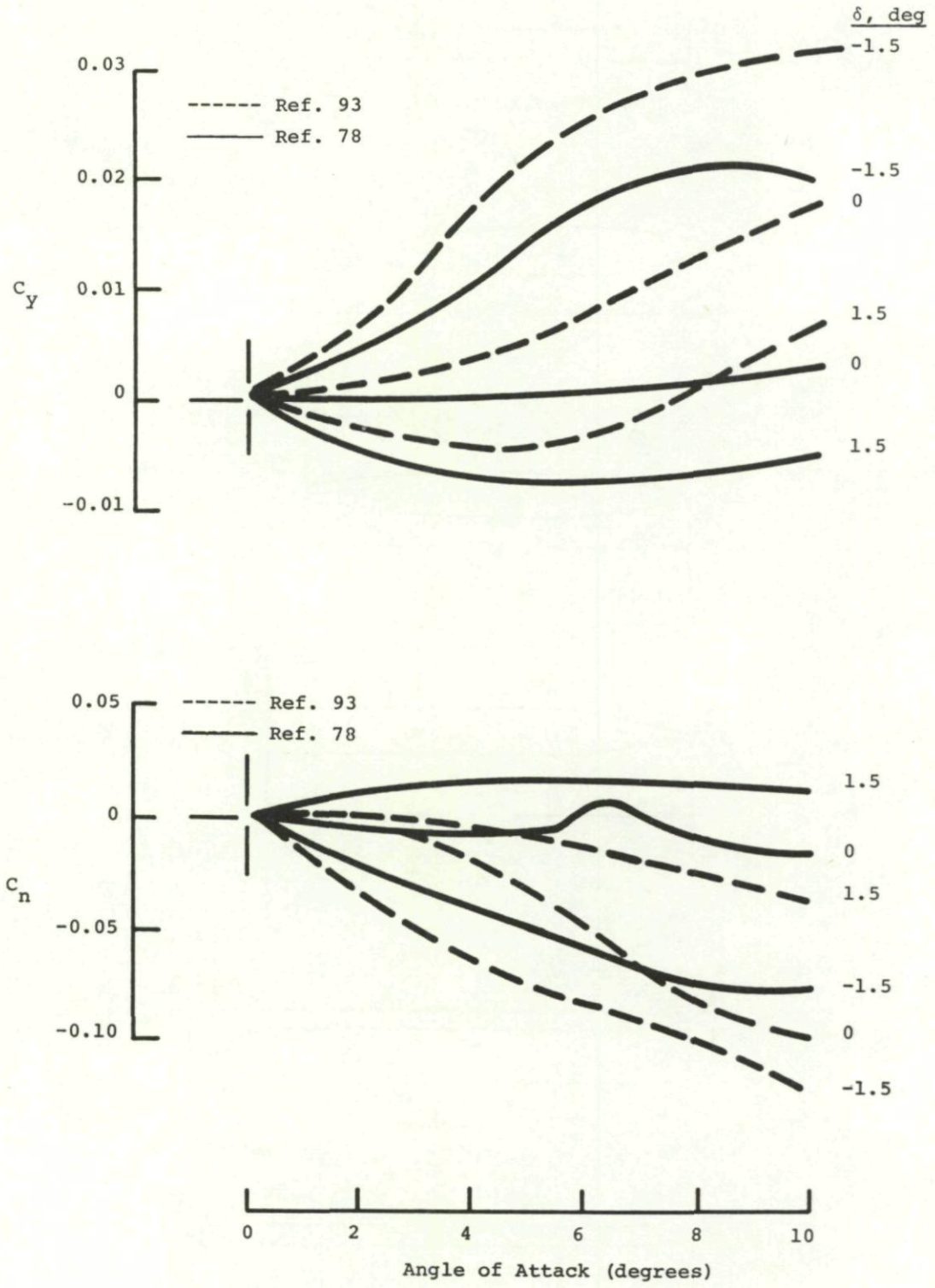

FIGURE 47. VARIATIONS OF C_y AND C_n WITH ANGLE OF ATTACK FOR THE POSITIVE AND NEGATIVE 1.5-DEGREE CANTED FINS AND FOR THE UNCANTED FINS AT $M_\infty = 5.0$, $Re_L = 27.3 \times 10^6$

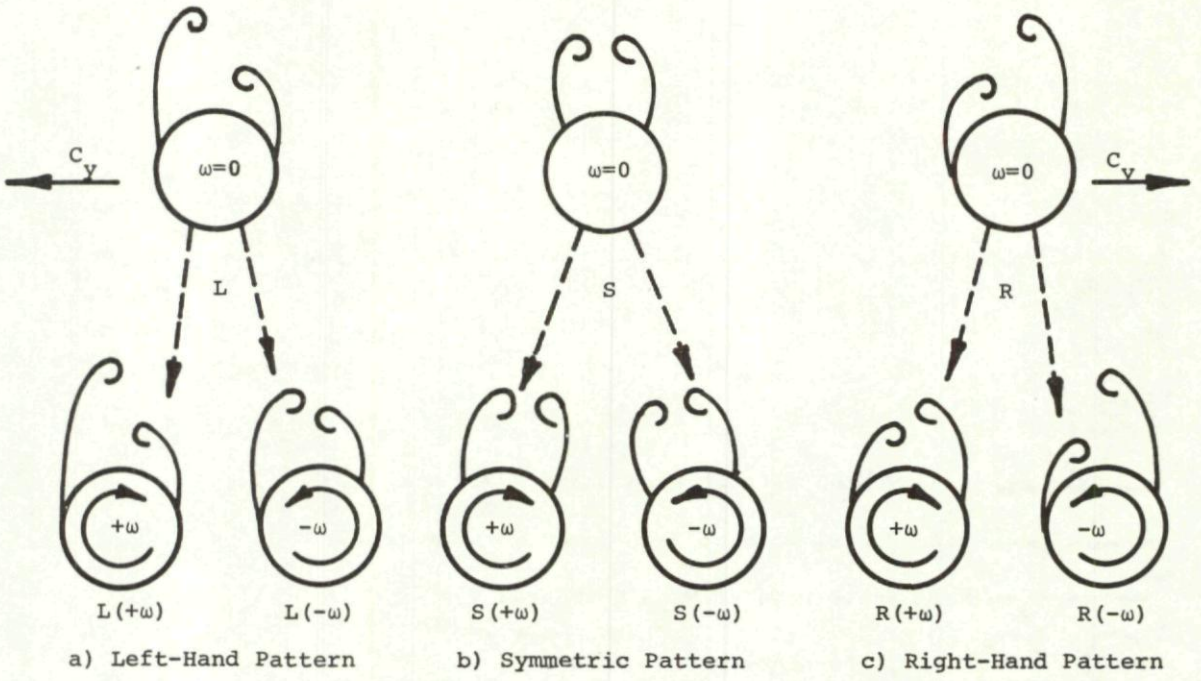

FIGURE 48. SCHEMATIC REPRESENTATION OF LEE SIDE FLOW PATTERNS ON THE TOMAHAWK WITH AND WITHOUT SPIN (from reference 93)

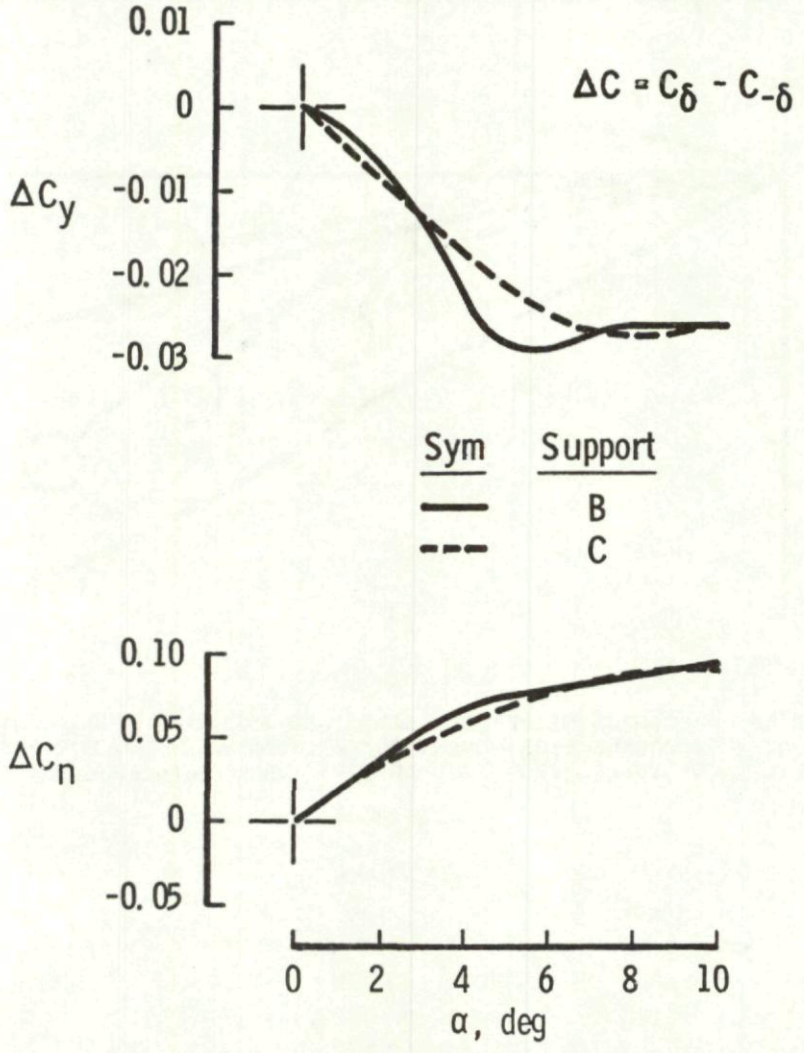

FIGURE 49. COMPARISON OF THE ΔC_y AND ΔC_n VARIATIONS BETWEEN THE MARCH AND JUNE TESTS FOR THE 1.5-DEG. CANT FINS AT $M_\infty = 5.0$, $Re_L = 27.3 \times 10^6$ (from reference 78)

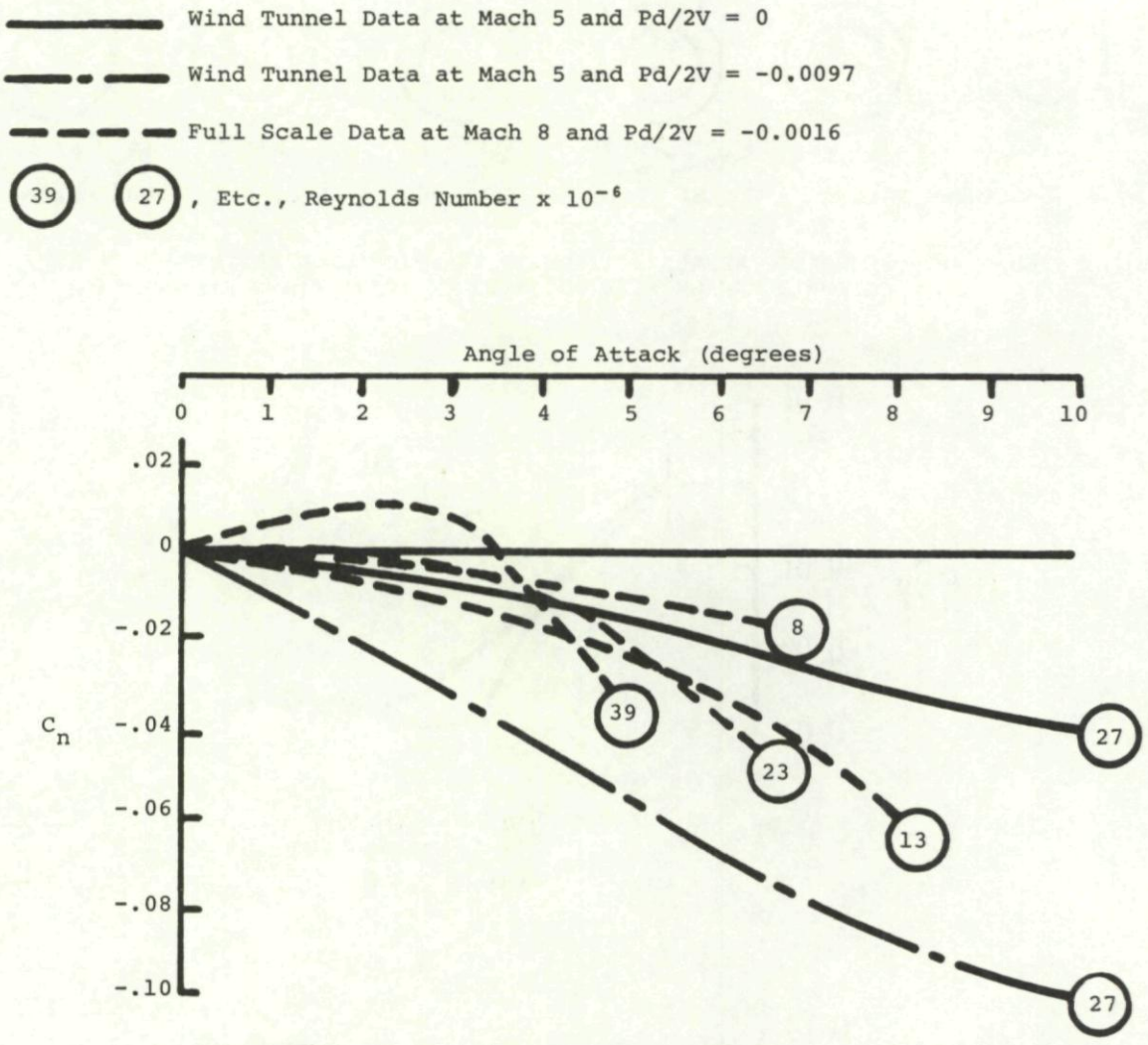

FIGURE 50. A COMPOSITE OF FULL SCALE AND AVERAGED WIND TUNNEL DATA ON THE TOMAHAWK SIDE MOMENT COEFFICIENT ADJUSTED FOR POSSIBLE EFFECTS OF TUNNEL FLOW ANGULARITIES (from reference 93)

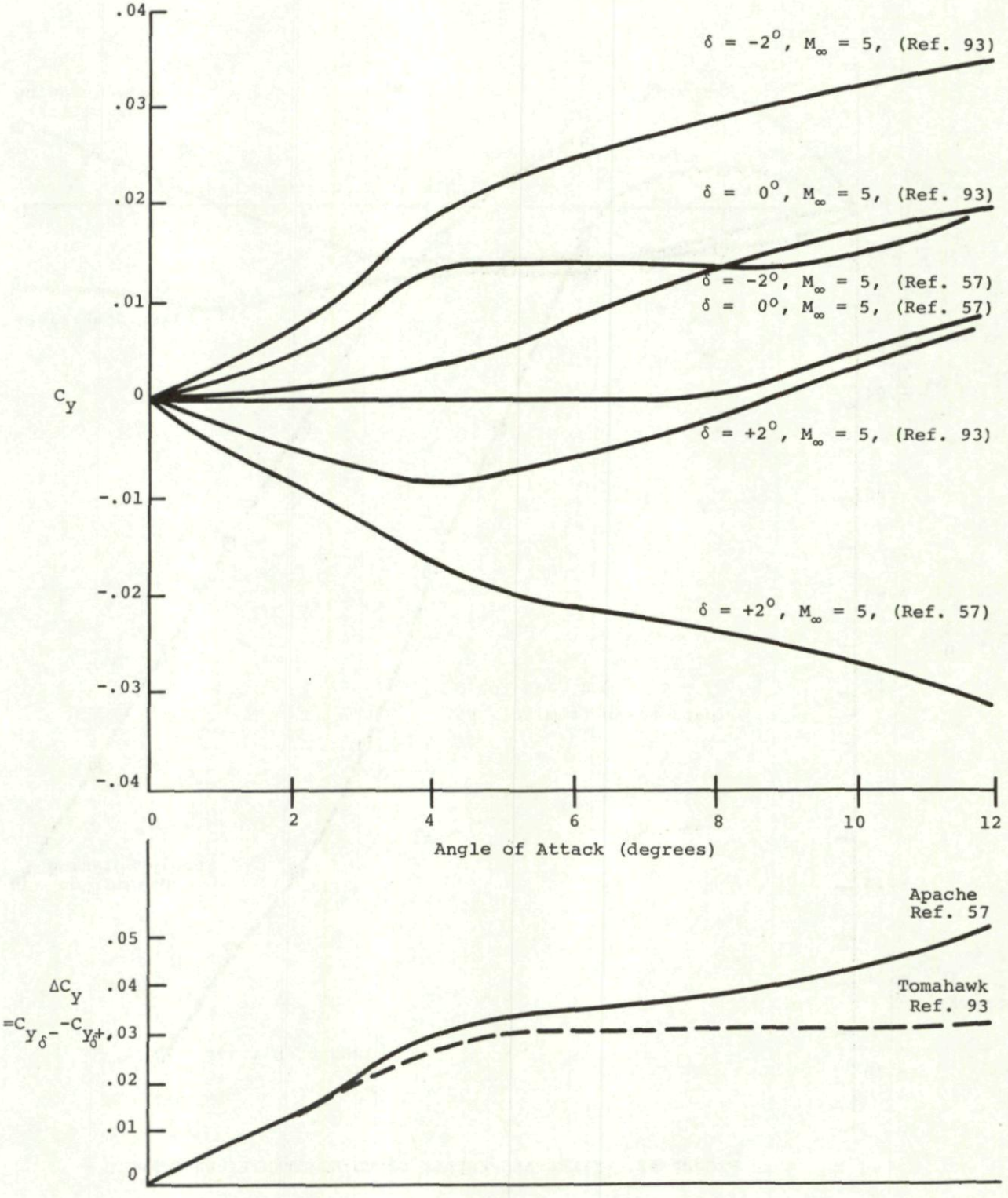

FIGURE 51. COMPARISON OF MAGNUS FORCE FOR TOMAHAWK AND APACHE VEHICLES

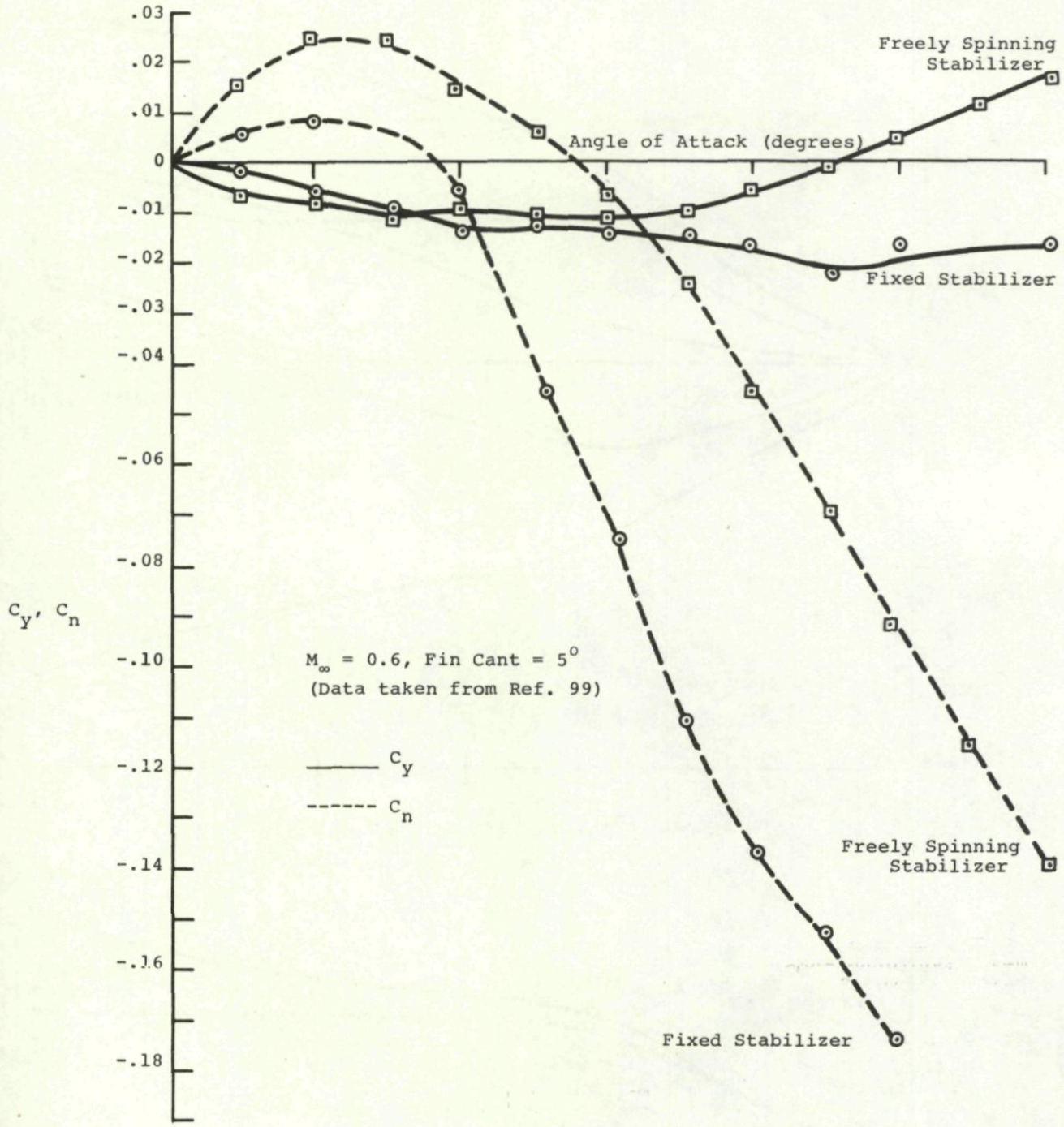

FIGURE 52. FIXED AND FREELY SPINNING STABILIZER EFFECTS

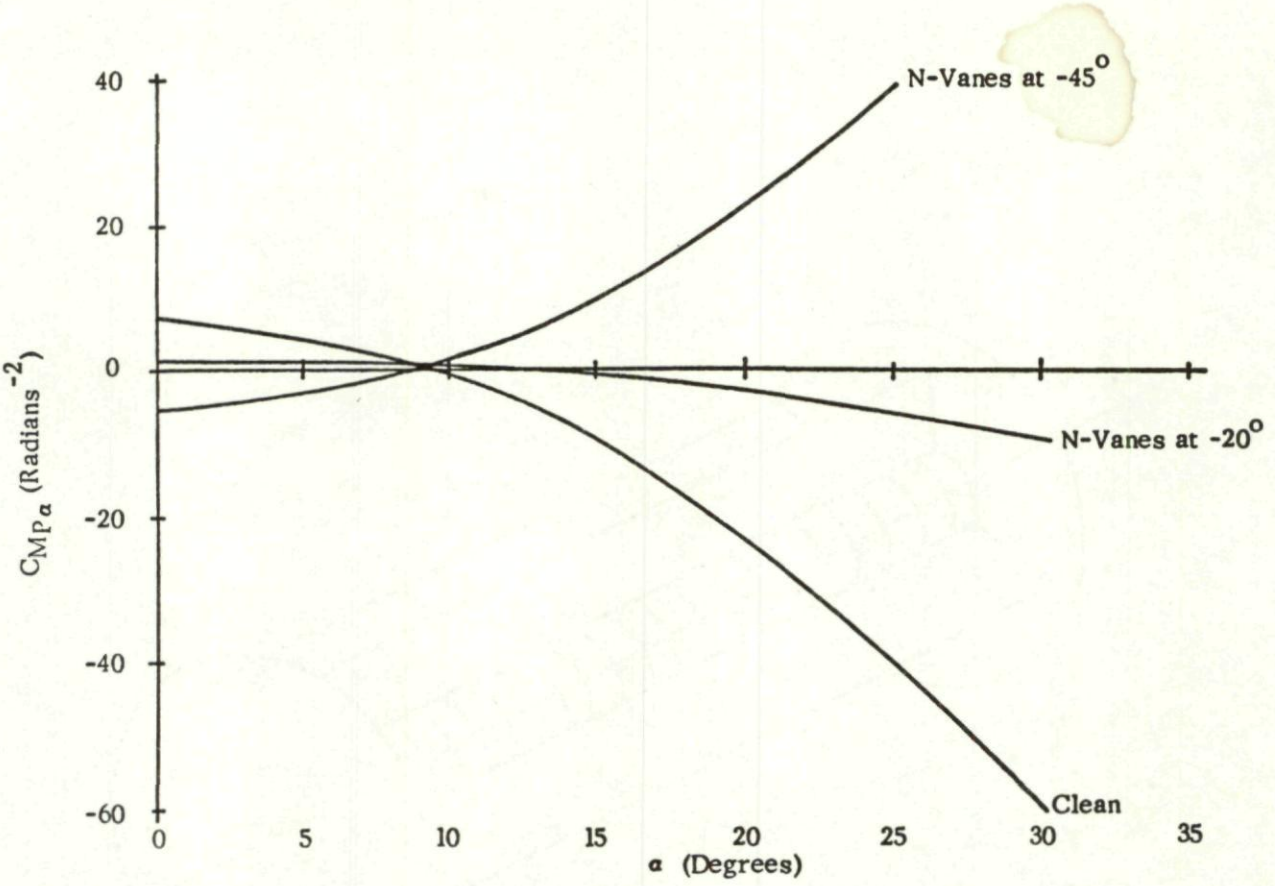

FIGURE 53. NONLINEAR MAGNUS MOMENTS VERSUS α (STRAIGHT AFT SECTION) N-VANES ON NOSE SECTION (from reference 33)

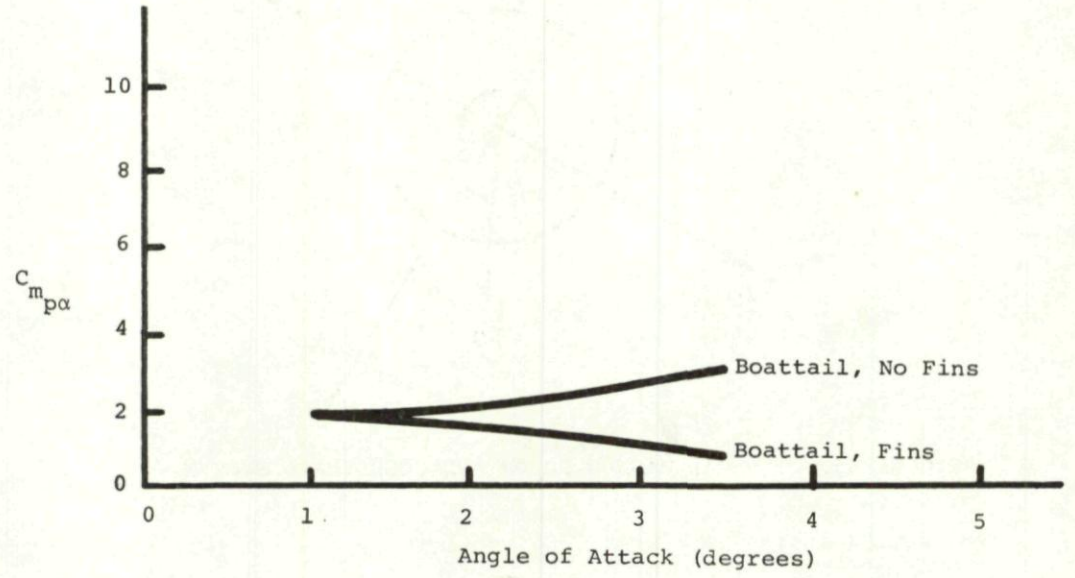

FIGURE 54. EFFECT OF BOATTAIL FINS ON MAGNUS MOMENT COEFFICIENT DERIVATIVE (from reference 89)

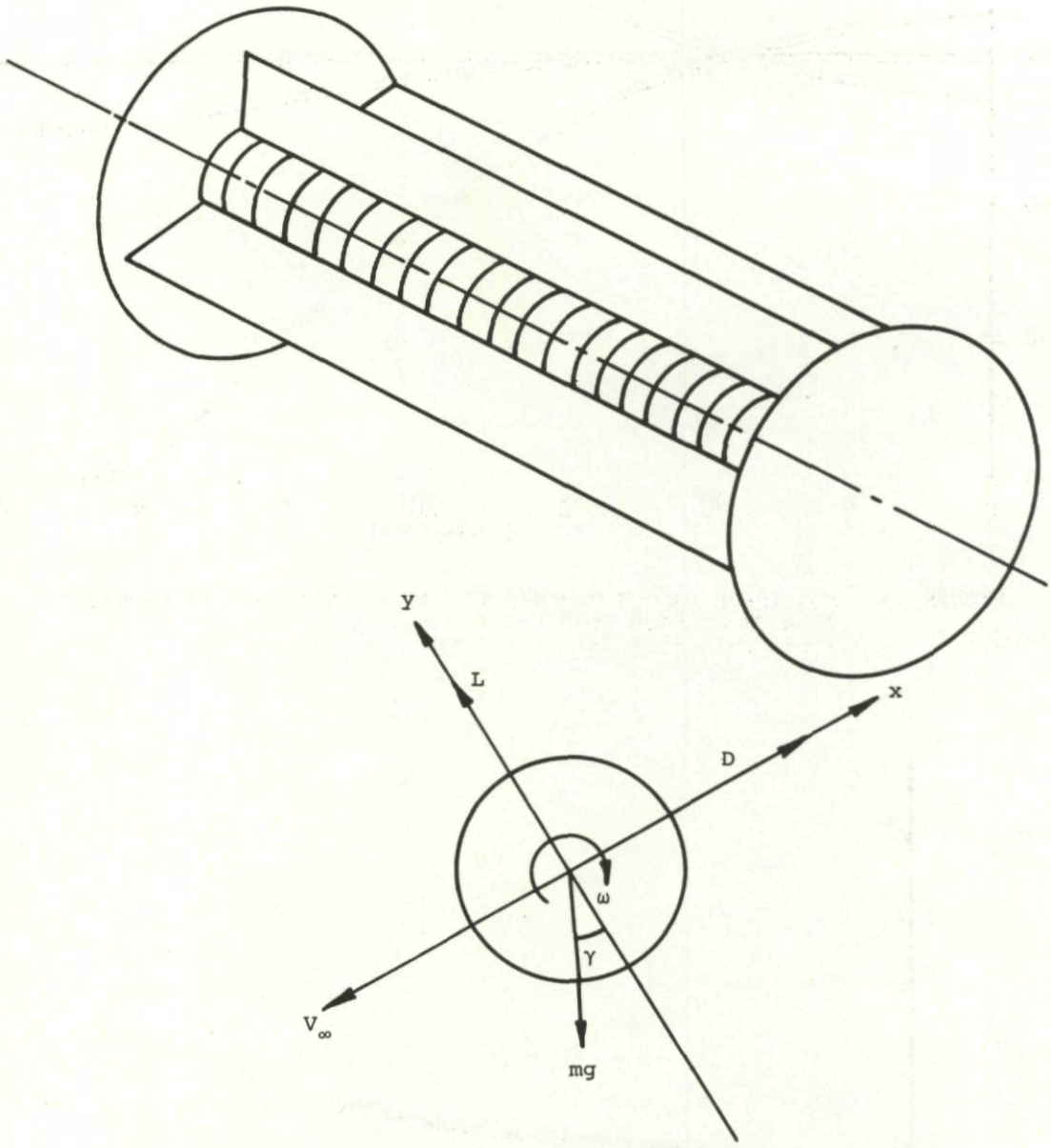

FIGURE 55. TYPICAL MAGNUS ROTOR AND COORDINATE SYSTEM

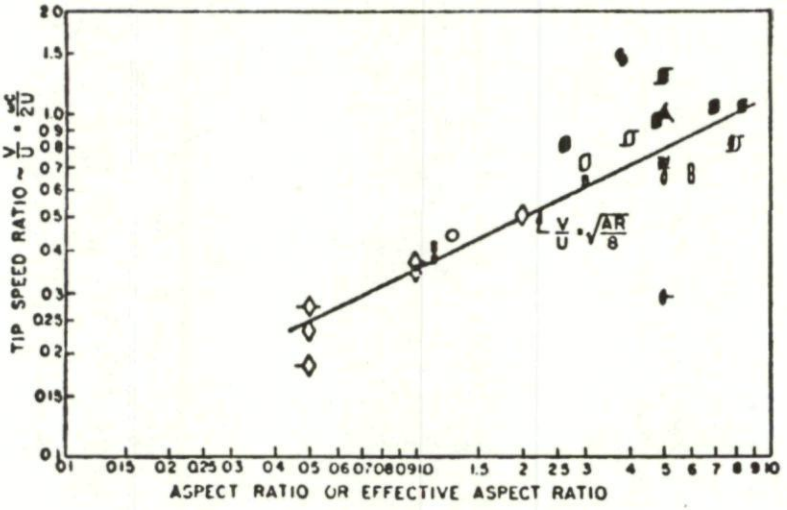

	Savonius	1.5 diameter end plates	AR = 1.45
	Modified rect.	1.5 diameter end plates driving vanes	AR = 2.32
	Modified rect.	1.0 diameter end plates	AR = 2.32
	Triangle	1.5 diameter end plates driving vanes	AR = 2.32
	Circle	1.5 diameter end plates driving vanes	AR = 2.32
	Modified rect.	Driving vanes	
	Modified rect.		
	Circular arc	$\tau = 0.2$	
	Circular arc	$\tau = 0.333$	
	Flat plate		
	Flat plate	Circular planform	
	Double wedge	Mounted hemisphere-cyl. $\tau = 0.1$	
	Double wedge	Mounted tunnel wall $\tau = 0.1$	
	Double wedge	$\tau = 0.1$	
	Double wedge	$\tau = 0.1$ wood	

FIGURE 56. ROTOR TIP SPEED RATIO VS. EFFECTIVE ASPECT RATIO (from reference 102)

AGARDograph No.171
Advisory Group for Aerospace Research and Development, NATO
MAGNUS CHARACTERISTICS OF ARBITRARY ROTATING BODIES
I.A.Jacobson, edited by P.F.Yaggy
Published November 1973
64 pages

This survey paper reviews both theoretical and experimental investigations of the Magnus effect on arbitrary bodies of revolution. The main emphasis is on spinning projectiles at angles of attack, both with and without fins. Flow visualization measurements are used to assess the accuracy of the existing theories. Laminar turbulent, and mixed boundary layers are considered.

AGARD-AG-171
532.582.82 :
533.696.5 : 623.451

Magnus effect
Rotation
Bodies of revolution
Projectiles
Spin stabilized ammunition
Flow visualization
Boundary layer

AGARDograph No.171
Advisory Group for Aerospace Research and Development, NATO
MAGNUS CHARACTERISTICS OF ARBITRARY ROTATING BODIES
I.A.Jacobson, edited by P.F.Yaggy
Published November 1973
64 pages

This survey paper reviews both theoretical and experimental investigations of the Magnus effect on arbitrary bodies of revolution. The main emphasis is on spinning projectiles at angles of attack, both with and without fins. Flow visualization measurements are used to assess the accuracy of the existing theories. Laminar turbulent, and mixed boundary layers are considered.

AGARD-AG-171
532.582.82 :
533.696.5 : 623.451

Magnus effect
Rotation
Bodies of revolution
Projectiles
Spin stabilized ammunition
Flow visualization
Boundary layer

AGARDograph No.171
Advisory Group for Aerospace Research and Development, NATO
MAGNUS CHARACTERISTICS OF ARBITRARY ROTATING BODIES
I.A.Jacobson, edited by P.F.Yaggy
Published November 1973
64 pages

This survey paper reviews both theoretical and experimental investigations of the Magnus effect on arbitrary bodies of revolution. The main emphasis is on spinning projectiles at angles of attack, both with and without fins. Flow visualization measurements are used to assess the accuracy of the existing theories. Laminar turbulent, and mixed boundary layers are considered.

AGARD-AG-171
532.582.82 :
533.696.5 : 623.451

Magnus effect
Rotation
Bodies of revolution
Projectiles
Spin stabilized ammunition
Flow visualization
Boundary layer

AGARDograph No.171
Advisory Group for Aerospace Research and Development, NATO
MAGNUS CHARACTERISTICS OF ARBITRARY ROTATING BODIES
I.A.Jacobson, edited by P.F.Yaggy
Published November 1973
64 pages

This survey paper reviews both theoretical and experimental investigations of the Magnus effect on arbitrary bodies of revolution. The main emphasis is on spinning projectiles at angles of attack, both with and without fins. Flow visualization measurements are used to assess the accuracy of the existing theories. Laminar turbulent, and mixed boundary layers are considered.

AGARD-AG-171
532.582.82 :
533.696.5 : 623.451

Magnus effect
Rotation
Bodies of revolution
Projectiles
Spin stabilized ammunition
Flow visualization
Boundary layer

AGARDograph No.171
Advisory Group for Aerospace Research and Development, NATO
MAGNUS CHARACTERISTICS OF ARBITRARY ROTATING BODIES
I.A.Jacobson, edited by P.F.Yaggy
Published November 1973
64 pages

This survey paper reviews both theoretical and experimental investigations of the Magnus effect on arbitrary bodies of revolution. The main emphasis is on spinning projectiles at angles of attack, both with and without fins. Flow visualization measurements are used to assess the accuracy of the existing theories. Laminar turbulent, and mixed boundary layers are considered.

AGARD-AG-171
532.582.82 :
533.696.5 : 623.451

Magnus effect
Rotation
Bodies of revolution
Projectiles
Spin stabilized ammunition
Flow visualization
Boundary layer

AGARDograph No.171
Advisory Group for Aerospace Research and Development, NATO
MAGNUS CHARACTERISTICS OF ARBITRARY ROTATING BODIES
I.A.Jacobson, edited by P.F.Yaggy
Published November 1973
64 pages

This survey paper reviews both theoretical and experimental investigations of the Magnus effect on arbitrary bodies of revolution. The main emphasis is on spinning projectiles at angles of attack, both with and without fins. Flow visualization measurements are used to assess the accuracy of the existing theories. Laminar turbulent, and mixed boundary layers are considered.

AGARD-AG-171
532.582.82 :
533.696.5 : 623.451

Magnus effect
Rotation
Bodies of revolution
Projectiles
Spin stabilized ammunition
Flow visualization
Boundary layer

AGARDograph No.171
Advisory Group for Aerospace Research and Development, NATO
MAGNUS CHARACTERISTICS OF ARBITRARY ROTATING BODIES
I.A.Jacobson, edited by P.F.Yaggy
Published November 1973
64 pages

This survey paper reviews both theoretical and experimental investigations of the Magnus effect on arbitrary bodies of revolution. The main emphasis is on spinning projectiles at angles of attack, both with and without fins. Flow visualization measurements are used to assess the accuracy of the existing theories. Laminar turbulent, and mixed boundary layers are considered.

AGARD-AG-171
532.582.82 :
533.696.5 : 623.451

Magnus effect
Rotation
Bodies of revolution
Projectiles
Spin stabilized ammunition
Flow visualization
Boundary layer

AGARDograph No.171
Advisory Group for Aerospace Research and Development, NATO
MAGNUS CHARACTERISTICS OF ARBITRARY ROTATING BODIES
I.A.Jacobson, edited by P.F.Yaggy
Published November 1973
64 pages

This survey paper reviews both theoretical and experimental investigations of the Magnus effect on arbitrary bodies of revolution. The main emphasis is on spinning projectiles at angles of attack, both with and without fins. Flow visualization measurements are used to assess the accuracy of the existing theories. Laminar turbulent, and mixed boundary layers are considered.

AGARD-AG-171
532.582.82 :
533.696.5 : 623.451

Magnus effect
Rotation
Bodies of revolution
Projectiles
Spin stabilized ammunition
Flow visualization
Boundary layer

NATIONAL DISTRIBUTION CENTRES FOR UNCLASSIFIED AGARD PUBLICATIONS

Unclassified AGARD publications are distributed to NATO Member Nations through the unclassified National Distribution Centres listed below

BELGIUM
Coordonnateur AGARD – VSL
Etat-Major de la Force Aérienne
Caserne Prince Baudouin
Place Dailly, 1030 Bruxelles

CANADA
Director of Scientific Information Services
Defence Research Board
Department of National Defence – 'A' Building
Ottawa, Ontario

DENMARK
Danish Defence Research Board
Østerbrogades Kaserne
Copenhagen Ø

FRANCE
O.N.E.R.A. (Direction)
29, Avenue de la Division Leclerc
92, Châtillon-sous-Bagneux

GERMANY
Zentralstelle für Luftfahrtdokumentation
und Information
Maria-Theresia Str. 21
8 München 27

GREECE
Hellenic Armed Forces Command
D Branch, Athens

ICELAND
Director of Aviation
c/o Flugrad
Reykjavik

ITALY
Aeronautica Militare
Ufficio del Delegato Nazionale all'AGARD
3, Piazzale Adenauer
Roma/EUR

LUXEMBOURG
Obtainable through BELGIUM

NETHERLANDS
Netherlands Delegation to AGARD
National Aerospace Laboratory, NLR
P.O. Box 126
Delft

NORWAY
Norwegian Defense Research Establishment
Main Library,
P.O. Box 25
N-2007 Kjeller

PORTUGAL
Direccao do Servico de Material
da Forca Aerea
Rua de Escola Politecnica 42
Lisboa
Attn of AGARD National Delegate

TURKEY
Turkish General Staff (ARGE)
Ankara

UNITED KINGDOM
Defence Research Information Centre
Station Square House
St. Mary Cray
Orpington, Kent BR5 3RE

UNITED STATES
National Aeronautics and Space Administration (NASA)
Langley Field, Virginia 23365
Attn: Report Distribution and Storage Unit

* * *

If copies of the original publication are not available at these centres, the following may be purchased from:

Microfiche or Photocopy

National Technical
Information Service (NTIS)
5285 Port Royal Road
Springfield
Virginia 22151, USA

Microfiche

ESRO/ELDO Space
Documentation Service
European Space
Research Organization
114, Avenue Charles de Gaulle
92200, Neuilly sur Seine, France

Microfiche

Technology Reports
Centre (DTI)
Station Square House
St. Mary Cray
Orpington, Kent BR5 3RE
England

The request for microfiche or photocopy of an AGARD document should include the AGARD serial number, title, author or editor, and publication date. Requests to NTIS should include the NASA accession report number.

Full bibliographical references and abstracts of the newly issued AGARD publications are given in the following bi-monthly abstract journals with indexes:

Scientific and Technical Aerospace Reports (STAR)
published by NASA,
Scientific and Technical Information Facility,
P.O. Box 33, College Park,
Maryland 20740, USA

United States Government Research and Development Report Index (USGDRI), published by the Clearinghouse for Federal Scientific and Technical Information, Springfield, Virginia 22151, USA

Printed by Technical Editing and Reproduction Ltd
Harford House, 7-9 Charlotte St, London. W1P 1HD